Structural studies of LWC paper coating layers using SEM and image analysis techniques

by

Gary Chinga

Thesis submitted in partial fulfilment of the doktor ingeniør degree
February 2002

Norwegian University of Science and Technology
Department of Chemical Engineering

ABSTRACT

The ever rising need for detailed knowledge of the structure of paper coating urges the improvement and development of new techniques for gaining new and valuable information. The assessment, study and characterisation of factors that are assumed to affect the interaction between printing inks and coated paper surface may be accomplished by microscopy and image analysis techniques. The scanning electron microscope (SEM) is a most suitable tool for morphometrical studies of fibres and paper. Digital images acquired in a SEM, by the secondary electron imaging (SEI) or backscattered electron imaging (BEI) mode have suitable quality and resolution for further image processing and analysis.

The present study exemplifies how microscopy and image analysis may be applied for structural studies of the coating layer. Image processing and analysis routines for acquiring information on the coating layer surface roughness and porosity details like the pore shape, size and orientation are described. A routine, based on the Sobel operators, for measuring the pigment particle orientation, is also described. The developed semi-automatic image analysis routines are useful methods for morphometric analysis of paper structure details, thus facilitating numerical data acquisition of the pores and the pigment particles' geometry. Parts of the obtained information is assumed to be unattainable by other methods at this point.

To discern the binder in the coating layer from the embedding epoxy and thus observe individual pores in the coating, the binder has to be stained before embedding. In the study, osmium tetroxide (OsO_4) was used to stain the latex binder in the coating layer. Morphometric analyses of paper cross-sections using SEM, BEI-mode images and stereo images were used to quantify the paper coating structure details. The smallest details to be quantified are approaching the limitations given by the imaging methods.

It is shown that the staining procedures allow a quite accurate determination of pore fraction in the coating, and individual readings of the pores like pore area, aspect ratio and orientation. Two compared staining methods differed somewhat in their effect on the paper. OsO_4 dissolved in water gave good staining throughout the base paper/coating sandwich, allowing good visualisation and assessment of the coating structure. However, moisture tends to make the base paper fibre expand, raising the paper thickness and thus the macro-roughness. When staining by dry OsO_4 crystals, the base paper expansion is avoided, however, even the staining of the fibres is reduced. Critical coating parameters like mean pore area and micro-roughness of the coating layer do not differ between the two methods

In the study, the structure of commercial LWC paper coating layers were assessed and quantified by SEM, BEI-mode and digital image analysis of cross sections. It is quantified how clay particles cause a more densely packed coating structure compared to coatings containing mainly $CaCO_3$. The pores of clay coatings have a larger aspect ratio and are oriented more parallel to the paper surface. Pore orientation is affected by the pigment particle orientation. Besides the size of the pores, their orientation is proved to be an essential parameter affecting the achieved

print gloss level for a given paper grade. The pore's orientation/ diameter ratio seems to be a suitable parameter for describing its geometry and influence on print gloss. For a given pore diameter, the more horizontally oriented, the higher the delta gloss (print gloss-paper gloss).

Based on secondary and backscattered electron images, some detailed characterisation of the calendered paper samples' surface is undertaken. Surface areas differing in porosity and roughness are identified and characterised. Significant differences between "closed" and "open" areas with respect to pore area fraction and mean pore diameter are quantified. It is demonstrated that the larger the size of each closed area unit the larger the correlation between the surface variation and mottling. The observed structural differences are likely to cause a non-uniform ink vehicle absorption into the coating structure and may affect the printing ink density on the paper surface. It is also demonstrated that print gloss is influenced by the pore diameter. However, pore geometry, described by the pore size and orientation, seems also important for the gloss development.

Finally, the SEM in low-vacuum mode is used to acquire consecutive backscattered electron images after successive polishing. The high resolution achieved by this technique permits the visualisation of pigment particles and inter-particle volumes. Computer programs available on the Internet are used to process, render and visualise the reconstructed volume. Structures from the real coating layer like the inter-particle volume network and the pigment particles are volume rendered and visualised in 3-D space. The technique seems promising, however further work is required to improve the efficiency of the image acquisition and to control the thickness of the removed cross-sections which is very important in the quantification of structure details.

PREFACE

This thesis is submitted in partial fulfilment of the *doktor ingeniør* degree at the Norwegian University of Science and Technology (NTNU). The work has been carried out at the Norwegian Pulp and Paper Research Institute (PFI) and Department of Chemical Engineering at NTNU from 1998 to 2001, with Professor Torbjørn Helle as supervisor.

Funding of the doctoral study was provided by Norske Skog ASA and the Norwegian Research Council.

ACKNOWLEDGEMENTS

First of all, I would like to thank my supervisor, Professor Torbjørn Helle, for excellent guidance, invaluable support and discussions during this work. The linguistic revision of the thesis and manuscripts is also highly appreciated.

I am also grateful to Øyvind Gregersen (PFI) for his help, guidance and invaluable discussions.

Trond Forseth (Norske Skog, Follum) is also recognised for help and inspiration during this work.

I also would like to thank all my fellow doctoral students and staff at the pulp and paper group at NTNU and PFI for their help, good environment and positive experience gained during my thesis work.

The co-operation of Norske Skog Research – Runnability and Printability Department and Bruck is also appreciated.

Financial support was given by Norske Skog and the Norwegian Research Council. This is grateful acknowledged.

Finally, my warmest thanks to Hege, my friends and family for their support and especially to my two wonderful sons for enriching my life.

TABLE OF CONTENTS

ABBREVIATION LIST

2-D	Two-dimensional
3-D	Three-dimensional
AR	Aspect ratio
BSE	Backscattered electron
BEI	Backscattered electron imaging
Br_2	Bromine
$CaCO_3$	Calcium carbonate
CD	Cross direction
CMC	Carboxy methyl cellulose
D	Diameter (minor axis) of an ellipse fitted to an object
FIB	Focused ion beam
GCC	Ground calcium carbonate
ISO	International standard organisation
KCL	Oy keskuslaboratorio – Centrallaboratorium AB, Finland
$KMnO_4$	Potassium permanganate
LM	Light microscope
LWC	Light weight coated
MD	Machine direction
NIH	National institute of health (US)
NTNU	Norwegian university of science and technology
O	Orientation of an ellipse fitted to an object (pores or pigment particles)
OsO_4	Osmium tetroxide
PFI	Norwegian pulp and paper research institute
pph	Parts per hundreds
Ra	Arithmetic average (roughness parameter)
rpm	Rotation per minutes
Rq	Root mean square (roughness parameter)
SE	Secondary electron
SEI	Secondary electron imaging
SEM	Scanning electron microscope
TEM	Transmission electron microscope
VPSEM	Variable pressure scanning electron microscope
XRD	X-ray diffraction
ZD	Z-direction, perpendicular to the paper plane

DEFINITIONS

3-D Reconstruction: Structure reconstruction based on 2-D images

Binarizing:	The pixels in a greyscale digital image are set to either black or white
Erosion:	Binary morphological operation that uniformly reduces the size of objects in relation to the background
Major axis:	The longest axis of a best fitting ellipse
Minor axis:	The longest axis that can be drawn through an ellipse while maintaining it perpendicular to the major axis
Pixel:	Picture elements of a digital array (image)
Rendering:	Method to render a 3-D reconstruction
Segmentation:	The first step of image analysis. Objects of interest are extracted from the background
Skeletonization:	Binary morphological operation that reduces an object to a skeleton representation
Sobel operator:	Spatial edge enhancement filter
Stack:	Single file containing two or more digital images
Threshold:	Manually or automatically selected value used to segment an image into a foreground (object of interest) and background

For more details see Baxes (1994)

CHAPTER

1

INTRODUCTION

1.1 Problem statement

The ever rising demand on print quality urges a steady growth of knowledge of the physical and chemical aspects of coated paper. Understanding how raw materials, including pulp fibres, fillers, binders and pigment particles, interact with each other is fundamental for predicting the final paper and print quality. In this context, it is also important to gain more insight into how different production and finishing variables affect the paper structure and thus the end-use properties of printing paper.

The micro-structure of paper has been reported to affect different properties such as light scattering, gloss and homogeneity of prints. Mottling is also believed to have causes related to the structure of the coated paper surface. Understanding the micro-structure of the coating layer with respect to porosity, surface roughness and pigment particle details may thus clarify some unanswered questions and contribute to the increasing knowledge of paper structure.

During the years several techniques have been developed in order to assess the mentioned details of the coating layer. However, the study and characterisation of the paper structure is always limited by the limitations of the existing analysis techniques urging the application of improved and emerging methods in order to gain new and valuable information.

The scanning electron microscope (SEM) offers high magnification, good resolution and the possibility to discern between structures having different atomic number (BEI-mode). The SEM may yield digital images with suitable quality for further analysis. The acquisition of numerical information from these high quality images requires good and effective processing and analysis routines. The routines must be fast, reliable and objective. The developed and applied method must also be reproducible in order to validate its reliability.

1.2 Aim of the study

The present study deals with the development of new characterisation and measurement techniques based on microscopy and image analysis. Modern methods available for paper sample preparation and image acquisition are looked into and discussed. The development of image processing and analysis routines for acquiring information about the coating layer structure of lightweight coated (LWC) paper are also described.

The following parameters are supposed to affect the end-use properties of paper and have been considered important in the characterisation of the coating layer structure:

- Coating layer thickness
- Macro- and micro-roughness
- Surface and bulk porosity
- Pore shape and orientation
- Pore size distribution
- Pigment particle orientation

The continuous development of these measuring techniques will ensure a profound knowledge of the paper structure details and contribute to its improved performance. This may certainly facilitate the efficient use of raw materials and minimise production costs.

1.3 Outline of the thesis

This thesis is mainly a collection of papers comprising results that have been either presented in international conferences or submitted for publication in international journals. The papers have been arranged in a reasonable order to facilitate the reading.

Chapter 2 gives an overview of available microscopy and image analysis techniques for assessing the coating layer structure. Advantages and drawbacks are discussed.

Chapter 3 presents the image analysis routines developed to assess the coating layer cross-sectional macro-structure like the thickness and surface macro-roughness.

Chapter 4 presents the image analysis routines developed to assess the coating layer surface based on SEM images. The chapter focuses on the segmentation and characterisation of pores and surface structural variation. A detailed description of the developed techniques is given.

Chapter 5 deals with the staining of binders in the coating layer. Two different methods involving OsO_4 for the staining are described. Besides discussing the advantages of using OsO_4 and calculating pore characteristic details, this chapter verifies the presumptive changes of the paper structure due to the staining.

Chapter 6 describes a series of image analysis routines developed to segment and characterise the coating layer micro-structure. Special attention is given to the assessment of critical pore and pigment particle details. Routines for assessing the coating layer porosity, the pore area, pore shape, pore orientation as well as the particle orientation are described.

Chapter 7 applies the preparation, image acquisition and image analysis procedures described in chapter 5 and 6 to study the cross-sectional coating structure of commercial LWC papers. The chapter emphasises the influence of pore geometry on the development of print gloss.

Chapter 8 applies the image analysis routines described in Chapter 4 to study the surface of commercial LWC papers. A morphometric study of the surface structural variation and the pore characteristic details is performed and related to gloss and mottling.

Chapter 9 explores the possibilities of obtaining a 3-D dataset for reconstruction of a real coating layer volume. The technique is based on serial polishing and the images are acquired in the SEM, BEI mode in low vacuum. Volume renderings of pigment particles and inter-particle voids are presented.

Chapter 10 presents the main conclusions of this study and gives some suggestions for further work.

CHAPTER

2

MICROSCOPY AND IMAGE ANALYSIS TECHNIQUES APPLIED IN STRUCTURAL STUDIES OF PAPER

2.1 Introduction

New available technology in microscopy and image analysis has improved the acquisition of morphometrical data in different fields of investigation. In recent years, several authors have also applied microscopy and image analysis techniques for data acquisition of paper structure details like paper thickness, roughness and porosity (see e.g. Peterson and Williams, 1992; Allem, 1998; Dikson, 1999) as well as the coating layer micro-structure (Climpson and Taylor, 1976; Rissa et al., 2000).

Microscopy and digital image processing techniques seem suitable to study and characterise paper structure details. However good image quality is essential for further morphometric analysis. The image quality depends on the preparation technique and on the microscope used for image acquisition. This part of the thesis is thus aiming at reviewing some of the microscopy and image analysis techniques applied to the study of the paper structure. Special attention is given to the techniques used for assessing the coating layer on paper.

2.2 Staining techniques

During the years, several techniques have been used to enhance and improve the visualisation of structures in pulp and paper. The techniques mentioned here are applicable to sample preparation for image acquisition in the scanning electron microscope (SEM).

2.2.1 Potassium permanganate ($KMnO_4$)

Potassium Permanganate ($KMnO_4$) has been used in the study of lignin components in wood and pulp fibres (see e.g. Gregersen et al., 1995). $KMnO_4$ reacts with lignin, raising the structure's average atomic weight, thus improving the contrast in backscattered electron (BSE) images. Regions containing lignin appear brighter as is the case with the middle lamella that surrounds the fibres in wood samples. This

is a simple and fast method to better visualise lignin-containing structures in the SEM, backscattered electron imaging (BEI) mode. However, although the technique provides good staining, it is not suitable for quantitative analysis of lignin content. Besides the staining must be applied as water solution inducing changes in the paper structure.

2.2.2 Bromine (Br_2)

Besides $KMnO_4$, bromine has been used in the staining and study of lignin-containing structures (Gregersen et al., 1995). Br_2 has similar effects as $KMnO_4$. Staining, accomplished by exposing the material to bromine gas, can be used for improving the quality of images acquired in the SEM, BEI-mode (Gregersen et al., 1995). The procedure is easy and fast, however, due to its toxicity proper precaution must be taken. Forseth et al. (1997) applied this technique to the study of the moisture effect on paper roughening. The authors allowed supercalendered paper to react with bromine gas. Based on the obtained backscattered electron (BSE) images the authors visualised and quantified the behaviour of chemical and mechanical pulp fibres after exposing the paper samples to moisture.

2.2.3 Osmium tetroxide (OsO_4)

Osmium tetroxide (OsO_4) is widely used in biological sample preparation to preserve and fixate cell structures for further visualisation by electron microscopy. The chemical forms cross-linked complexes with C=C double bonds. Such bonds are present in latex which is used to bind pigment particles in coating. Examples of such latex components are butadiene and styrene. Thus, an improved visualisation of the pore structure is obtained by staining the latex films with OsO_4. The latex films appear brighter and may be clearly discerned from the epoxy resin used for embedding the paper samples (Fig. 2.1). This improves the final visualisation of the pore structure, allowing quantification of pore details. Image analysis of micrographs of OsO_4-stained paper sample cross-sections may thus offer an interesting way of assessing the pore structure of coating layers. However, due to its toxicity, proper precautions must be taken during staining.

A few researchers have reported the use of OsO_4 staining applied to paper studies. Mechanical pulp fibres, binders (Krishnagopalan and Simard, 1976; Matsubayashi et al., 1990; Matsubayashi and Saito, 1992; McCoy, 1998; Rissa et al., 1999) and printing inks (Ozaki and Kimura, 2000) are reported to be stained by this chemical to facilitate the characterisation of paper structure. According to McCoy (1998) OsO_4 will also stiffen the base sheet fibres, thus improving the sample polishing process.

McCoy (1998) used 1g of OsO_4 crystals to vapour-stain styrene-butadiene latex in coated paper. The author reported good staining of the latex material in the coating. Rissa et al. (1999) used OsO_4 dissolved in water to stain the latex of clay coatings in order to characterise the morphology of the coating structure based on SEM, BEI-mode cross-section images. In another study, OsO_4-staining was used to improve the visualisation of talc pigment particles allowing particle orientation to be assessed by image analysis (Rissa et al., 2000).

Whalen-Shaw and Eby (1991) applied OsO_4 to study binder concentration variation at the coating layer surface and its possible effect on the print quality defect termed

"backtrap mottle". Higher binder concentration was found on areas with low ink density.

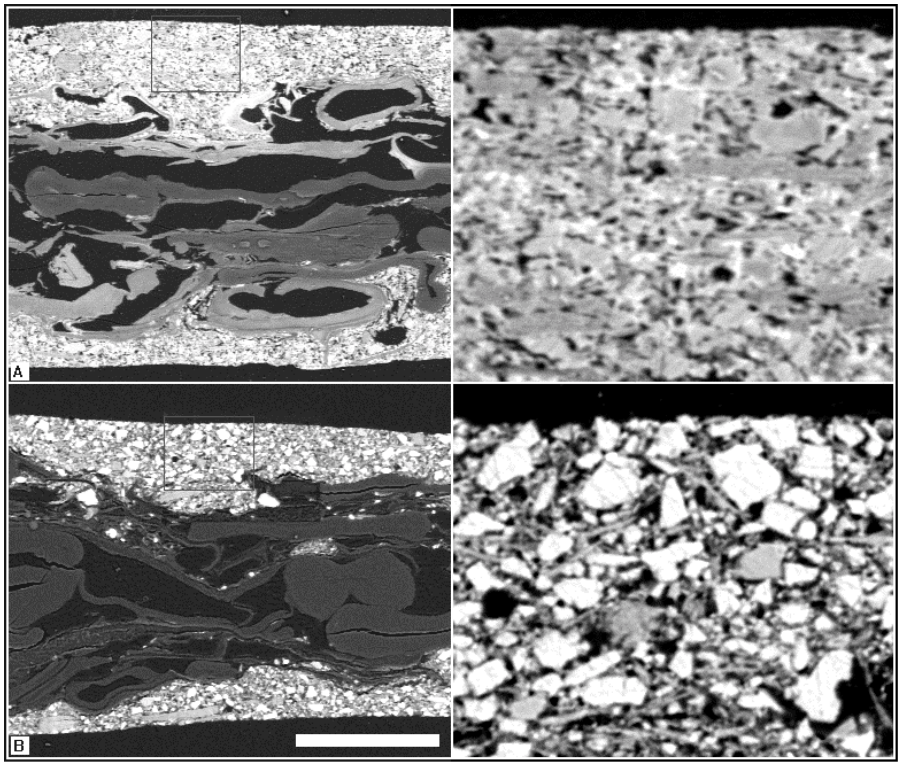

Figure 2.1 Cross-section images of LWC paper samples. A) Paper sample stained with OsO_4 before embedding in epoxy resin. B) Unstained LWC paper sample for comparison. The images on the right side are taken with 5000x magnification and show details of the regions marked on the left side respectively. Note the bright latex material around the pigment particles in A. Bar: 25 μm for 1000x magnification images (left side) and 5 μm for 5000x magnification images (right side).

2.3 Preparation techniques

Perhaps the most important step for good image quality is the preparation of the samples to be studied. The preparation varies depending on the microscope to be used and the structure to be studied and must be carefully performed.

2.3.1 Microtoming

Sample preparation for the light microscope (LM) and the transmission electron microscope (TEM) may imply a mechanical sectioning of the paper samples. Reported methods consist of trimming the block surface with vertical leading face and sides; only the trailing face keeps its usual shape in order to avoid flexure of the block during sectioning (Fahrenbach, 1984). The trimming may be performed using a microtome or manually with a razor blade. The blocks containing the samples can be sectioned with an ultra-microtome. The thickness is in the range of

approximately 50-100 nm for TEM sections and 0.5-5.0 μm for LM sections. According to Walbaum and Zak (1976), microtoming may introduce distortions into the sections making it difficult to obtain quantitative information. This is a major disadvantage when the structure and composition of the coating layer must be characterised. Cross-section preparation may also be tedious and time consuming.

However, Peterson and Williams (1992) used microtomed sections of paper samples and studied them in the SEM. Based on the acquired SEM images, the authors were able to measure the coating layer thickness. They also used the variation value of the coating layer thickness to estimate the base sheet roughness. Despite the obtained results the authors also found some problems related to the preparation of the paper samples. It was evident that the used glass knife had removed a certain amount of pigment particles in the coating layer. Besides, shrinkage and wrinkling were also visible on the cross-sections. The same authors claimed that using a diamond knife would improve this technique avoiding the mentioned problems. However, any cutting process may rip out pigment particles from the coating layer, affecting the morphometrical study.

2.3.2 Grinding and polishing

Scanning electron microscopy, BEI-mode requires distortion-free and smooth surfaces of the studied samples. Gibbon et al. (1989) described a detailed procedure for preparing large paper samples. The method was based on embedding the samples in epoxy resin, grinding and polishing. By using this method, distortions introduced by microtoming could be avoided. Williams and Drummond (1994) further developed the mentioned technique to prepare paper samples for image acquisition in the SEM. 10 samples could be placed vertically in the same plastic mould and embedded in epoxy resin (Fig. 2.2). The block surface was then ground using a series of abrasive papers (240, 400, 600, 800 and 1200 grit). Thereafter, the block face was polished on a nylon cloth using a 1-micrometer oil-based diamond paste. The block face was cleaned between each change to a finer abrasive paper to avoid contamination of the previous grinding. This method provided, according to the authors, high quality sections for high-resolution imaging. A major advantage is the fact that large samples can be studied in the SEM, providing good image quality and resolution.

2.3.3 Automatic polishing

More recently, several authors have reported improved techniques for the preparation of fibres and paper samples (see e.g. Forseth et al., 1997; Allem, 1998). The main steps are principally the same; the procedure may vary with respect to the type of abrasive paper, the polishing cloth, time, speed and force used in grinding and polishing. If modern equipment is available, blocks can be prepared quickly and effectively. This is of major importance since fewer steps are required to prepare the samples avoiding probable distortions on the cross-section surface.

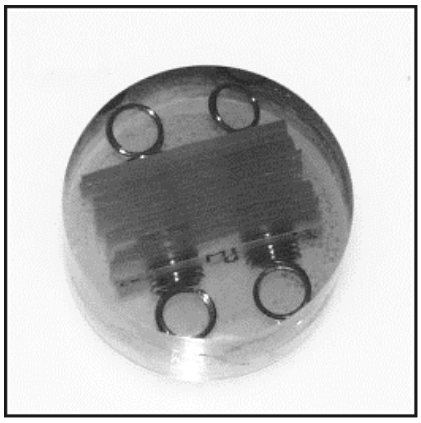

Figure 2.2 Paper samples placed in spring holders and embedded in epoxy resin for SEM analysis.

2.3.4 Alternative preparation methods

Although automatic grinding and polishing seems to be a well-established technique for the preparation of fibres and paper samples, other techniques appear to be promising. The focused ion beam (FIB) is a new reported method for preparation of transmission electron microscopy samples (see e.g. Kim and Dravid, 2000). The TEM has the ultimate optics for assessing the specimens' micro-structure, though the microscope requires a maximum cross-section thickness of approx. 100 nm for being electron transparent. The FIB instrumentation is reported to impose less mechanical stress to the samples during preparation, compared to grinding and polishing, avoiding matrix cracks into the prepared regions (Kim and Dravid, 2000). However, the method seems to be laborious, including embedding, sectioning, grinding and polishing. The samples are finally thinned using a gallium beam accelerated at 30 kV. Since the FIB is similar to a SEM, an electron image is formed while the beam is milling the sample. This may be considered a major advantage for obtaining consecutive images of a sample.

Alkemper and Voorhees (2001) reported the use of a micromiller for sample preparation. According to the authors, the advantages of using this kind of equipment is i) nearly scratch-free cross-sections, ii) serial sectioning and iii) automatic alignment of the cross-sections. This equipment thus provides a dataset with aligned cross-sections suitable for three-dimensional (3-D) reconstruction. The surface of the sample is milled off with a step-size between 1 and 20 μm. However, the accuracy of the distances between the cross-sections is affected by thermal changes during sectioning. A major drawback, with respect to the assessment of the coating structure, is the reported resolution (0.96 μm in x and y-direction).

2.4 Image acquisition

The resulting quality of the preparation step is an important factor affecting the image quality during image acquisition. The optimal microscope to be chosen depends on the structure to be analysed and the type of the study. In this review

only three types of microscopes will be described and commented, i.e. the light microscope, the transmission electron microscope and the scanning electron microscope (Fig. 2.3).

2.4.1 Light microscope (LM)

Light microscopy is one of the simplest techniques used for acquiring information about fibres and paper structures. Elton et al. (1990) pointed out the importance of optical microscopy in the study of paper structure. However, the obtained information is limited due to the optics of this microscope. As mentioned above, light microscopy may require microtomed sections of paper samples, introducing distortions into the paper structure (Walbaum and Zak, 1976). Besides, the resolution and magnification limitations of the light microscopes are limiting factors for the study of coating layer structures (see Table 2.1). Although the light microscope is not suitable for the study of the coating layer details, according to Quackenbush (1988) this kind of microscope is still applicable to different studies in pulp and paper research. Besides the microscope may facilitate the visualisation of e.g. ink penetration into the paper structure.

2.4.2 Transmission electron microscope (TEM)

The resolution of the TEM provides advantages for the study of fibre ultrastructure. However, the TEM requires microtomed cross-sections. Ultrathin cross-sections prepared for this microscope may cause severe problems and artefacts, yielding poor image quality. Despite this limitations Climpson and Taylor (1976) managed to use microtomed sections of clay coatings to quantify pore size distributions and correlate the results with light scattering. Although reasonable agreement was found between the measured pore dimensions and the coatings optical properties, ultramicrotoming requires careful preparation in order to preserve the structure of the samples. New preparation techniques like the FIB method (Kim and Dravid, 2000) may be useful in this respect.

2.4.4 Scanning electron microscope (SEM)

As mentioned above, the SEM is suitable for pulp fibre and paper studies. This microscope offers high quality imaging with high resolution (Helle and Johnsen, 1994). Commonly, the microscope can be operated in two modi; secondary electron imaging (SEI) and backscattered electron imaging (BEI). The SEI-mode is generally used for imaging the surfaces of structures. In the BEI-mode, the obtained images' contrast depends on the atomic number of the structure under the electron beam (Fig. 2.4 and 2.5A). The higher the average atomic weight the brighter the region will appear in the BSE image.

Images of coated paper are roughly composed of three regions; the base paper, the coating layer and the background. These structures differ in contrast due to the different average atomic weight (Fig. 2.5A). The base paper is primarily composed of fibres and may also contain fillers. Furthermore, the coating layer is composed of mineral particles and binders. Pigment particles, used in the coating layer, are produced from minerals having different atomic number and yielding different contrast in the obtained images. This fact is a major advantage when acquiring images in the BEI-mode improving the quality and contrast between structures.

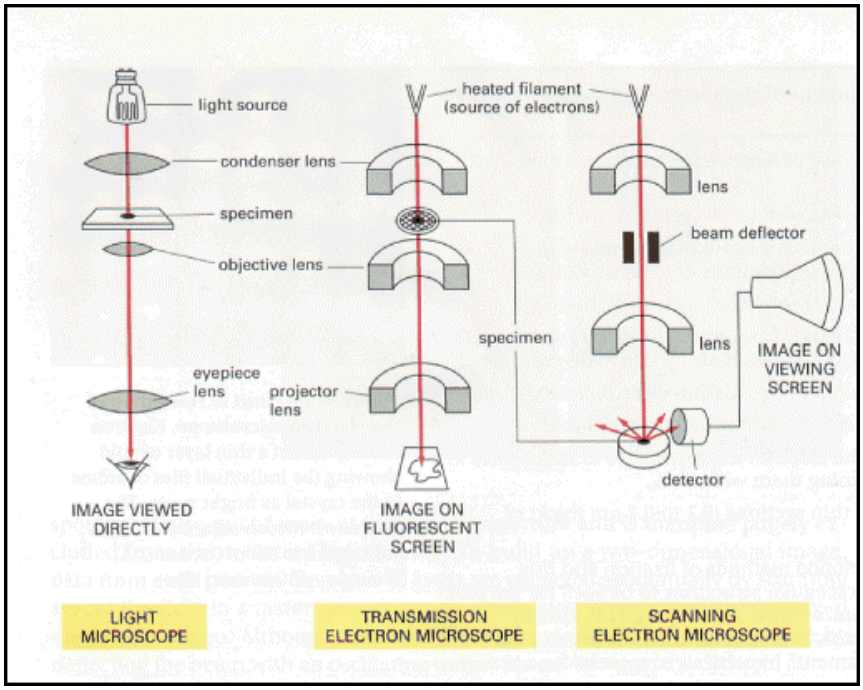

Figure 2.3 Schematic representation of the three type of microscopes discussed in this study (reproduced from Alberts et al., 1989).

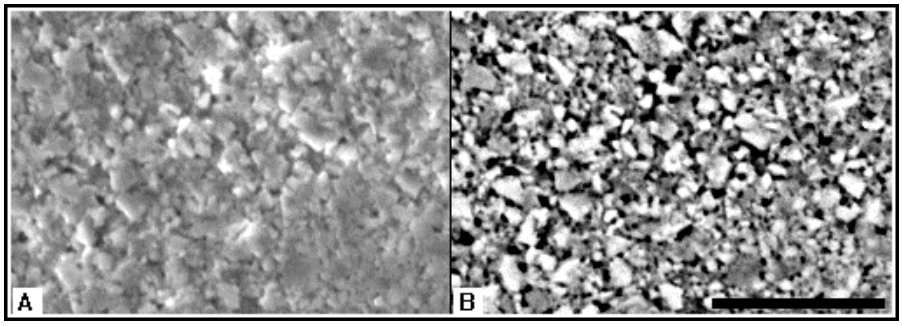

Figure 2.4 SEM surface images of a LWC paper sample. A) SEM image taken in SEI-mode. B) The same area taken in BEI-mode. Note the improved visualisation of the pores in BEI-mode. The different grey levels obtained in BEI-mode depends on the average atomic weight of the pigment particles. Bar: 10 µm.

Table 2.1 Microscopes used in fibre and paper structural studies.

Microscope	Resolution*	Comments
LM	0.2 µm	Poor magnification, resolution and image quality
TEM	0.1-0.2 nm	High resolution, image quality depends on preparation
SEM	5-10 nm	Good resolution and high image quality.

* According to Alberts et al., 1989.

2.5 Image analysis

Digital image processing techniques applied to study the fibres and paper are widely used. Details of the paper structure like the coating layer, the fillers and the base paper characteristics can effectively be assessed and quantified (Fig. 2.5).

2.5.1 Assessment of the coating layer thickness

Several authors have reported attempts to characterise the coating layer based on digital images acquired by microscopy (see e.g. Kent et. al., 1986; Gane et al., 1991; Peterson and Williams, 1992; Williams and Drummond, 1994; Allem, 1998). Peterson and Williams (1992) described a method based on the area comprised by the coating layer in the cross-section image and the length of the image. This method provides the mean thickness of the coating layer (Fig. 2.6B). However, the local variation is not assessed. Williams and Drummond (1994) pointed out that a representative quantification of the thickness and variation of a coating layer could be achieved using scanning lines. The lines should scan the coating layer randomly in order to get a representative value of the full sample length. However, no attempts were made by these authors to quantify the coating layer thickness.

Allem (1998) used a similar method to assess the uniformity of lightweight coated papers. He developed image analysis routines based on the above mentioned scanning lines (Fig. 2.6C). The greyscale images were thresholded and binarised. However, the binary images needed to be further edited to remove particles not belonging to the coating layer. This step was performed manually, requiring time and effort. The method proved, however, to be an effective way of acquiring data from the paper cross-section images.

2.5.2 Base sheet porosity and roughness assessed by image analysis

Allem and Uesaka (1999) developed the image analysis techniques further in order to include the base sheet porosity and interaction with the coating layer. Using scanning lines at regular intervals the base sheet and coating profile could be analysed and their roughness assessed. The roughness value was evaluated as the arithmetical mean deviation of the measured lines from the top of the image to the surface of the paper sample. The results of the image analysis method proved good agreement with conventional used methods.

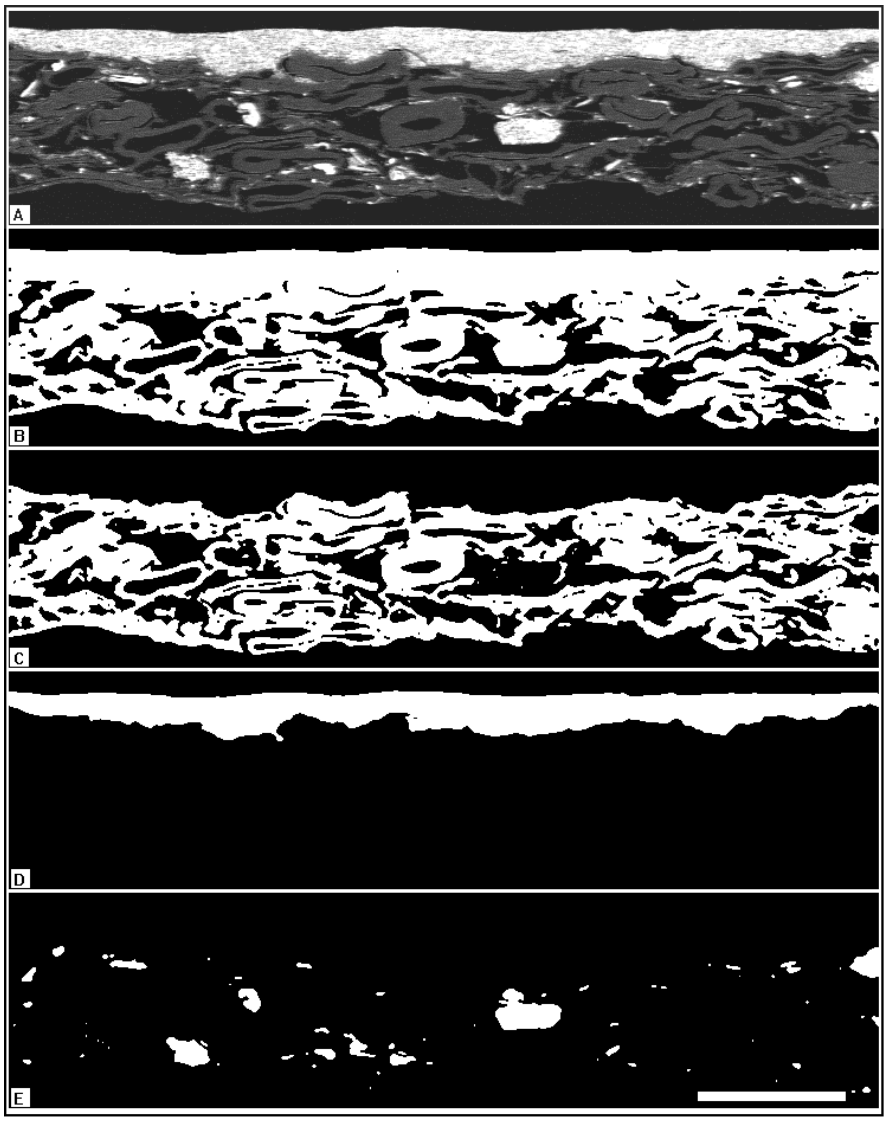

Figure 2.5 Segmentation of digital images of paper cross-sections. A) Original digital image, B) segmented cross-section, C) segmented base paper, D) coating layer and E) Fillers. Bar: 50 μm.

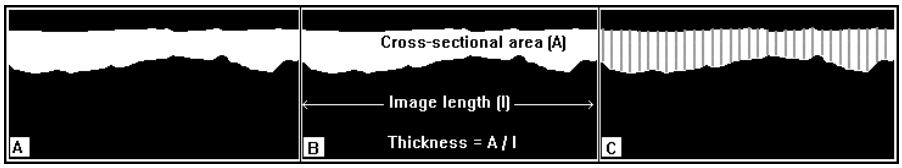

Figure 2.6 Schematic representation of thickness measurements of the coating layer. A) Segmented coating layer (white area). B) Thickness assessment based on the coating layer cross-sectional area and the image length. C) The same region with superimposed scanning lines for local thickness assessment.

2.5.3 Assessment of the coating layer's micro-structural details

Climpson and Taylor (1976) quantified pore dimensions of clay coatings by image analysis. The authors used a spheroid model to simplify the pore structure. They found that pores with diameters between 0.5 and 0.7 μm gave the largest contribution to light scattering. Distributions of the oriented spheroids were also compared to distributions obtained with the mercury intrusion method. An underestimation of the pore dimensions when using the intrusion method was found. According to the authors this phenomenon is due to the limitations of mercury porosimetry. The pore volume distribution assessed by porosimetry has thus been found to be much smaller than that found by image analysis methods (Dullien and Mehta, 1971; Climpson and Taylor, 1976; Lepoutre and Rezanowich, 1977). Several authors (see e.g. Climpson and Taylor, 1976; Wygant et al., 1995; Abrams et al.,1996; Gane et al., 1996) state that mercury porosimetry may have limitations like i) sample compressibility, ii) assumption of interconnected pores and iii) inability of identifying narrow necked voids. However, according to Gane et al. (1996) compressibility and shielding effects may be overcome by new reported correction procedures.

Coating pigment particle orientation is an important parameter. Besides affecting gloss and light scattering, particle orientation affect the runnability at the blade (Gane and Watters, 1989); the packing of the coating, and thus the porosity and barrier properties (Rissa et al., 2000). X-ray diffraction (XRD) techniques are used to assess clay particle orientation (Gane et al., 1995; Elton et al., 1999). Rissa et al. (2000) measured talc pigment particles' orientation by X-ray diffraction, comparing the results with manual image analysis assessments. Semi-automatic image analysis was not applied due to touching edges of adjacent particles. Albeit good correlation, manual procedure is tedious and time consuming. XRD is also limited to comparative studies of pigment particles having similar crystallinity (Elton et al., 1999).

2.6 Concluding remarks

This study was aiming at reviewing the different microscopy techniques used in structural studies of pigment coating layers. The preparation step is perhaps one of the most important ones in order to get good images for further analysis. The sample preparation described above is mainly applied for the study of the coating structure. However, the same preparation could be used to assess the base paper and fibres' details. Even if several microscopes are described, the preparation techniques mentioned in this study are principally applicable to scanning electron microscopy. The SEM, due to its high resolution, magnification power and image quality seems suitable for morphometrical studies. This microscope, in combination with image analysis techniques, thus offers excellent possibilities to study e.g. fibres dimensions, pore details, base paper morphology and coating layer structure details.

Although several authors have reported the assessment of e.g. paper surface roughness, pore details and particle orientation, much remain to be done regarding the automation and standardisation of the image processing and analysis methods. Moreover, the accuracy of the obtained results depends considerably on the number of images and objects analysed. Manually assessment of e.g. pore and pigment particles dimensions may be tedious and work laborious thus urging the development of automatic routines for image analysis of the coating layer structure details. In addition, manual assessment always imply a certain degree of subjectivity leading to individual differences.

CHAPTER

3

ASSESSMENT OF THE COATING LAYER MACRO-STRUCTURE

3.1 Introduction

The quantification of different aspects of the coating layer is of primary importance for controlling the quality of coated paper. A smooth and even coating layer structure is desirable in order to avoid variations in structural properties of the paper surface. However, due to the rough formation of the base paper, the coating process may lead to an uneven coating layer having regions differing in thickness and surface roughness (Fig. 3.1). This factors may affect the optical and printing properties of the paper. This chapter describes thus the methods developed for assessing the coating layer macro-structure.

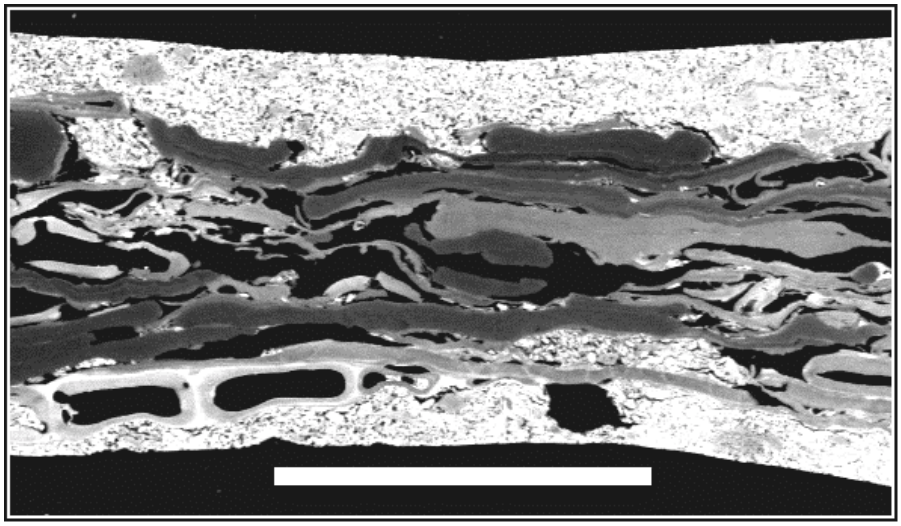

Figure 3.1 BSE image of a LWC paper cross-section. The paper sample has been treated with OsO_4 before embedding in epoxy resin. Bar : 50 μm.

3.2 Paper sample preparation

The paper samples for cross-section analysis were dried at 105ºC for 1 hour, then placed vertically in spring holders, evacuated in a vacuum chamber for 15 min and impregnated with epoxy resin. After curing, the blocks were ground, using 320 grit abrasive paper, removing approximately 1mm from the block surface. The blocks were then placed in an automatic STRUERS RotoForce-4 and polished in a STRUERS RotoPol-22 for 5 min using abrasive cloths with 9 and 1 μm diamond particles. Applied pressure and speed for polishing were 5N and 150 rpm respectively. The blocks were finally carbon coated.

3.3 Image acquisition

Digital images for further inspection were acquired using a SEM, Hitachi S-3000 VPSEM instrument. The BSE images were generated using 5kV accelerating voltage and 8-10 mm working distance. The applied magnifications were 250x and the resolution was 0.4 μm/pixel. The spatial resolution of digital images was 1280x960 pixels with 256 grey levels.

3.4 Image processing

For the image processing and analysis of the SEM images the Scion Image program was used, available on the Internet at http://www.scioncorp.com. Several routines were written to automate the Image program for use in the morphometric analysis.

The image quality obtained during acquisition in the SEM is well suited for further processing and analysis. If necessary, digital filters may be used to remove noise before segmentation. For this purpose a median filter has been used. This filter consists of running a 3x3 mask over the images. The filter sorts the pixel values in the 3x3 mask and replaces the centre pixel by the median pixel. This is an effective way of removing noise, enhancing image quality.

3.5 Image analysis

Image analysis deals with the acquisition of numerical information from digital images. One of the most important steps is thus segmentation, separation of features and objects from the background. Segmentation may be accomplished by thresholding greyscale histograms in such a way that the image will be divided into foreground and background. Once segmented, the objects of interest can be assessed and characterised.

3.5.1 Thresholding

The segmentation was accomplished by thresholding the greyscale histogram as explained by Ridler and Calvard (1978). The optimum threshold is obtained automatically by an iterative procedure yielding refined threshold levels that converge to an optimum value midway between two peaks. This procedure yields white objects on a black background. According to the authors the approach seems

suitable for high and low contrast images. Automatic thresholding is also important for the reproducibility of the developed method and is used in the present study. Manual thresholding tends to vary between operators and even for the same person over a period of time (Russ, 1999).

3.6 Segmentation and thickness measurements of the coating layer

Prior to thresholding a median filter was applied on every image to remove noise. As the coating layer primarily consists of bright mineral pigments, it is easily segmented by thresholding the greyscale histogram automatically, isolating the coating layer from the rest of the image (see Fig. 3.2).

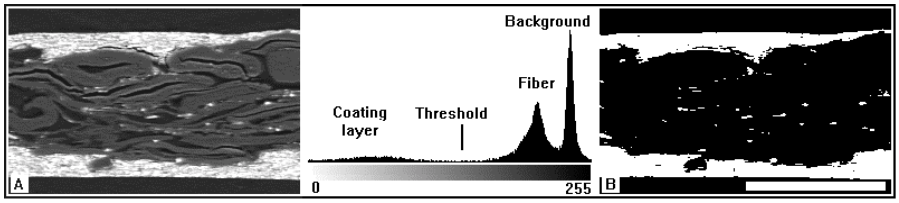

Figure 3.2 A) Digitised micrograph of a paper cross-section and the respective histogram showing the coating layer, the base paper and the background tops. B) The image was thresholded by using the in-built algorithm in the Scion Image program. Bar: 50 μm.

The whole paper cross-section can also be segmented by the same procedure. Applying histogram equalisation to the image before segmenting, enhances the paper cross-section to background contrast, thus improving the segmentation process. Subtracting the coating layer from the paper cross-section yields an image of the base paper. Finally, agglomerates not part of the coating layer may also be segmented by subtraction.

The routine used to segment the paper cross-section images (Fig. 3.3A) yields stacks composed of the whole cross-section (Fig. 3.3B), the base paper (Fig. 3.3C), the coating layer (Fig. 3.3D and E) and the base paper fillers (Fig. 3.3F). The segmented structures may then be assessed for analysis and quantification of e.g. the thickness and structural variation of the coating layer. For this purpose, several techniques and ways of measuring the thickness are available (Fig. 3.4). Fig. 3.4D also describes a simple way of measuring the thickness of a structure. Instead of applying measuring lines along the coating layer, the routine calculates the complete solids area of the structure in the image. The mean thickness is easily calculated by dividing the whole area by the length of the cross-section image as described by Peterson and Williams (1992).

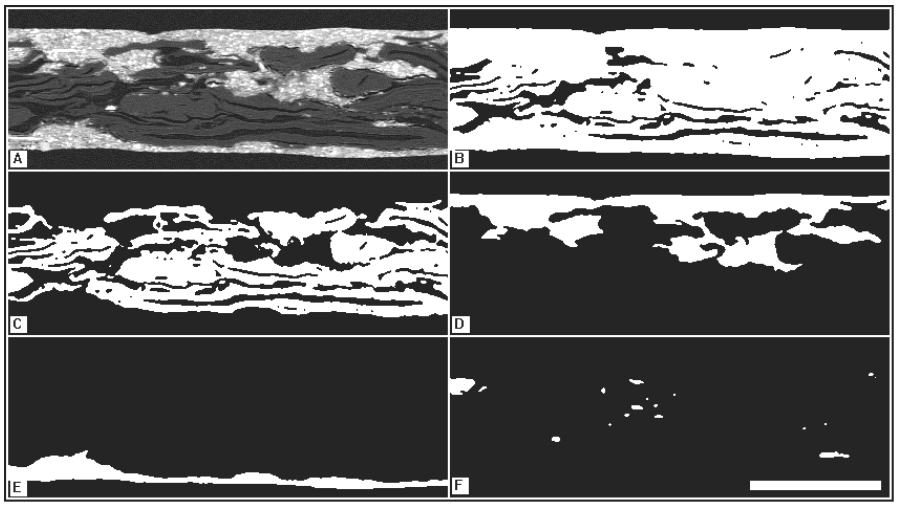

Figure 3.3 Segmentation of a paper sample cross-section image. A) Original digital image, B) segmented cross section, C) segmented base paper, D) top coating layer, E) bottom coating layer and F) base paper fillers. Bar: 50 μm.

It is important to find the right parameters both for segmentation and for measuring the objects of interest. During this study different aspects were investigated. Both the necessary step size between measuring chords on low and high magnification images were defined in order to measure parameters like the thickness and thickness variation. Although measuring chords at regular intervals, as exemplified in Fig. 3.4, has been used, the high capacity power of modern computers allows measuring at every pixel along the image without requiring any step size. However, a step size of 3 μm were used for measuring thickness and macro-roughness and 0.2 μm for micro-roughness.

3.7 Assessment of the coating surface macro-roughness

To assess roughness value a regression line is put along the paper surface. The routine scans the surface, registers the profile and calculates the regression line. The roughness is based on the measured distances from the calculated line to the surface (Fig. 3.5). Roughness parameters like the mean square root (Rq) and the arithmetic average (Ra) may be obtained according to the ISO 4287/2000 standard,

$$Rq = \sqrt{\frac{1}{n} \times (y_i - y_m)^2} \qquad \text{(I)}$$

$$Ra = \frac{1}{n} \times \left| y_i - y_m \right| \qquad \text{(II)}$$

Here, n is the number of measured distances, y_i the distance at x_i and y_m the average distance.

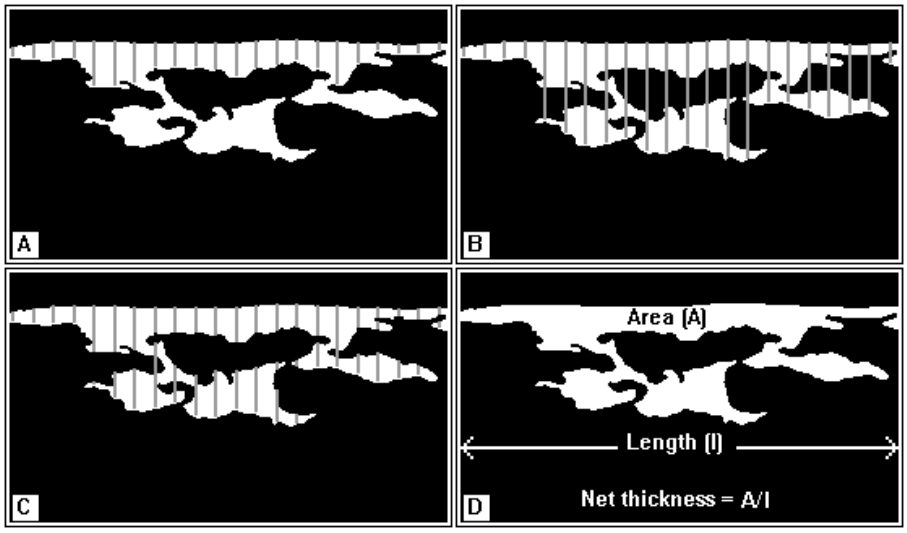

Figure 3.4 Schematic representation of measurements of the coating layer thickness. A) Only the thickness of the coating layer over the fibres is measured. The routine also calculates the thickness from top to bottom, B) including and C) excluding the voids. D) The thickness is calculated based on the area of the coating layer in the cross-section image divided by the length of the image.

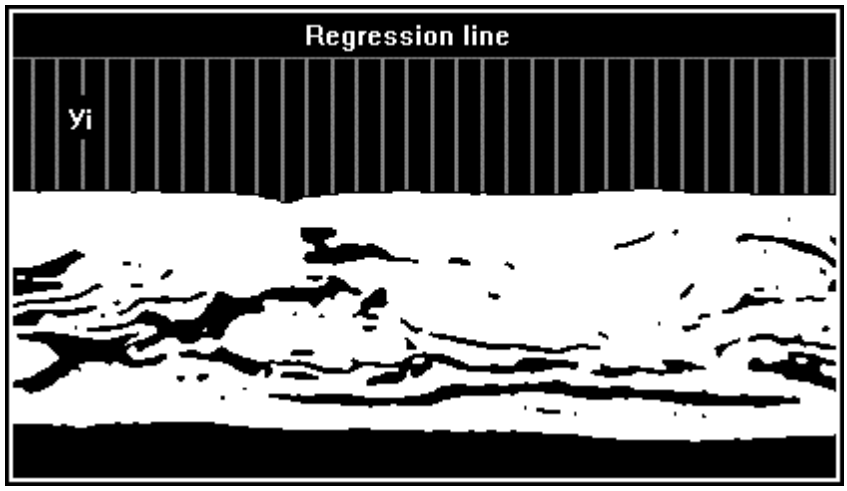

Figure 3.5 Schematic calculation of the surface roughness based on digital images. The white areas correspond to the paper cross-section. The step length may be chosen at will.

CHAPTER

4

MICROSCOPY AND IMAGE ANALYSIS OF SURFACE DIGITAL IMAGES

4.1 Introduction

The ideal paper surface should be smooth with optimal pore sizes to improve gloss and keep a good interaction between the paper surface and the applied inks during printing. Imperfections and irregularities on the paper surface structure should be avoided. However, paper surfaces have variations with respect to structural parameters like roughness and porosity that may affect the uniformity of the printing ink film formation. Such variations may be observed in Fig. 4.1. Techniques developed to identify and quantify such variations are described in this chapter.

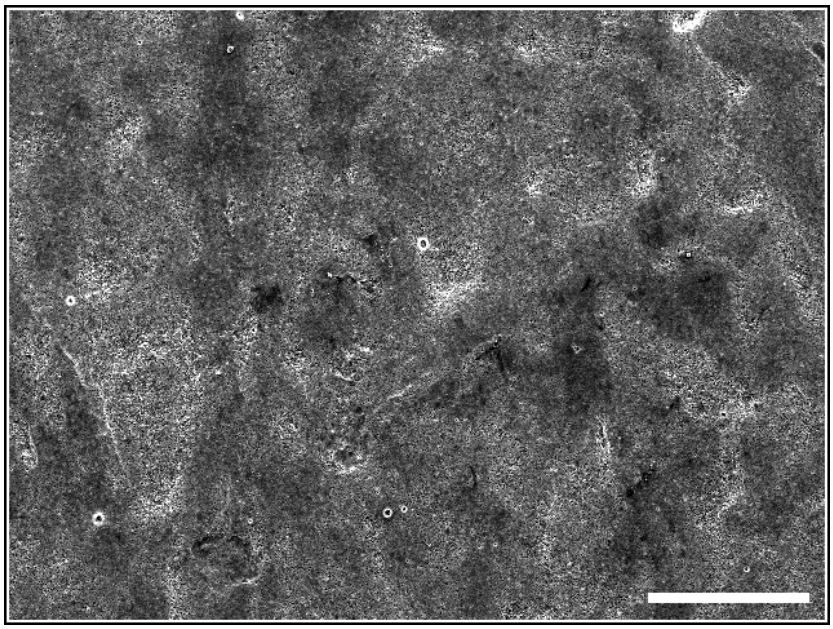

Figure 4.1 Secondary electron image of a LWC paper surface. Note the differences in surface appearance in dark (closed) and light (open) areas. The dark areas appear smoother having smaller pores than the more open, less dark areas. Bar: 100 μm

4.2 Sample preparation and image acquisition

10x10 mm^2 samples were taken from each paper grade and gold sputtered for 30 sec before visualisation in the SEM, SEI and BEI-mode. Table 4.1 presents the operation parameters used during image acquisition.

4.3 Image processing and analysis

Image analysis routines were developed in order to segment and characterise the coating surface. The segmentation was based on thresholding greyscale histograms. The segmented binary images were then filtered with an "eroding" filter in order to remove excessive noise as explained in Fig. 4.2 and 4.3.

Table 4.1 SEM conditions during image acquisition in secondary electron imaging (SEI) and backscattered electron imaging (BEI) mode.

	Low magnification	**High magnification images**
SEM-mode used	SEI, BEI	BEI
Magnification	250x	5000x
Accelerating voltage	10 kV	5 kV
Working distance	10 mm	8 mm
Image size	1280x960 $pixels^2$	1280x960 $pixels^2$
Image resolution	0.4 μm/pixel	0.02 μm/pixel

4.3.1 Development of the segmentation method applied to low magnification images

By microscope inspection, "closed" and "open" areas can easily be observed. They are also observed in SEM micrographs, where the closed areas seem to be smoother, having lower surface porosity than the open areas. The compact closed areas have less specific surface available for electron emission. Fewer electrons being captured by the secondary electron detector may cause the darker grey area level, characteristic for these areas (Fig. 4.1).

If not performed with caution, any kind of image processing and analysis may lead to significant changes in the numerical data acquisition. Thus, care must be taken in order to find the optimal segmentation procedure avoiding removal of important data. Image analysis routines were developed to automate this part of the process.

The greyscale images were histogram equalised, segmented using automatic thresholding and binarised (Fig. 4.3). The segmented images were then subjected to erosion in order to remove the small noise particles. Binary erosion removes pixels from the edges of a segmented structure. A 3x3 mask (Fig. 4.2, left) was run over each pixel on the image where the regions of interest are black and the background is white. By determining the number of neighbour pixels to be considered if the middle pixel (pixel 5 in the mask) will be removed, it is possible to limit the degree of pixel removal from the edges. Choosing a limit of 8

neighbour pixels will only remove single noise particles (1 pixel size) contributing little to the image segmentation. Reducing the neighbour pixel limit increases the erosion of the edges and thus reduces the remaining region of interest in the image, as exemplified in Fig. 4.2 (right).

The erosion parameters used in Fig. 4.3, like the number of surrounding neighbour (white) pixels and the number of iterations were found based on Fig 4.2. An erosion filter with limit 5 and 20 iterations was found to be suitable and is used in our study.

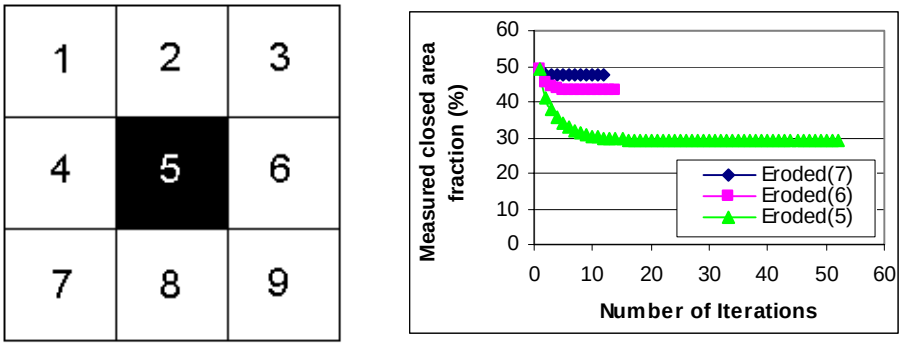

Figure 4.2 Left: 3x3 mask exemplifying the 8 neighbour pixels and the middle pixel (pixel 5). Right: closed area measurement after using erosion filters with three different numbers of neighbour-pixel limits (given by parenthesis in the legend).

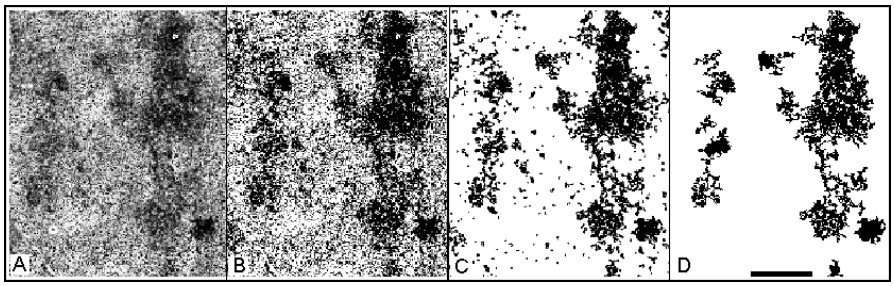

Figure 4.3 Segmentation procedure of closed areas on images of LWC paper surfaces. A) Original equalised image reflecting differences in topography, B) thresholded image, C) the same area after running erosion filter with limit 5 and 20 iterations and D) noisy particles smaller than 100 pixels have been removed. Bar: 50 μm.

4.3.2 Assessment of pore details on closed and open areas

As explained above, topographical information may be gained from secondary electron images. However, backscattered electron images may also contribute to the surface characterisation by improving the surface pore visualisation in high magnification micrographs (see Fig. 4.4) and further quantification. Parameters such as pore area fraction, pore shape and size may be easily quantified on the segmented images.

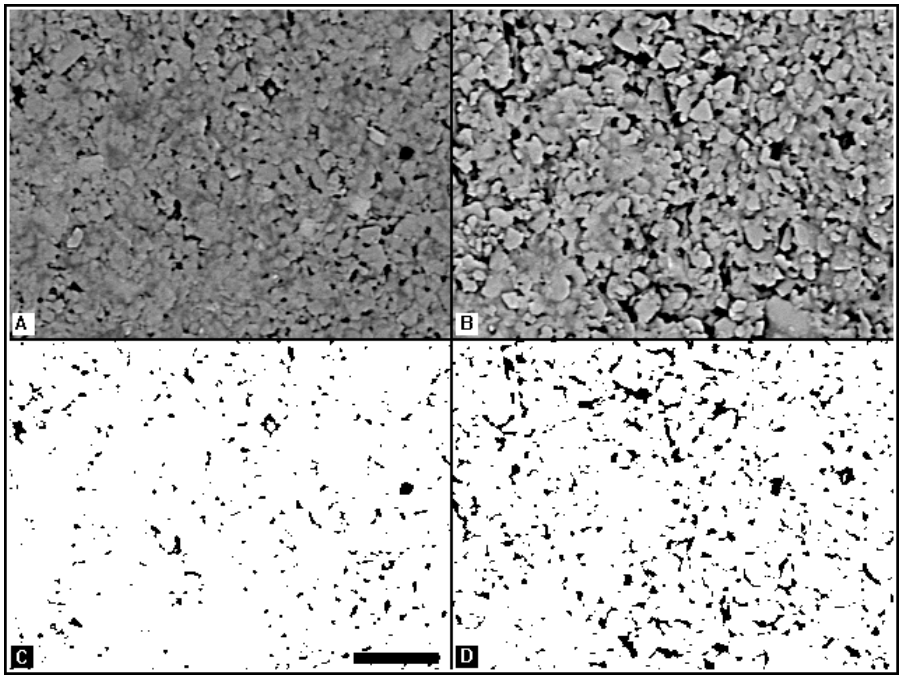

Figure 4.4 A) and B): Backscattered electron images of closed and open areas resp. C) and D) Surface pore segmentation based on the images shown in A) and B). Bar: 5 μm.

The surface pore segmentation exemplified in Fig. 4.4C and D is based on the same routine developed to segment closed areas on the paper surface. In order to enhance the segmentation procedure the first threshold value was subtracted from the histogram and the resulting image was thresholded again. For low contrast images, as is the case with extreme closed areas (Fig. 4.5A), an extra subtraction of the threshold value may be required, otherwise the pore area fraction may be over estimated (Fig. 4.5B). After thresholding and binarisation a erosion filter was run over the images. 10 iterations and a neighbour pixel limit of 6 seems to be enough for removing most of the noise particles (Fig. 4.5C).

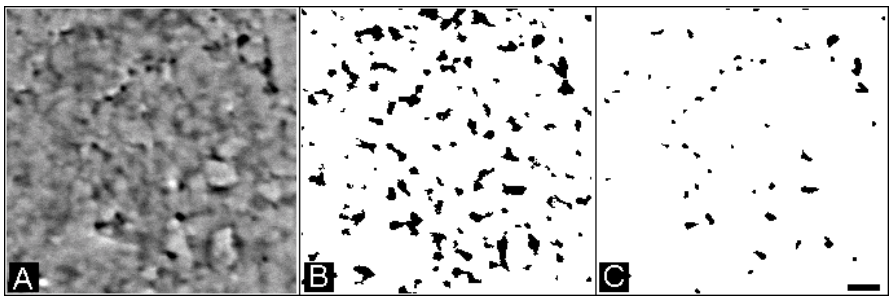

Figure 4.5 Pore segmentation on low-contrast images. A) Original low-contrast image of a region from the closed areas. B) Pore segmentation by subtracting the first threshold value. C) The same image after subtracting the second threshold value. Bar: 1 μm.

4.3.3 Paper coating coverage

Low-magnification images in BEI-mode may also be helpful in studying coverage on the paper surface (see. e.g. Kartovaara, 1989, Dickson et al., 2000). However, the information gained from such images depends on the penetration depth of the electron beam (see Fig. 4.6). 10 kV accelerating voltage seems to be suitable for coverage characterisation and may represent information from some 0.5 μm of the uppermost part of the coating layer (see e.g. Helle and Johnsen, 1994; Allem, 1998).

The same procedure used to segment the surface pores in high magnification images was used to segment the low magnification images having areas with little coverage (Fig. 4.7).

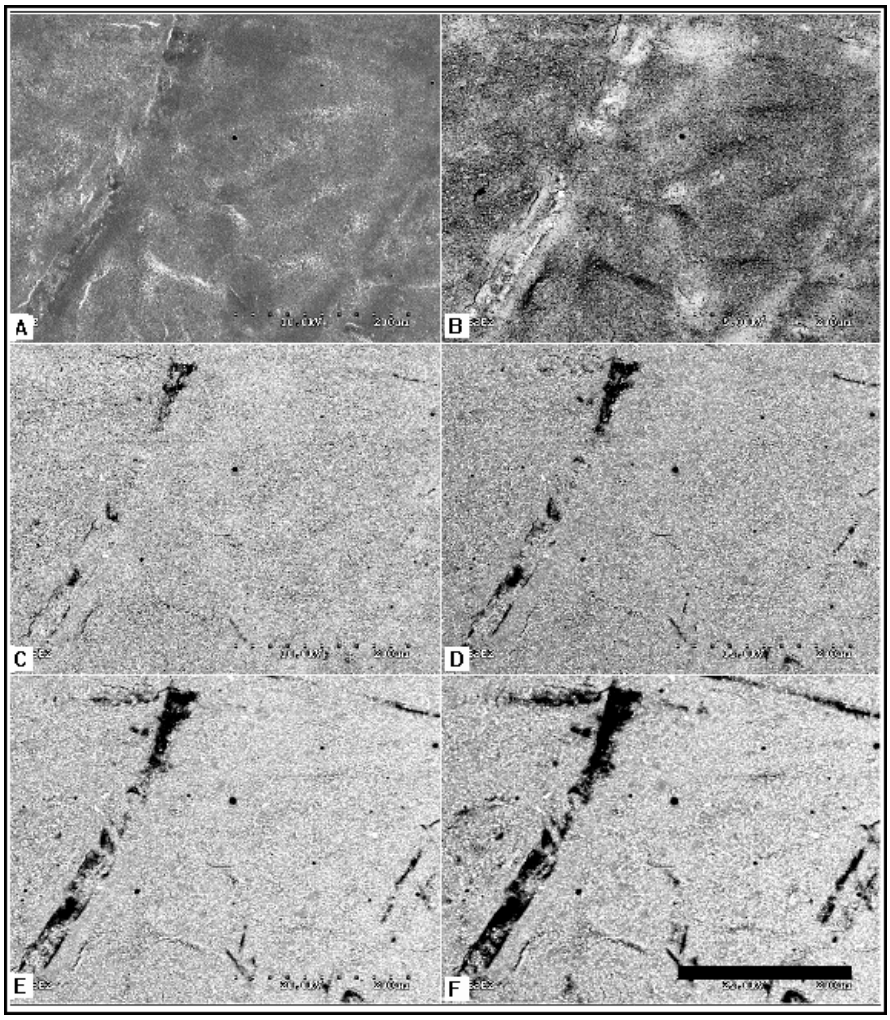

Figure 4.6 A) Secondary electron image showing surface variations. B)-F) Images showing the same area, taken in BEI-mode with raising accelerating voltage: 5, 10, 15, 20 and 25 kV resp. Note the gradually emerging fibres when raising the accelerating voltage. Bar: 200 μm.

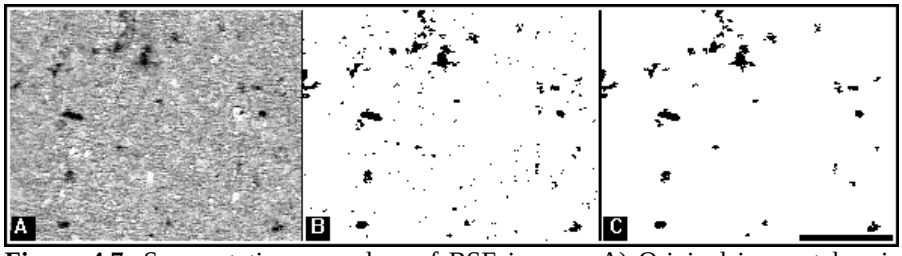

Figure 4.7 Segmentation procedure of BSE images. A) Original image taken in BEI-mode at 250x magnification and 10 kV. B) The same image after thresholding, and erosion. C) Particles smaller than 20 pixels have been removed by automatic filtering. Bar 50 μm.

4.4 Stereo Images

The use of stereo images for structure visualisation and analysis has been amply proven (see e.g. Gregersen et al., 1994; Helle and Johnsen, 1994; Reme and Kure, 2000). Stereo images of the paper surface were also obtained in order to explore their characteristic differences in roughness and surface structure. The SEM parameters used during image acquisition are summarised in Table 4.2. To create a stereo image two images from the same area were acquired using 0 resp. 10º tilt angle. The images were then calibrated and processed by the image analysis system AnalySIS (Soft Imaging System). Even height differences profiles from the paper surface may be obtained with the available computer program being a powerful tool for surface data acquisition (Fig. 4.8).

Table 4.2 SEM parameters used during the acquisition of stereo images.

Signal	Vacuum-mode	Accelerating voltage (kV)	Working distance (mm)	Magnification	Resolution (µm/pixel)
SEI	Low	10	10	3000	0,03

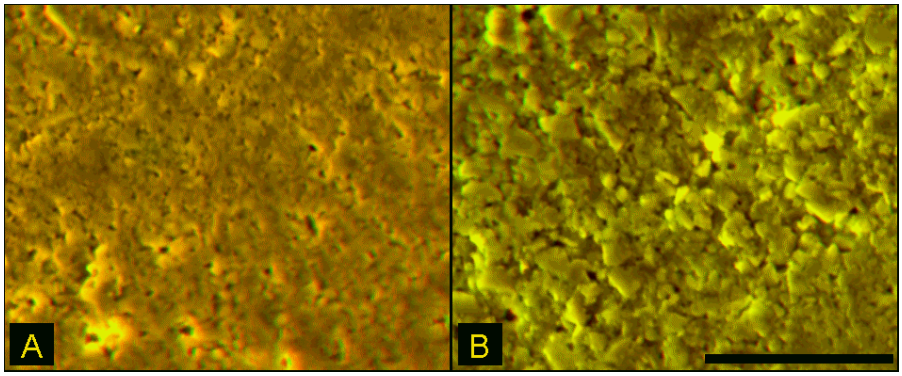

Figure 4.8 Stereo images of closed (A) and open (B) areas taken from the same paper sample surface. Note the differences in roughness and apparent porosity. Red-green glasses should be used for visualisation. Bar: 10 µm.

CHAPTER

5

STAINING WITH OsO_4 AS A MEANS TO EXPLORE PAPER COATING STRUCTURE (PAPER I)

G. Chinga
Department of Chemical Engineering
Norwegian University of Science and Technology (NTNU)
N-7491 Trondheim
Norway
e-mail: gary.chinga@pfi.no

T. Helle
Department of Chemical Engineering
Norwegian University of Science and Technology (NTNU)
N-7491 Trondheim
Norway
e-mail: torbjorn.helle@pfi.no

Submitted for publication in Paperi ja puu.

Abstract

The void volume (pore) fraction and the surface roughness of the coating layer are two factors that critically affects the interaction between printing inks and coated paper surface. The assessment, study and characterisation of these factors may be accomplished by microscopy and image analysis techniques. To discern the binder in the coating layer from the embedding epoxy and thus observe each pore in the coating, the binder has to be stained before the embedding. In the study, osmium tetroxide (OsO_4) was used to stain the latex binder in the coating layer. Morphometric analyses of paper cross-sections using SEM, BEI-mode images and stereo images were used to quantify the paper coating structure details. The smallest details to be quantified are approaching the limitations given by the imaging methods. Nevertheless, it was shown that the procedures allow a quite accurate determination of pore fraction in the coating, and individual readings of the pores like pore area, aspect ratio and orientation. The two compared stained methods differed somewhat in their effect on the paper. OsO_4 dissolved in water gave good staining throughout the base paper/coating sandwich, allowing good visualisation and assessment of the coating structure. However, the moisture tends to make the base paper fibre expand, raising the paper thickness and thus the macro-roughness. When staining by dry OsO_4 crystals, the base paper expansion was avoided, however, even the staining of the fibres was reduced. Critical coating parameters like mean pore area and micro-roughness of the coating layer did not differ between the two methods.

Keywords: Staining, Image analysis, SEM, Paper coating, Porosity, Surface roughness.

5.1 Introduction

5.1.1 Coated paper structure

Pigment coated paper has two main parts; the base paper and the coating layer. Most base paper contains both chemical and mechanical pulp fibres. They will even contain fillers, i.e., pigment powders used to e.g. raise opacity and brightness. The coating contains high quality pigment particles and binders. The particles, like clay, calcium carbonate and titanium dioxide differ in size and shape, consequently affecting the forming of pores during the consolidation of the coating layer on the base paper. Furthermore, the coating layer's pore volume fraction and the surface roughness affect the interaction between printing inks and the paper. Thus, how well a coated paper sheet will reproduce images when printed depends on the uniformity and the surface characteristics like roughness, pigment particle orientation and porosity of the coating layer.

It is customary to distinguish between two kinds of surface roughness; micro-roughness mainly affected by pigment particles and macro-roughness mainly due to variations of the base paper. Proper characterisation of these parameters will be of major importance for predicting the printing ink behaviour in printing. The assessment, study and characterisation of the mentioned factors may be accomplished by means of microscopy and image analysis techniques /1/.

To analyse the size and shape of pores in the coating layer, the resolution of optical microscopes is not sufficient. Besides, the presence of hard mineral particles in the coating layer will obscure the microtoming of the paper sample. On the other hand, grinding of paper cross sections, embedded in epoxy with subsequent curing, leaves a cross section suited for SEM, backscattered electron imaging (BEI). In SEM, BEI-mode, the brightness increases with the average atomic number of the imaged components. The epoxy and the coating binders differ too little in atomic weight to be properly discerned unless the binder has been tagged by some high-atomic weight element, like osmium. To observe the coating pores, one thus has to stain the binder material before embedding. OsO_4 may be a suited material for such a staining.

5.1.2 OsO_4 staining

Several techniques have been used to enhance and improve the visualisation of paper and fibre structures for SEM, BEI-mode. Potassium Permanganate ($KMnO_4$) has been used in the study of lignin components in wood and pulp fibres /2/. Bromine is used in staining and studying of lignin-containing structures /2/. Forseth et al. /3/ applied this technique to study the effect of moisture on paper roughening.

Osmium tetroxide (OsO_4) is widely used in biological sample preparation to preserve and fixate cell structures for further visualisation in electron microscopy. The chemical forms cross-linked complexes with C=C double bonds. Such bonds are present in latex which is used to bind pigment particles in coating. Examples of such latex components are butadiene and styrene. Thus, an improved visualisation of the pore structure is obtained by staining the latex films with OsO_4. The latex

films will then appear brighter and may be clearly discerned from the epoxy resin used for embedding the paper samples. This improves the final visualisation of the pore structure, allowing quantification of pore details. Image analysis of micrographs of OsO_4-stained paper sample cross-sections may thus offer an interesting way of assessing the pore structure of coating layers.

A few researchers have reported the use of OsO_4 staining applied to paper studies. Mechanical pulp fibres, binders /4,5,6,7/ and printing inks /8/ are reported to be stained by this chemical to facilitate the characterisation of paper structure. According to McCoy /4/ OsO_4 will also stiffen the base sheet fibres, thus improving the sample polishing process. However, it is essential to do the staining in a way that does not change the coating structure. Some of the reported techniques may be questionable in this respect.

McCoy /4/ used 1g of OsO_4 crystals to vapour-stain styrene-butadiene latex in coated paper. The author reported good staining of the latex material in the coating. Rissa et al. /5/ used dissolved OsO_4 in water to stain the latex of clay coatings in order to characterise the morphology of the coating structure based on SEM, BEI-mode cross-section images. In another study, OsO_4-staining was used to obtain visualisation of talc pigment particles allowing particle orientation to be assessed by image analysis /6/.

Whalen-Shaw and Eby /9/ applied OsO_4 to study binder concentration variation at the coating layer surface and its possible effect on the print quality defect termed “backtrap mottle”. Higher binder concentration was found on areas with low ink density.

No comparative study of the staining methods utilising OsO_4 has been published. Besides, when staining, the binders and pigments can be discerned, leaving the actual pore voids to be analysed, as a total volume fraction and in details. Despite this fact, the real pore structure has not been quantified. The purpose of the present study is to analyse and compare the effect the different OsO_4-staining procedures on coated paper structure. In order to quantify important pore details this point is critical for judging the reliability of the morphometric results by image analysis of stained paper samples.

5.2 Materials and methods

5.2.1 Paper sample description

The paper used in this study had been commercially coated with a pigment mix of 70% ground calcium carbonate (GCC), 30% kaolin (clay) (90% <2μm). The binder had 11 parts styrene-butadiene latex and 0.25 parts CMC per 100 parts of pigment. The coat-weight was 11.0 g/m^2 on the top side and 12.0 g/m^2 on the wire side of the paper. The paper was stiff blade coated at 1300 m/min. The paper grade was calendered on a 12 nip supercalender applying a linear load of ~300kN/m, at 800m/min.

5.2.2 OsO_4 staining and paper sample preparation

2x1 cm^2 paper samples were used. The samples were divided into 4 groups to compare the characteristics of the staining procedures listed in Table 1. The procedures A and B involves OsO_4, procedure C water vapour only and D was used as the control sample without staining.

Table 1 Solution and exposure time used in order to stain the paper sample.

Procedure	Staining mix	Reaction time (hrs)
A	100 mg OsO_4 dissolved in H_2O	48
B	1 g OsO_4 in air	48
C	H_2O	48
D	Control	

The paper samples were put into a staining chamber along with the staining mix, without any direct contact. After finished reaction and neutralising the OsO_4, the paper samples were left in the fume hood for another 24 hrs. The temperature in the fume hood was 23°C.

After staining, the paper samples for cross-section analysis were dried at 105°C for 1 hour, then placed vertically in spring holders, evacuated in a vacuum chamber for 15 min and impregnated with epoxy resin (Fig. 1). After curing, the blocks were ground, using 320 grit abrasive paper, removing approximately 1 mm from the block surface. The blocks were then placed in an automatic STRUERS RotoForce-4 and polished in a STRUERS RotoPol-22 for 5 min using abrasive cloths with 9 and 1 μm diamond particles. Applied pressure and speed for polishing were 5N and 150 rpm respectively. The blocks were finally carbon coated.

5.2.3 Image acquisition and analysis

For comparison, SEM stereo images of paper surfaces were taken before and after staining. The surface and cross-section images were obtained using a Hitachi S-3000 VPSEM as explained in Table 2.

The stereo images were calibrated and processed by the image analysis system AnalySIS (Soft Imaging System). The Scion Image program was applied for image processing and analysis of the SEM, cross-section images. The Scion Image program is available at http://www.scioncorp.com. Several routines were written to automate the Image program in the morphometric analysis.

Table 2 SEM parameters used during the acquisition of surface and cross-section images.

Images	Signal	Vacuum-mode	Accelerating voltage (kV)	Working distance (mm)	Magnification	Resolution (μm/pixel)
Surface (stereo)	BEI*	Low	10	10	3000	0.03
Cross-section	BEI	High	5	8	250 1000 5000	0.4 0.1 0.02

BEI* - The backscatter electron detector was applied in 3D-mode.

After thresholding and binarising the images, the void or pore characteristics was measured and described by e.g. pore size, an aspect ratio factor (AR) and pore orientation relative to the paper surface. The pore orientation and aspect ratio are calculated using a best fitting ellipse on every pore, yielding the minor and major axis of the corresponding ellipse. The angle between the major axis and a horizontal reference line (the paper plane) yields the orientation of the individual pores. The aspect ratio is obtained by dividing the major by the minor axis on the corresponding ellipse. Even the pore area fraction was calculated by determining the total area comprised by the pores relative to a predefined region in the cross-section image.

The roughness value is based on measuring lines from the top of the image to the surface of the paper sample. Parameters such as the mean square root (Rq) and the arithmetic average (Ra) may be obtained according to the ISO 4287/2000 standard. For details about image measurements see Chinga and Helle /1/.

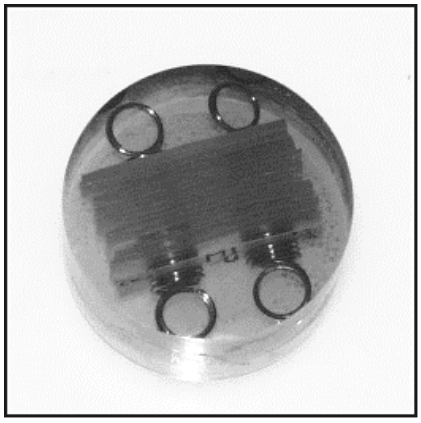

Figure 1 Paper samples placed in spring holders and embedded in epoxy resin for SEM analysis.

5.3 Results

5.3.1 Qualitative assessment of the paper structure

Fig. 2 depicts three micrographs from the paper samples described in Table 1. The OsO_4 reaction is observed in the stained samples (A and B). Here, the coating binder appears bright, whereas the black areas are epoxy filled voids or pores. On the other hand, in the unstained sample (Fig. 2c), the pigment particles only are clearly visualised, the binder however appears dark and can not be discerned from the epoxy filled voids. Due to the high atomic weight of the osmium, the structures reacted with OsO_4 get a lighter grey shade on the backscattered electron images. Thus, the latex binder, distributed throughout the coating layer surrounding the pigment particles, appears as light areas (Fig. 2a, right side). Besides latex, even the lignin of the base paper's fibres reacts strongly with the OsO_4. Apparently, the lighter fibre cross-sections seen from procedure A proves a larger degree of staining on the lignin containing structures, than can be see from procedure B.

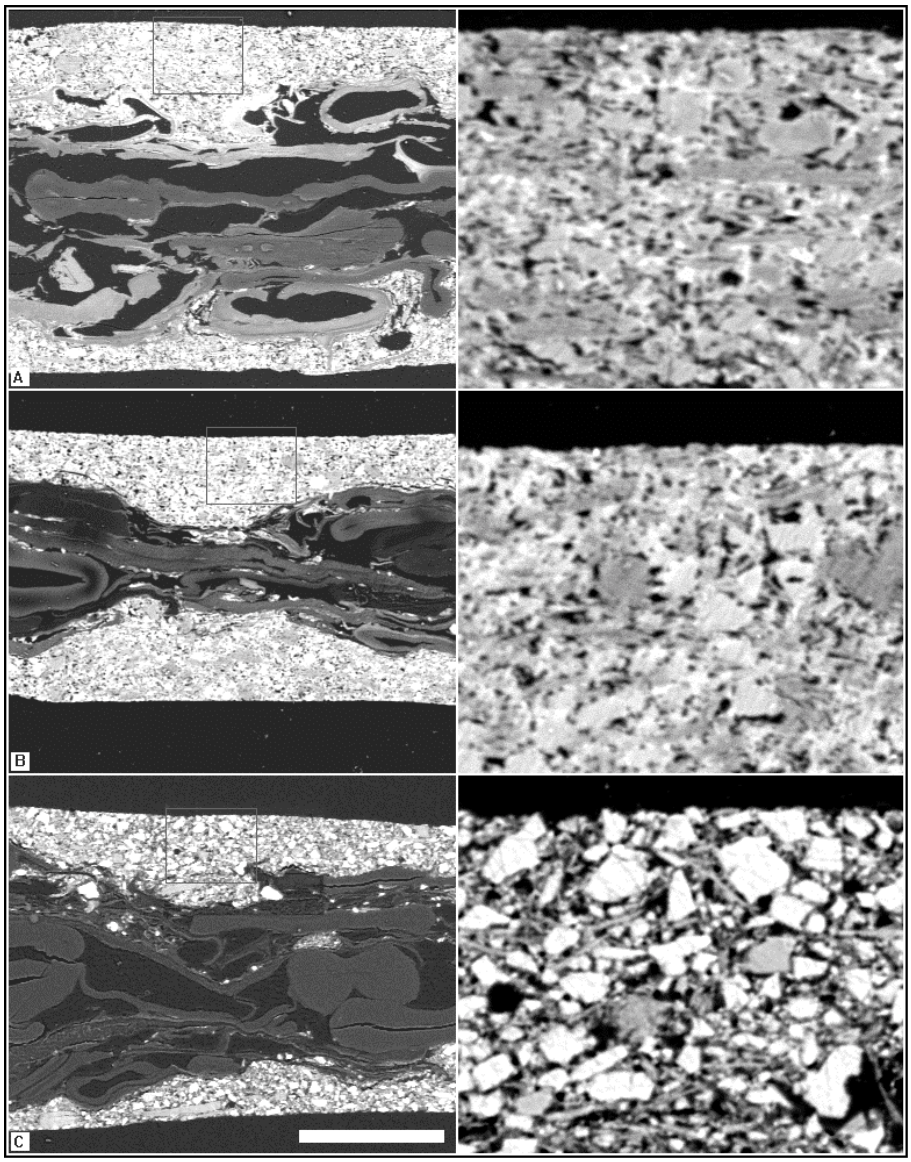

Figure 2 Cross-section images of the paper samples stained by procedure A, B and C of Table 1 respectively. Images on the right side are taken with 5000x magnification and show details of the regions marked on the left side respectively. Note the bright latex material around the pigment particles of A and B. Bar: 25 μm for 1000x magnification images (left side) and 5 μm for 5000x magnification images (right side).

5.3.2 Quantification of surface micro-roughening on stereo images

Stereo images of the paper surface are suitable for assessment of the small scale paper surface topography variations. This technique was used to explore possible differences in surface structural changes induced by the staining procedures. Stereo

images of the same region were made before and after the reaction (Fig. 3). Height differences on specific regions on the paper surface were measured (Fig. 3 and 4).

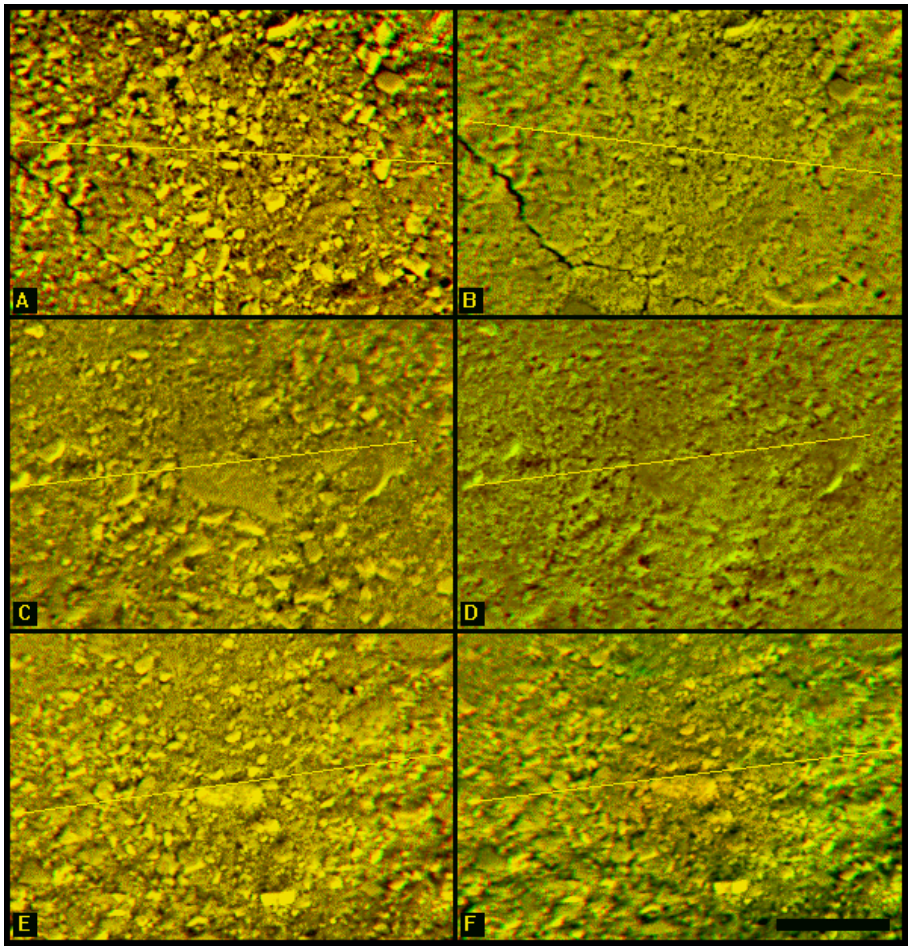

Figure 3 Stereo images of the analysed samples. Left column: Micrographs taken before staining treatment. Right column: Same surface area, after staining treatment. The bright line across the micrographs indicates the line along which the height measurements were made. A) and C) correspond to the staining procedures A and B respectively. E) and F) depict the sample before and after H_2O-vapour exposure (procedure C). Red-green glasses should be used for visualisation. Bar: 10 μm.

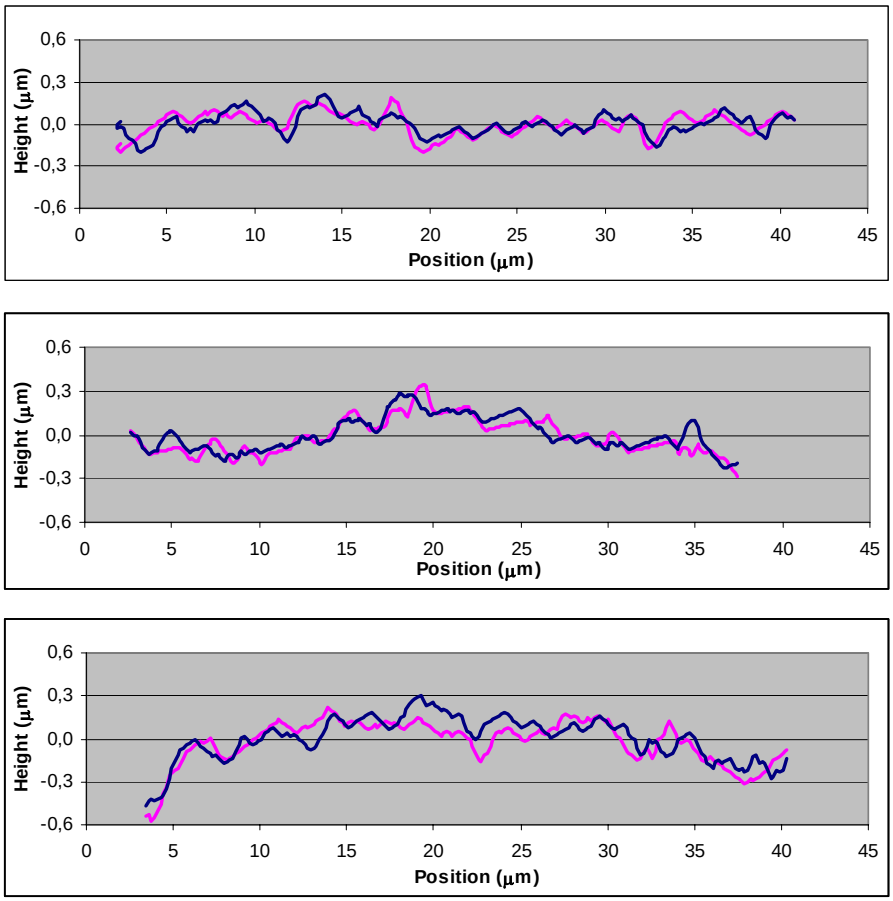

Figure 4 Height differences measured using the stereo images shown in Fig. 3. Top, middle and bottom figures correspond to sample A, B and C respectively (Table 1). The blue and red curves correspond to the measurements taken before and after the reaction as described in Fig. 3.

5.3.3 Quantification of structure details on cross-section images

In the evaluation of the different staining procedures, it is important to compare the effects on paper characteristics being essential to paper's end-use properties. Several important parameters were therefore measured on the cross-section images to assess the effect by the OsO_4 staining on the paper structure. Total pore volume, along with parameters like mean pore area, pore orientation, shape and surface roughness were measured. The quantification of the listed parameters may be important for understanding the influence by different process variables on paper quality and also to predict the paper/printing ink interaction. Fig. 5 compares the obtained results with respect to coating layer pore and surface details for samples stained by procedure A, B, C and D. Fig. 6 compares the pore area fraction whereas the paper thickness and the surface macro-roughness is given in Fig. 7.

Estimation of the latex binder volume fraction may be performed taking into consideration the pore area fraction before and after the OsO_4-treatment,

$$\text{latex volume fraction (\%)} = A_b - A_a \qquad \text{(I)}$$

where A_b denotes the apparent pore area fraction before OsO_4-treatment and A_a the area fraction after OsO_4-treatment. The calculation, based on samples A and B relative to the control sample D, yields a latex area (volume) fraction of 20 and 19 % resp. This is in well agreement with the known latex volume fraction in the coating layer, as calculated in Table 3.

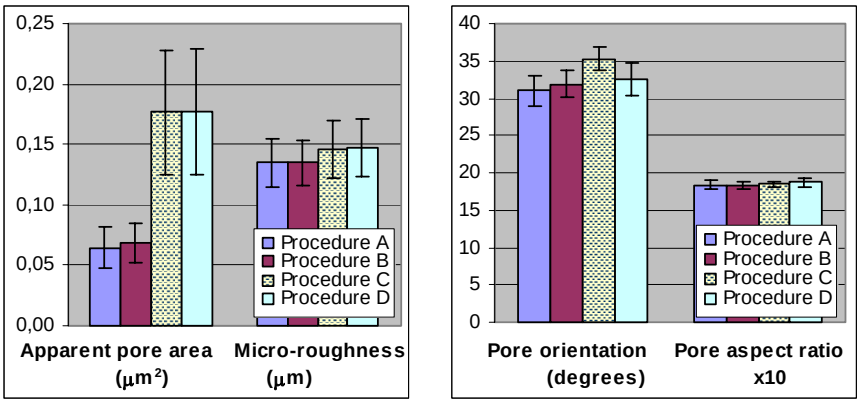

Figure 5 Structure details measured on paper samples, procedure A,B,C and D. Left: Mean pore area and surface micro-roughness. Note that the apparent pore area fraction of samples C and D includes both the real pore structure and the binders. Right: Coating layer pore orientation and aspect ratio. The pore orientation is given in degrees relative to a horizontal reference line.

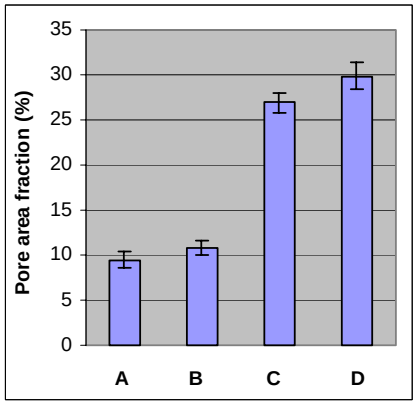

Figure 6 Apparent pore area fraction (pore volume) throughout the coating layer on the four analysed samples. Note that the apparent pore area fraction of samples C and D includes both the real pore structure and the binders.

Table 3 Comparison of the calculated latex volume fraction based on known specifications (supplier information) with the estimates obtained from the cross-sectional image analysis.

	pph	Density * (kg/dm^3)	Component volume (dm^3/kg)	Calculated volume fraction (%)	Measured cross-sectional area fraction (%)	
					Proc. A	Proc.B
Piment particles	100	2.5	40	78	80	81
Latex	11	1.0	11	22	20	19

(*) Values obtained from Lehtinen /10/.

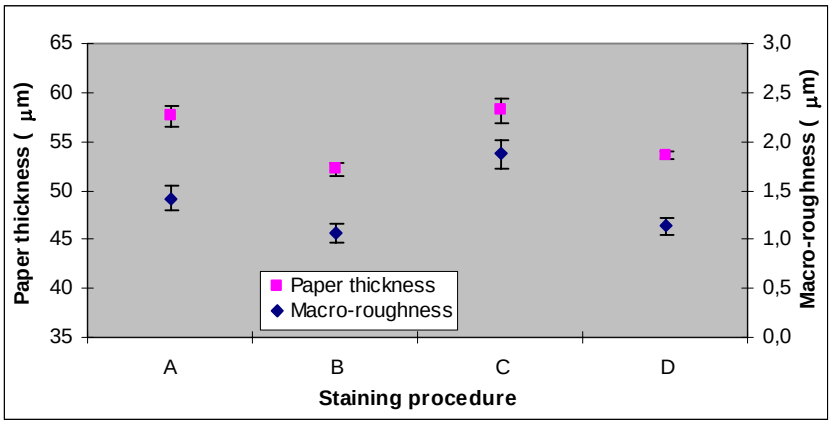

Figure 7 Paper thickness and macro-roughness (Rq) measured on cross-section images taken at 250x.

5.4 Discussion

The results obtained during this study confirm an effective reaction of OsO_4 with material components like mechanical pulp fibres and latex binders for pigment coated paper. The reaction of the binder allows SEM backscattered electron imaging with sufficient resolution to discern details of the small pores to be analysed. Pore details like mean pore area, pore orientation and aspect ratio are quantified.

With respect to the two staining methods that are compared, OsO_4 dissolved in water (procedure A) causes the best staining of the combined coating/base paper structure (see Fig. 2). Unfortunately, although the paper samples are not in direct contact with water, the humidity in the sealed containers causes a swelling of the hydroscopic pulp fibres, inducing a roughening of the paper surface. Analysis of the samples suggests that the moisture causes an expansion of the base paper

raising its surface roughness (Fig. 6). The base paper expansion is caused by moisture induced release of stresses in the fibres, created by the paper calendering, as explained by Forseth and Helle /3/. In this expansion, compressed mechanical pulp fibres recover their tube-like shape. It should be mentioned, that a base paper made from bleached pulp only, is likely to reveal much less expansion.

In the dry procedure B, using crystalline OsO_4 only, no water- induced expansion of the base paper occurs, yielding a paper with less macro-roughening than procedure A. On the other hand, the base paper appears to be less reacted by this procedure. This may be due to the low vapour pressure of OsO_4. The absence of the macro-roughening will be of importance when the whole coating/base paper sandwich is under study. Procedure B may possibly be improved by heating the sealed container.

The more through reaction by procedure A may be explained as a result of the H_2O's polarity. Water has a great ability to dissolve compounds, increasing the number of OsO_4 surface molecules and hence the evaporation rate. The solution mix (A) facilitates the evaporation of OsO_4 molecules, easing the reaction with the paper structure and improving the image quality.

With respect to the effects of the staining methods on the micro-roughness of the coating surface, and the coating pore details, methods A and B appear to be more or less equivalent (Figs. 3-5), A possibly having somewhat better image quality. Where only the coating layer is under study, either method may be recommended. Where even the base paper has to be considered, procedure B should be preferred.

Considering the interesting potentials offered by OsO_4 staining, the method is likely to become a quite common step in the preparation and analysis of fibres and paper even besides coated grades. The chemical is well-suited for visualisation of lignin-containing structures in the base paper and latex films in the coating structure, thus improving the quantification of parameters like porosity and roughness. However, OsO_4 is highly toxic, hence inhalation, ingestion or direct contact may cause severe damage. Proper precautions must be taken to ensure safety and health.

References

1. Chinga, G., Helle, T.: Structure characterisation of pigment coating layer on paper by scanning electron microscopy and image analysis. Submitted for publication in Nordic Pulp Pap. Res. J., 2001.
2. Gregersen, O.W. et al. Qualitative Methods for the Study of Lignin Distribution in Wood and Surface Layers of Unbleached Pulp Fibres and Paper. J. Pulp Pap. Sci., 21(1995):8, 285-287.
3. Forseth, T., Helle, T.: Effect of moistening on cross-sectional details of calendered paper containing mechanical pulp. J. Pulp Pap. Sci. 23(1997): 3, 95-102.
4. McCoy, J.W.: Metallographic Preparation of Coated Papers for Backscattered Electron Imaging of Coating Structure in Cross-Section. Proceedings from the 1998 Coating/Papermakers Conference, p. 121.

5. Rissa, K., Lepistö, T., Vähä-Nissi, M., Savolainen, A.: Characterization of Pigment and Dispersion Coatings using Atomic Force Microscopy and Scanning Electron Microscopy. Proceedings from the 1999 Microscopy as a Tool in Pulp and Paper Research and Development Symposium, p. 195.
6. Rissa, K., Lepisto, T., Vaha-Nissi, M., Lahti, J., Savolainen, A.: Orientation of talc particles in dispersion coatings. Nordic Pulp Pap. Res. J., 15(2000): 5, 357- 361.
7. Krishnagopalan, A., Simard, G.L.: An improved technique for studying binder migration in coated paper, Tappi J. 12 (1976): 96- 99.
8. Ozaki, Y., Kimura, M.: Visualisation of printing ink vehicle on paper surfaces by a SEM technique, Appita J. 3 (2000): 216-219.
9. Whalen-Shaw, M., Eby, T.: An investigation of factors related to backtrap mottle in coated papers using electron probe microanalysis, Proceedings from the 1991 Tappi Coating Conference and Trade Fair, p. 401.
10. Lehtinen, E.: Pigment coating and sizing of Paper, Fapet Oy, Helsinki 2000, p. 61.

CHAPTER

6

STRUCTURE CHARACTERISATION OF PIGMENT COATING LAYER ON PAPER BY SCANNING ELECTRON MICROSCOPY AND IMAGE ANALYSIS (PAPER II)

G. Chinga
Department of Chemical Engineering
Norwegian University of Science and Technology (NTNU)
N-7491 Trondheim
Norway
e-mail: gary.chinga@pfi.no

T. Helle
Department of Chemical Engineering
Norwegian University of Science and Technology (NTNU)
N-7491 Trondheim
Norway
e-mail: torbjorn.helle@pfi.no

Submitted for publication in Nordic Pulp and Paper Research Journal.

Abstract

The ever rising need for detailed knowledge of the structure of paper coating urges the improvement and development of new techniques for gaining new and valuable information. The scanning electron microscope (SEM) is a most suitable tool for morphometrical studies of fibres and paper. Digital images acquired in a SEM, by the secondary electron imaging (SEI) or backscattered electron imaging (BEI) mode have suitable quality and resolution for further image processing and analysis. However, to discern the binder in the coating layer from the embedding epoxy and thus observe each pore in the coating, the binder has to be stained before the embedding. In the study, osmium tetroxide (OsO_4) was used to stain the latex binder. The present study exemplifies how microscopy and image analysis can be applied in structural studies of the coating layer. Image processing and analysis routines for acquiring information on the coating layer surface roughness and porosity details like the pore shape, size and orientation are described. A routine, based on the Sobel operators, for measuring the pigment particle orientation, is also described. The developed semi-automatic image analysis routines are useful methods for morphometric analysis of paper structure details, thus facilitating numerical data acquisition of the pores and the pigment particles' geometry. Part of the obtained information is assumed to be unattainable by other methods at this point.

Keywords : SEM, image analysis, coating structure, porosity, particle orientation.

6.1 Introduction

As quality demands on paper and print are rising, better knowledge and understanding of the coating layer structure details and its interactions with printing inks is imperative. The coating layer has a complex structure, pigment particles and binders separated by air-filled voids. These components establish the layer's micro-characteristics, and thus the end-use properties of the paper. It is important to explore how production variables affect coated paper structure. Several methods have been used in such studies (see e.g. Wygan et al., 1995). Image analysis of digital micrographs appears be suitable for numerical data acquisition of surface and internal coating structure details.

The SEM is well suited for morphometrical studies of fibres and paper. Digital images, both based on secondary (SEI) or backscattered electron imaging (BEI) modes are suitable for further image processing and analyses. The SEM may reveal details hardly detectable by other techniques. Several authors used such techniques to study details like paper thickness, roughness and base paper porosity (Peterson and Williams, 1992; Williams and Drummond, 1994; Allem, 1998; Allem and Uesaka, 1999; Dickson, 1999)

6.1.1 Assessment of the coating layer micro-structure

The coating layer's pore structure affects decisively the printing ink absorption. However, the pore details cannot be studied directly by BEI on epoxy embedded samples, as the binder material cannot be discerned from the epoxy. Reacting with OsO_4 before embedding may circumvent the problem. Image analysis of OsO_4-stained paper cross-sections allows the exploration of the pore structure. Besides, mechanical pulp fibres, binders (Krishnagopalan and Simard, 1976; MacCoy, 1998; Rissa et al., 1999) and printing inks (Ozaki and Kimura, 2000) may be stained by OsO_4, making paper structure characterisation more effective.

6.1.2 The pore structure of the coating layer

Although techniques for staining binders in the coating layer have been reported, little has been done to quantify the coating's micro-structure details. Most pore structure studies have been based on mercury intrusion methods. However several authors (see e.g. Climpson and Taylor, 1976; Abrams et al.,1996; Wygant et al., 1995) state that mercury porosimetry may have limitations like i) sample compressibility, ii) assumption of interconnected pores and iii) inability of identifying narrow necked voids.

Digital image processing and analysis have been used to study the micro-structure of e.g. grains, graphite and concrete (Janowski et al., 1998; Yang and Buenfeld, 2001; Inagaki and Suwa, 2001). Parameters like pore area fraction, distribution and shape have been quantified. The quantification requires segmenting the regions of interest. Hence, segmentation is essential in image analysis, being critical for further quantification of the parameters. Segmentation based on thresholding greyscale histograms of digital images is a common approach. However, manual thresholding will vary between operators and even for one person over time (Russ, 1999). This has been repeatedly demonstrated (see e.g. Tovey and Hounslow, 1995; Barratte et al., 1997). Although segmentation methods may vary in different

applications, one should find objective, reliable and reproducible methods. Procedure automation is thus important to reduce subjectivity and laborious work.

6.1.3 Pigment particle orientation

Coating pigment particle orientation is an important parameter. Besides affecting gloss and light scattering, particle orientation affect the runnability at the blade (Gane and Watters, 1989); the packing of the coating, and thus the porosity and barrier properties (Rissa et al., 2000). X-ray diffraction (XRD) techniques are used to assess clay particle orientation (Gane et al., 1995). Rissa et al. (2000) measured talc pigment particles' orientation by X-ray diffraction, comparing the results with manual image analysis assessments. Semi-automatic image analysis was not applied due to touching edges of adjacent particles. Albeit good correlation, manual procedure is tedious and time consuming. XRD is also limited to comparative studies of pigment particles having similar crystallinity (Elton et al., 1999).

The coating layer presents a complex structure in backscatter electron (BSE) images, due to its many components. Digital images have, however, a greyscale variation suited to detect edges in between particles and at particles/voids interfaces. Detection of edges depends on the grey-level variations in digital images. Two regions having different grey-level may have boundaries detectable using horizontal and vertical masks (for details see Gonzalez and Woods, 1993). Here, the Sobel operators are useful (see e.g. Davies and Celano, 1993; Gadala-Maria and Parsi, 1993). This operator seems to be applicable for calculating pigment particle orientation.

This study aims at describing improved and new techniques within microscopy and image analysis for the characterisation of important coating structure details. Automation of image analysis techniques is described in detail. Such automation improves numerical data acquisition and reduces the involvement of operators and hence subjective assessments. The quantified paper characteristics are surface smoothness and coating layer pore details like area, shape and orientation as well as particle orientation.

6.2 Materials and methods

The studied paper was a commercially coated grade with a pigment formulation of 70% GCC, 30% clay (90% <2μm). The binder contained 11 parts styrene-butadiene latex and 0.25 parts CMC, based on 100 parts of pigments. The coat-weight was 11.0 g/m^2 on the top-side and 12.0 g/m^2 on the wire side. The paper was coated with a stiff blade at 1300 m/min. and calendered in a 12 nip supercalender using a line load of ~300kN/m at 800m/min.

6.2.1 Sample Preparation

The samples were stained by Osmium tetroxide (OsO_4) before embedding in epoxy resin (see Chinga and Helle, 2001). After staining, the samples were dried at 105 ºC for 1 hour. After being in a vacuum chamber for 15 min, the samples were impregnated with epoxy. Cured blocks were ground hand-held, using 320 grit abrasive paper, removing some 1mm from the block surface, then put in a STRUERS RotoForce-4 and polished in a STRUERS RotoPol-22 using abrasive

cloths with 9 and 1 μm diamond particles, using pressure and speed, 5 N and 150 rpm respectively. The blocks were dried between the grinding and polishing to avoid cracks in the coating layer. The blocks were finally carbon coated to become conductive.

6.2.2 Image acquisition and analysis

Images were obtained by a Hitachi S-3000 VPSEM. BSE images were generated using 5kV accelerating voltage, 8-10 mm working distance and 5000x magnification. The size of the digital images was 1280x960 pixels using 256 grey levels. The resolution was 0.02 μm/pixel for high magnification images. The segmentation was accomplished by thresholding the greyscale histogram as explained by Ridler and Calvard (1978). The optimum threshold is obtained automatically by an iterative procedure, consisting in finding the middle between tops corresponding to two different structures in the paper samples cross-sections. For the image processing and analysis of the SEM images the Scion Image program was used, available on the Internet at http://www.scioncorp.com. Several routines were written to automate the Image program for use in the morphometric analysis.

6.3 Results

6.3.1 Backscattered electron images of paper cross-sections

High quality BEI requires samples with smooth and distortion free surfaces, being well met by the applied technique. The embedding epoxy appears black, the base paper fibres grey. Mechanical pulp fibres are brighter than chemical pulp fibres, as OsO_4 reacts with lignin (Fig. 1). In high magnification micrographs, the OsO_4 reaction allows the light grey binder to be discerned from the black epoxy and the grey pigments (Fig. 1 and 2). For printed samples, gold sputtering before epoxy embedding establishes a border layer between the printing ink and the epoxy, allowing the darker layer of printing ink to be observed (Fig. 1B).

6.3.2 The pore details of the coating layer assessed on high magnification images

Image analysis of the high magnification images allows assessment of additional details (Fig. 2). Prior to thresholding, a median filter was applied to remove noise. Pores may be segmented as shown in Fig. 2B. The threshold value to convert the greyscale image to binary is found automatically only for images with a well-balanced contrast. To minimise subjective segmentation in the definition of the surface, a routine was written to scan the surface with a “rolling” sphere (Fig. 2D) and close the pore openings, Fig. 2E. The sphere’s diameter may be chosen at will. The pores may be characterised inside a predefined area, by e.g. the aspect ratio (AR), pore minor axis, orientation relative to the paper surface and size (Fig. 2F). Pore orientation and aspect ratio are calculated using a best fitting ellipse on every pore. The orientation is calculated as the angle between the major ellipse axis and a horizontal reference line, Fig. 2F. The pore’s AR is the ellipse’s major/minor axis ratio. Some readings of the numerated pores in Fig. 2E are given in Table 1. Even

the pore area fraction distribution was calculated, giving the pore area fraction (average porosity) throughout 10 layers from surface to bottom (Fig. 3).

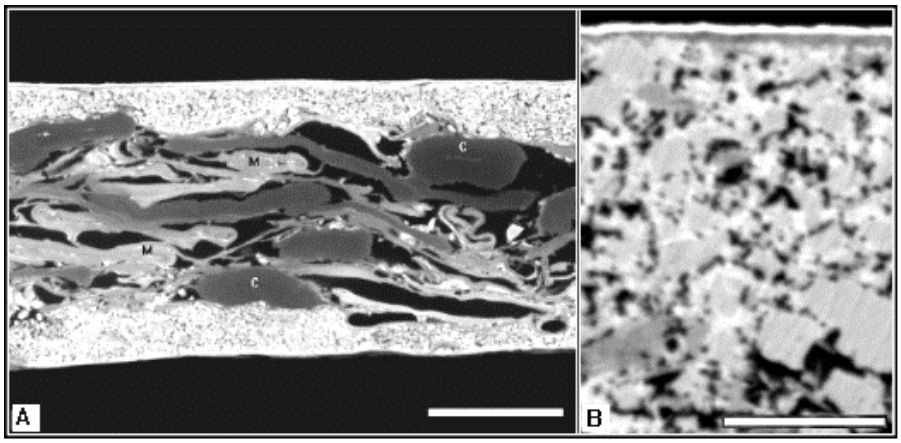

Figure 1 BSE images of coated paper reacted with OsO_4. ***A)*** Mechanical pulp fibres (**M**), and chemical pulp fibres (**C**) can be distinguished in the low-magnification image (Bar: 25μm). ***B)*** High magnification image of the coating layer. *Top:* Gold sputtering establishes a bright borderline between the (grey) printing ink and the (black) epoxy. *Main part:* The binder films are also observed as bright areas surrounding the (grey) pigment particles and (black) voids, filled with epoxy (Bar: 5 μm).

Table 1 Pore details assessed by image analysis. The numbers refer to the pores numerated in Fig. 2E. The orientation is the ellipse's main axis' in degrees relative to a horizontal reference line.

Pore number	**Area (μm^2)**	**Orientation (degrees)**	**Aspect ratio**
1	0,81	16,3	2,8
2	0,36	16,9	4,5
3	0,23	7,2	3,4
4	0,27	7,8	4,6
5	1,24	25,8	1,2

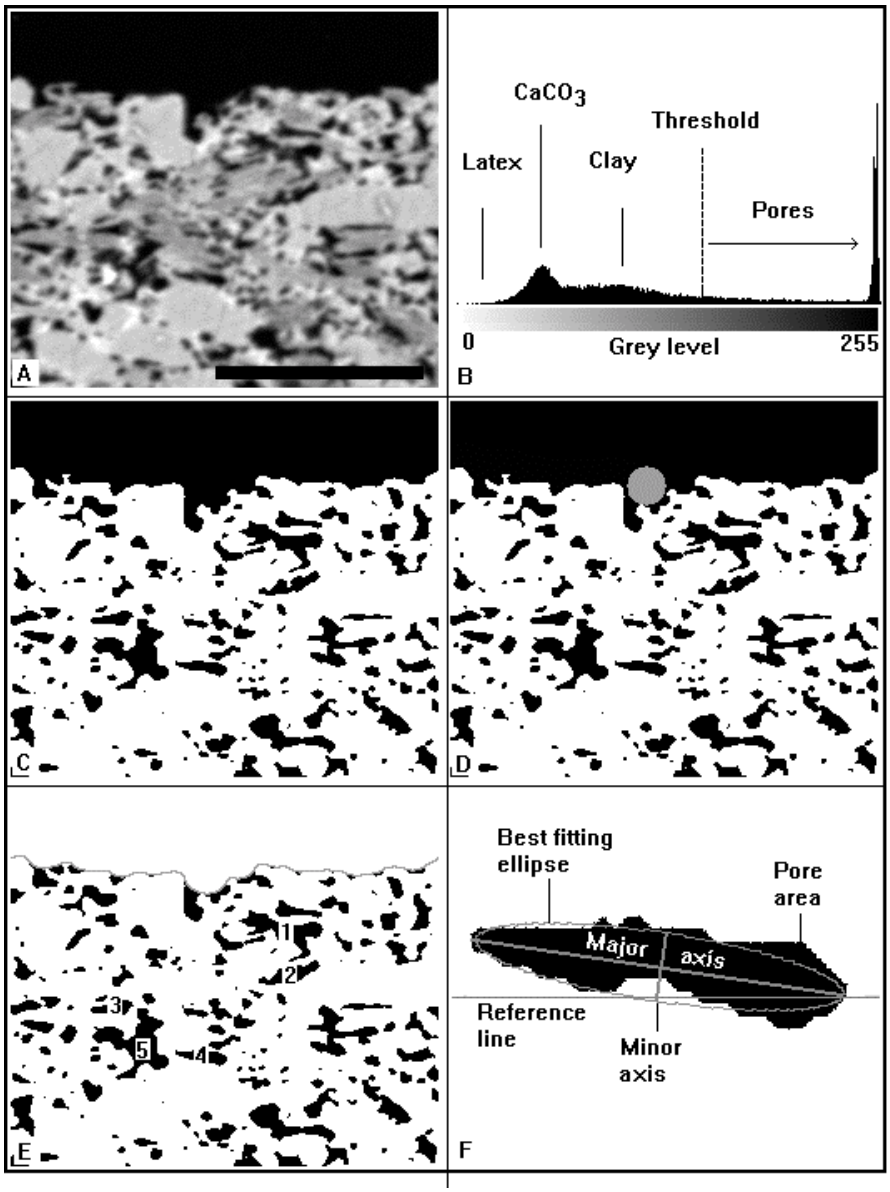

Figure 2 Calculation of characteristic pore details in the coating layer. ***A)*** Original image showing the top coating layer stained with OsO_4. ***B)*** Greyscale histogram showing the different structures visualised in BSE images of the coating layer and the corresponding threshold level for pore segmentation. ***C)*** Segmented image presenting the pore distribution. ***D)*** Sphere used to segment the surface pores. ***E)*** Segmented surface pores. Some pores are numerated for analysis (see Table 1). ***F)*** Details measured on pore number 4 showing the actual area and the major and minor axis used to calculate the orientation and AR of the single pores. Bar in A: 5 μm.

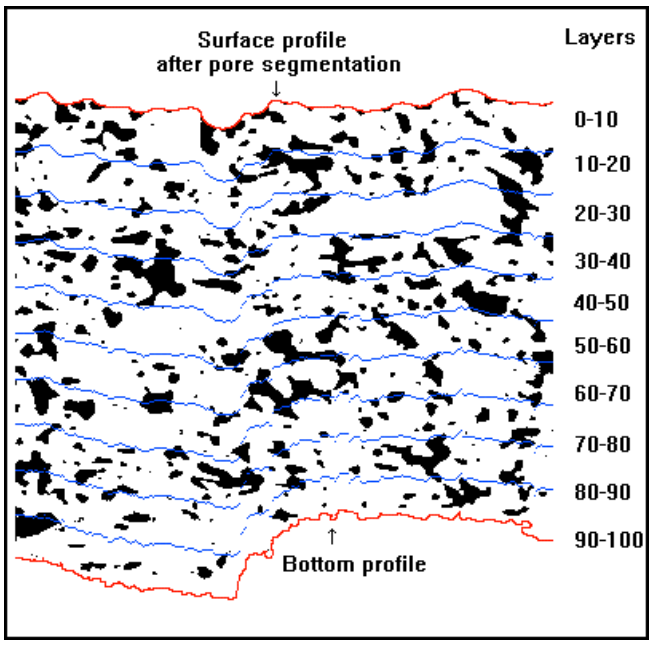

Figure 3 Schematic calculation of the pore area fraction throughout the coating layer. The black areas represent pores. The surface and bottom profiles of the coating layer are indicated along with the layer divisions used to calculate the pore area fraction distribution. The 0-10 level represents the topmost layer and the 90-100 level the one closest to the base paper.

6.3.3 Pigment particle orientation

Particle orientation was measured by a semi-automatic procedure. The routines are based on the Sobel operators for edge detection (Fig. 4). The routine detects the edges in the image, thresholds the resulting image and applies a thinning algorithm to make the skeletons of the edges (Fig. 4C and D). For images of unstained paper samples one may run an eroding filter with limit 5 and 10 iterations before skeletonising. This will reduce the amount of branched edges and enhance accuracy. These skeletons' orientation to a horizontal plane is measured automatically. Only detected edges with lengths between 25 and 150 pixels were measured. This eliminates the small-scale noise and the long continuous edges that may reduce the method's accuracy. Likewise, branched edges like e.g. 19, 20 and 21 in Fig. 4F are excluded from the calculation of the mean orientation, based on the AR of the measured edges. As exemplified in Fig. 4C and D, most of the segmented edges are curved and branched skeletons and can thus be represented by best fitting ellipses having a corresponding AR (Fig. 2F). The more branched the edge is, the lower the AR. For straight skeletons the AR solely depends on the length (in pixels) of the edge. Each detected edge's AR was thus verified and only those edges having an AR larger than 5 were taken into account. This yields two partial orientations, one for the horizontal (Fig. 4C) and one for the vertical images

(Fig. 4D). Thus, the final orientation of the particles in the image was measured using the following equation:

Particle orientation = $(n_h * Ø_h + n_v * Ø_v) / (n_h + n_v)$ (I)

Here, n_h is the number of horizontal edges, n_v the number of vertical edges, $Ø_h$ the mean orientation for the horizontal edges and $Ø_v$ the mean orientation for the vertical edges. Good correlation was found between particle orientation values found based on the best fitting ellipse, Fig. 2F and calculation based on the Sobel edge detectors. The routine was tested on the segmented pores of Fig. 2E. The two methods yielded the same average pore orientation, namely 31 degrees. This method thus appears to be a simple, yet powerful tool for application on images where particles are difficult to segment from the background and from each other.

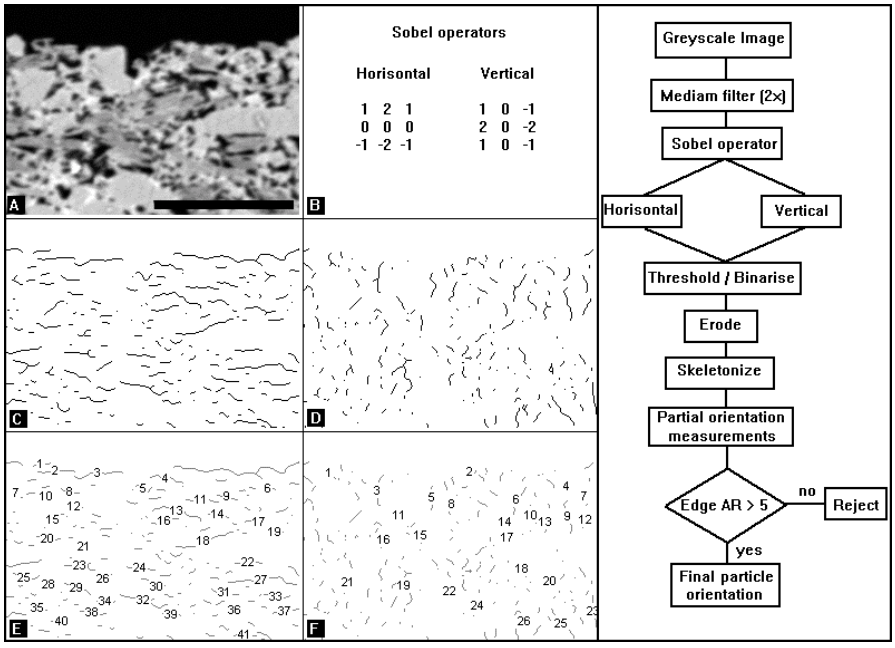

Figure 4 Calculation of pigment particle orientation in the coating structure. ***A)*** Original image. ***B)*** The Sobel operators used to detect the horizontal and vertical edges of the pigment particles. ***C)*** Image after running the horizontal mask, thresholding and skeletonizing the thresholded edges. ***D)*** Image after running the vertical mask. ***E)*** and ***F)*** The edges taken into consideration during measuring. The right side of the figure exemplifies the procedure used to detect the edges, rejection of the edges having aspect ratios (AR) less than 5 and calculation of the final average particle orientation. Bar in A: 5 μm.

6.3.4 Assessment of the coating surface micro-roughness

To assess the roughness value, a regression line is put along the paper surface. The routine scans the surface, registers the profile and calculates the regression line. The roughness is based on the measured distances from the calculated line to the surface (Fig. 5). Roughness parameters like the mean square root (Rq) and the arithmetic average (Ra) may be obtained according to the ISO 4287/2000 standard,

$$Rq = \tilde{a}\ \frac{1}{n} \times (y_i - y_m)^2 \qquad \text{(II)}$$

$$Ra = \frac{1}{n} \times b\ y_i - y_m b \qquad \text{(III)}$$

Here, n is the number of measured distances, y_i the distance at x_i and y_m the average distance.

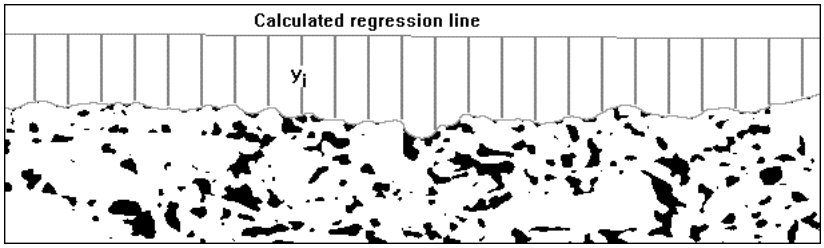

Figure 5 Calculation of surface roughness based on digital images. The step length may be chosen at will. A step size of 0.2 µm is usually applied.

6.3.5 Validity of the segmentation procedure

Thresholding is a most important step in image analysis. Quantification of pore details depends strongly on the image segmentation. It was desirable to compare automatic to subjective segmentation. A stack composed of 10 digital images was given to 7 students. They undertook a subjective segmentation of the pore structure. The same images were segmented automatically by the routine explained above. The 8 segmented stacks were processed in the same way. Coating layer details were finally measured (Fig. 6).

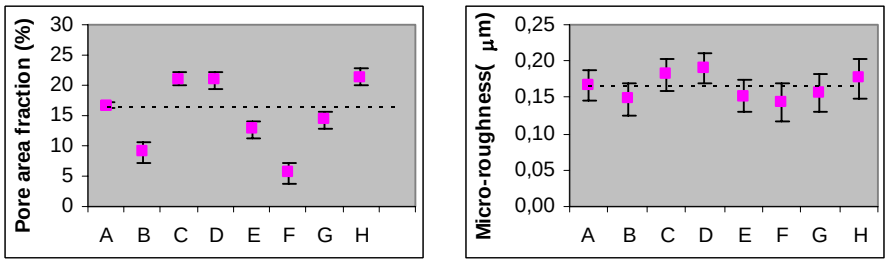

Figure 6 Coating layer details as measured on subjective and objective segmented digital images. Point A and the dotted line indicates values obtained from the automatic segmentation. B-H give values obtained after subjective segmentation by 7 students.

Fig. 6 shows a significant spread of the subjective segmentations from the objective one, which however gives a good average. Pore area fraction differing by over 15 % was calculated when using manual thresholding. This is due to an over and under representation of the areas comprised by the pores by subjective segmentation.

6.4 Discussion

6.4.1 Preparation of paper samples

Staining samples by OsO_4 is important. OsO_4 stabilises cross-sections, easing the sample preparation (McCoy, 1998). The reaction with the styrene/butadiene in the coating improves the contrast between binders and epoxy filled voids (Fig. 1). The method yields good results for visualisation and quantification of binders and pore details (see Chinga and Helle, 2001). Even the reaction between OsO_4 and the ink (Fig. 1B) is important for ink quantification. Finally, the fixative appears to prevent the mechanical pulp fibres from being damaged during SEM image acquisition, thus securing the final image quality.

6.4.2 Image processing and analysis

Despite the complex cross-sectional structure, the automatic thresholding yielded suitable segmentation. The procedure is reproducible, avoiding the large variation of manual segmentation (Fig. 6). For surface definition, the scanning-sphere yields surface pores segmented objectively. Small noisy pores arising at the surface as a result of segmentation are removed automatically by erosion without affecting the bulk pore structure. The procedure is easy to use and batch processing may be performed easing the work. Fig. 3 exemplifies the calculation of the pore area fraction distribution throughout the cross-section. Such information, otherwise hard to obtain, add to our knowledge of the coating layer structure.

The routine to measure particle orientations (Fig. 4) is simple yet powerful for assessing particle details avoiding manual assessment. Good correlation was found when compared to images with known particle orientation. By this technique one may measure pigment particle orientation throughout the coating layer. Coating layers with platy particles like clay and talc prove clear orientation and may yield the most reliable results. Although the orientation of blocky particles like ground $CaCO_3$ is difficult to measure, the routine detects the orientation of edges interfacing other pigment particles, pores or the paper surface, thus yielding valuable information. The used Sobel operators detect grey-level variations between regions in digital images. The most pronounced variation is found between particles and pores. It is conceivable that the routine calculates the pore orientation rather than particle orientation. However, the pore structure is strongly dependent on the particle distribution and packaging. There obviously will be a positive correlation between particle and pore orientation.

Restoration algorithms like the reported wiener filter (Tovey and Hounslow, 1995) might be used to enhance the pores and particles' edges to improve segmentation of small pores and easing the particle orientation assessment. The absence of sharp edges between the small pores and surrounding matrix is caused by the spreading of the electron beam when interacting with the specimens surface. A low

acceleration voltage (5 kV) was used to reduce this problem, thus improving the image resolution.

In judging the findings, one should keep in mind that paper is a three-dimensional structure and the present analytical method only describes two-dimensional cross-sections. On the other hand, it is widely known that e.g. the area fraction of an object in a cross-section may be a good estimate of the volume fraction of that object in the entire 3-D structure (see e.g. Cruz-Orive, 1997; Janowski et al., 1998). Although the aspect ratio appears to be a proper pore descriptor, the pores may have complex shapes in 3-D space and estimation of the 3-D pore characteristics details may require more than 2-D images. Systematic serial sectioning and 3-D reconstruction may give more insight into the coating layer structure, making it possible to apply new techniques like the equivalent pore concept (see e.g. Holmstad et al., 2001). However, nowadays 3-D reconstruction techniques have limitations regarding preparation, resolution and visualisation and can hardly be applied for making 3-D reconstructions of the coating layer.

6.5 Conclusion

A series of routines were developed during this study, yielding new and valuable information about the coating layer on paper. Structure details, possibly unattainable by other current methods have been assessed. The outlined automation improves the morphometric analysis of coating layers, allowing a direct assessment of critical pore and pigment particle details as well as the paper surface smoothness. Besides, the limited operator involvement in the measurement procedures raise the objectivity and reproducibility of the results. Finally, the complementary information obtained by the described methods may be useful for an increased knowledge of the coating layer structure, how it is affected by different process variables and how it will affect the paper end-use properties.

References

Abrams, L., Favorite, C.W., Capano, P.J. and Johnson, R.W. (1996) Using mercury porosimetry to characterise the coating pore structure and its relation to coating optical performance, *Proceedings from the TAPPI Coating Conference*, 185-192

Allem, R. (1998) Characterization of Paper Coatings by Scanning Electron Microscopy and Image Analysis, *J. Pulp Pap. Sci.*, 24(10) 329-336.

Allem, R. and Uesaka, T. (1999) Characterization of Paper Microstructure: A New Tool for Assessing the Effects of Base Sheet Structure on Paper Properties", *Proceedings from the Microscopy as a Tool in Pulp and Paper Research and Development Symposium*, 43-52.

Barratte, C., Dalphond, J.E., Mangin, P.J. and Valade, J.L. (1997) An automatic determination of threshold for the image analysis of prints, *Advances in Printing Science and Technology: Proceedings of the 23rd research conference of IARIGAI*, 451-469

Chinga, G. and Helle, T. (2001) Staining with OsO_4 as a Means to Explore Paper Coating Structure. *Submitted for publication to Pap. puu.*

Climpson, N.A. and Taylor, J.H. (1976) Pore distributions and optical scattering coefficients of clay structures, *Tappi J.59* (7) 89-92.
Cruz-Orive, L.M. (1997) Stereology of single objects. *J. Micros.*, 186 (5): 93-107.
Davies, E.R. and Celano, D. (1993) Orientation accuracy of edge detection operators acting on binary and saturated grey-scale images, *Electronics letters* 29(7): 603-604.
Dickson, A. (1999) Quantitative analysis of paper cross-sections. *Appita*, 735-738
Elton, N.J., Gate, L.F. and Hooper, J.J. (1999) Texture and orientation of kaolin in coatings, *Clay Minerals* 34: 89-98.
Gadala-Maria, F. and Parsi, F. (1993) Measurement of fiber orientation in short-fiber composites using digital image processing, *Polymer composites 14 (2): 126-131*.
Gane, P. A. C., Hooper, J. J. and Grunwald, A. (1995) Coating pigment orientation: A comparative analysis of the application mechanisms and properties of blade and roll coatings. *Proceedings from 1995 Coating Conference*, 383-390.
Gane, P. and Watters, P. (1989). Pigment particle orientation, *Pap. puu* 71(5): 517-533.
Gonzalez, R.C. and Woods, R.E. (1993) *Digital image processing, Eds. Addison-Wesley publishing company, Inc*. ISBN 0-201-60078-1.
Holmstad, Antoine, C., Silvy, J., Costa A-P. and Antoine, J. (2001) Modelling paper sheet structure according to the equivalent pore concept, Proceedings from the *Cost Action E11, Characterization methods for fibres and paper* 15-25.
Inagaki, M. and Suwa, T. (2001) Pore structure analysis of exfoliated graphite using image processing of scanning electron micrographs, *Carbon* 39: 915-920.
Janowski, J., Sadowski, A., Kraj, W. and Ratajczak, T. (1998) Determination of porosity of reduced hematite by stereologic methods , *J. Mat. Sci.* (33): 477-486.
Krishnagopalan, A. and Simard, G.L. (1976) An improved technique for studying binder migration in coated paper. *Tappi J.* (12): 96- 99.
McCoy, J.W. (1998) Metallographic Preparation of Coated Papers for Backscattered Electron Imaging of Coating Structure in Cross-Section. *Proceedings from the Coating/Papermakers Conference*, 121-132.
Ozaki, Y. and Kimura, M. (2000) Visualisation of printing ink vehicle on paper surfaces by a SEM technique. *Appita J.* (3): 216-219.
Peterson, A. and Williams, L.C. (1992) Determining Paper-Coating Thickness with Electron Microscopy and Image Analysis, *Tappi J.*, (10) 122-126.
Ridler, T.W. and Calvard, S. (1978) Picture Thresholding Using an Iterative Selection Method. *IEEE Transactions on Systems, Man, and Cybernetics*, smc-8 (8): 630-632.
Rissa, K., Lepisto, T., Vaha-Nissi, M., Lahti, J. and Savolainen, A. (2000) Orientation of talc particles in dispersion coating, *Nord. Pulp Pap. Res. J.* 15(5): 357-361.
Rissa, K., Lepistö, T., Vähä-Nissi, M. and Savolainen, A. (1999) Characterization of Pigment and Dispersion Coatings using Atomic Force Microscopy and Scanning Electron Microscopy. *Proceedings from the Microscopy as a Tool in Pulp and Paper Research and Development Symposium*, 195-206.
Russ, J.C. (1999) The image processing handbook. 3rd Ed. ISBN 3-540-64747-3.
Tovey, N.K. and Hounslow, M.W. (1995) Quantitative micro-porosity and orientation analysis in soils and sediments, *J. Geological Society* 152: 119-129.

Wygant, R.W., Pruett, R.J. and Chen, C.Y. (1995) A review of techniques for characterizing the paper coating surfaces, structures and printability. *Proceedings from the Coating Fundamentals Symposium*, 1-15.
Williams, G.J. and Drummond, J.G. (1994) Preparation of Large Sections for the Microscopical Study of Paper Structure, *Proceedings from the Papermakers Conference*, 517-523.
Yang, R. and Buenfeld, N.R. (2001) Binary segmentation of aggregate in SEM image analysis of concrete, *Cement and concrete res.* 31: 437-441.

CHAPTER

7

QUANTIFICATION OF STRUCTURE DETAILS OF LWC PAPER COATING LAYERS (PAPER III)

G. Chinga
Department of Chemical Engineering
Norwegian University of Science and Technology (NTNU)
N-7491 Trondheim
Norway
e-mail: gary.chinga@pfi.no

T. Helle
Department of Chemical Engineering
Norwegian University of Science and Technology (NTNU)
N-7491 Trondheim
Norway
e-mail: torbjorn.helle@pfi.no

T. Forseth
Norske Skog ASA
Follum
e-mail: trond.forseth@norske-skog.com

Submitted for publication in Nordic Pulp and Paper Research Journal.

Abstract

Quantification of the pigment coating layer characteristics is essential for the quality control of coated paper and achieve a true understanding of how the coating and calendering processes affect the coating structure. In this study, the structure of commercial LWC paper coating layers were assessed and quantified by SEM, BEI mode and digital image analysis of cross sections. To enhance the visualisation of the pores in the coating, the binder was stained with osmium tetroxide (OsO_4) before embedding in epoxy. Image analysis techniques were applied to obtain information on the pore size distribution in the Z-direction, the pore shape and orientation. A routine, based on the Sobel operators, for measuring the pigment particle orientation, was also applied. It is quantified how clay particles cause a more densely packed coating structure compared to coatings containing mainly $CaCO_3$. The pores of clay coatings have a larger aspect ratio and are oriented more parallel to the paper surface. Pore orientation is affected by the pigment particle orientation. Besides the size of the pore, its orientation is proved to be an essential parameter affecting the achieved print gloss level for a given paper grade. The pore's orientation/ diameter ratio seems to be a suitable parameter for describing its geometry and influence on print gloss. For a given pore diameter, the more horizontally oriented, the higher the delta gloss (print gloss-paper gloss). The described techniques may enrich our knowledge about the coating layer structure, its relationships to the end-use properties, and how it is affected by process variables.

Keywords: SEM, image analysis, coating structure, porosity, particle orientation

7.1 Introduction

7.1.1 Characterisation of pigment coating layer structure details

Improved characterisation of the coating layer is essential for the quality control of coated paper and a thorough understanding of the coating process. The coating layer should be smooth and uniform to avoid variations in structural properties of the paper surface. However, due to e.g. the roughness of the base paper, the coating process yields a somewhat rough and uneven coating layer. Some regions of the paper may be more compressed, smoother and contain more particles aligned parallel to the surface than others. Such differences will affect the uniformity of the paper surface and its interaction with printing inks.

7.1.2 Assessment of structure details in pigment coating layers

Mercury porosimetry is widely used to characterise coating layer porosity. The pore volume fraction and size distribution is assessed by the volume of mercury intruding into the sample as pressure is increased (see e.g. Wygant et at., 1995). However, the authors claim that sample elasticity and narrow necked, or bottle shaped voids may cause erroneous results. Thus, due to the irregular pore shapes the calculated size distribution may underestimate the volume of small pores. The method also assumes the pores to be interconnected. The pore volume distribution assessed by porosimetry has thus been found to be much smaller than that found by image analysis methods (Dullien and Mehta, 1971; Climpson and Taylor, 1976; Lepoutre and Rezanowich, 1977). The assumed cause for the striking difference was that mercury porosimetry measures the void entry radii while image analyses assess the void themselves. Several authors have tried to characterise the coating layer macrostructure and uniformity based on digital micrographs (Peterson and Williams, 1992; Williams and Drummond, 1994; Allem, 1998). However, only few studies have dealt with the microstructure (see e.g. Climpson and Taylor 1976; Rissa et al., 2000, Chinga and Helle,2001a).

7.1.3 The effect of the coating layer characteristic details on print paper quality

The coating layer pore structure is considered to be a main parameter for the printing ink behaviour on the paper surface. The pore diameter and volume fraction may affect the absorption and setting of the ink vehicle. Structures with small pores may cause faster ink setting (see e.g. Donigian et al., 1997; Xiang and Bousfield, 2000). Fukui et al. (1996) studied how coating layer pore diameters affected the setting of offset inks on $CaCO_3$ based coating layer surfaces. The authors found the optimal pore diameter for ink setting to be between 0.12 and 0.15 μm. The pore diameters were obtained from mercury porosimetry analysis. Intrusion does not allow differentiation between surface and bulk pore geometry. Arai and Nojima (1998) stated that the surface coating pore structure plays an essential role for the gloss development in printed paper samples. Coating layers having small surface pores and large inner pores will be advantageous for gloss development, because of slower ink setting. Donigian et al. (1997) quantified the effect of pore dimension on

gloss development. The authors reported that print gloss dropped below the paper gloss when the average pore diameters of the coating layer were below 0.1 μm. An explanation for this may be that the capillary forces acting in the small pores are pulling the ink solvent into the coating structure, thus preventing the ink film from levelling (Donigian et al., 1997). Recently, mechanisms related to inertial capillarity (Schoelkopf et al, 2000) and the formation of an ink filter cake on the coated paper surface (Xiang and Bousfield, 2000) have been proposed to explain the ability of the small pores to absorb the ink components faster than the large ones.

Although there is an agreement that the pore structure affects ink setting and thus probably print gloss as well as printing ink density on the paper surface, it has been difficult to determine what kind of pore characteristics the coating layer structure should have to yield the best print quality. Moreover, due to the limitations of e.g. mercury porosimetry, critical parameters like pore size distribution in the Z-direction, pore shape and orientation have been hard to assess. Such parameters are however crucial in characterising the geometry of the coating pores but have not been measured in the referred studies. Besides some mathematical models of pore morphology and its influence on liquid absorption (see e.g. Kent and Lyne, 1989; Senden et al., 2000), most studies have focused on the pore size as the sole parameter to characterise coating pore geometry.

The purpose of this study is a more detailed characterisation of the coating of commercially available LWC paper. Direct assessment of pore geometry is essential to predict the printing ink vehicle absorption into the coating. The study analyses how pore geometry affects the end-use properties of printed paper. The information thus obtained will complement morphometrical studies.

7.2 Materials and methods

Commercial LWC paper samples from different suppliers were used. The samples had been coated with different pigment formulations, mainly clay and $CaCO_3$ pigment particles. Further details for the paper samples are found in Table 1. Production details were not known.

Table 1 Properties of the studied commercial LWC paper grades. The clay fraction values are based on residue on ignition (ash) determination of the given paper grades.

Paper samples		**Clay fraction (%)**	**Tappi paper gloss**	**Tappi print gloss**	**Delta gloss (Print gloss-paper gloss)**
A	High clay content samples	92	54,3	80,6	26,3
B		95	49,0	73,5	24,5
C		82	54,9	72,1	17,2
D		98	55,3	80,7	25,4
E	Low clay content samples	54	46,0	68,9	22,9
F		54	55,6	80,2	24,6
G		53	47,6	68,1	20,5
H		27	48,0	67,8	19,8

7.2.1 Preparation and analysis

The paper samples were stained by Osmium tretroxide (OsO_4) before embedding in epoxy resin (Chinga and Helle, 2001b). Digital images were obtained using the Hitachi S-3000 VPSEM. Backscatter images were generated using 5 kV accelerating voltage and 8-10 mm working distance. 30 digital images of high magnification (5000x) were acquired from each paper sample. The resolution was 0.02 μm/pixel for the high magnification images.

After thresholding and binarising the high magnification images, the void or pore characteristics were measured and described. The pore orientation and aspect ratio were calculated using a best fitting ellipse on every pore, yielding the minor and major axis of the corresponding ellipse. The angle between the major axis and a horizontal reference line (the paper plane) yields the orientation of the individual pores. The aspect ratio is obtained by dividing the major by the minor axis on the corresponding ellipse. Even the pore area fraction was calculated by determining the total area comprised by the pores relative to a predefined region in the cross-section image. The apparent particle orientation was measured relative to the paper surface. Sobel operators were used for detecting the edges of the particles in combination with erosion and skeletonizing. For further details about image processing and analysis see Chinga and Helle (2001a). In the present study the mean values are given with the corresponding standard errors.

7.2.2 Calculation of the clay content in the paper samples

The coating layers contained both $CaCO_3$ and kaolin. To assess the relative amounts of the two components, the samples were burnt, first at 490 ^oC. After weighing, the ash was further heated to 800^oC and weighed again. Based on the two readings, and knowledge of the ash for the two components at the two temperatures, the relative and then the absolute amounts were calculated by a procedure recommended by Zellcheming.

7.2.3 Print gloss measurements

Paper and print gloss were assessed by the TAPPI 75^o specular gloss method (T 480 om-92). Print gloss was measured 24 h after printing the sample on a Prüfbau test printer. 0.3 g ink (Reflecta Magenta 42F8000) was used on every test strip. Printing speed and temperature were 0.5 m/s and 23 ^oC respectively.

7.2.4 Mercury porosimetry

Since the morphometrical analysis was concentrated on the top coating layer, the coating layer on the wire side was removed by adhesive tape on this side and splitting the paper in two. The remaining parts of the samples, being the top coating layer and parts of the base paper, which was difficult to remove completely, were used for porosimetry analysis. The porosimetry measurements were performed in a Carlo Erba Macropores unit 120 and a Carlo Erba Porosimeter 2000.

7.3 Results

7.3.1 Morphometric analysis of the coating layers' outermost region

Digital images of the 8 studied paper samples are presented in Fig. 1. There are clear differences regarding the coating formulation and the pulp fibres composition used in the paper grades. Image analysis based on digital micrographs is a well-suited technique for accurate assessments of critical parameters affecting the print quality of a given paper grade. Direct assessment of the pore and pigment particles' details may be obtained at different depths in the coating structure, a point unattainable by other present methods where local variations cannot be registered.

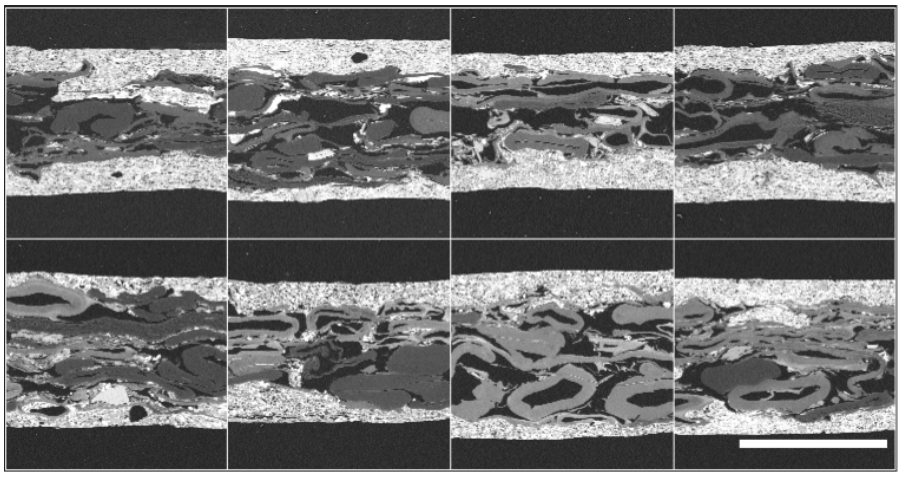

Figure 1 Digital images of the studied paper samples. Top row, left to right: A, B, C, D. Bottom row: E, F, G and H. Note the difference in base paper composition. Dark fibres indicate poor reaction with OsO_4 due to low lignin content (bleached pulp fibres). Bar 50 μm

To assess the coating/printing ink interaction one should obviously quantify pore and pigment particle details in the uppermost layer of the coating structure. Here, the pores in the top 2.5 micrometers were characterised. The pore area fractions of the studied coating layers were measured (Fig. 2). A reduction of porosity with increasing clay fraction is observed, indicating a denser structure. The correlation is somewhat poor, which is reasonable considering the different blends of pigment particles for different samples. One should also keep in mind that the clay content has been calculated using an ash determination procedure, allowing only an estimate of the clay fraction. The limited knowledge of the coating formulations does not allow further analysis of the variation. However, the found correlation is in well agreement with the expected results, that is, the clay pigment particles will contribute to forming a rather compressed coating structure as depicted in Fig. 2.

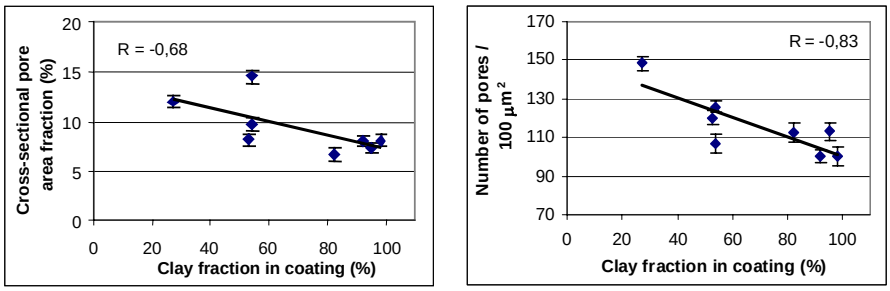

Figure 2 Left: The pore (void) fraction in the coating layer of the different paper grades. Right: number of pores pr. square micrometer as a function of clay fraction.

Analysis of the pore details also demonstrates how pigment particles affect the pore shape and orientation (Fig. 3). It has been suggested that the pigment particle shape determines the shape of the pores, at least at low binder level (Lepoutre, 1996) thus affecting even the total porosity of the coating structure (Lohmander, 2000). The influence of the clay content on pore details may possibly be more easily studied using specific pigment particles and known blends of coating colours. A clear relationship between the pigment particle shape and pore shape and orientation has been established here, showing the influence of the pigment particle grade on pore geometry (Fig. 3). The pore orientation may also provide an indirect measurement of the pigment particle orientation, especially for particles of high aspect ratio like the platy clay particles. This relationship is established in Fig. 6.

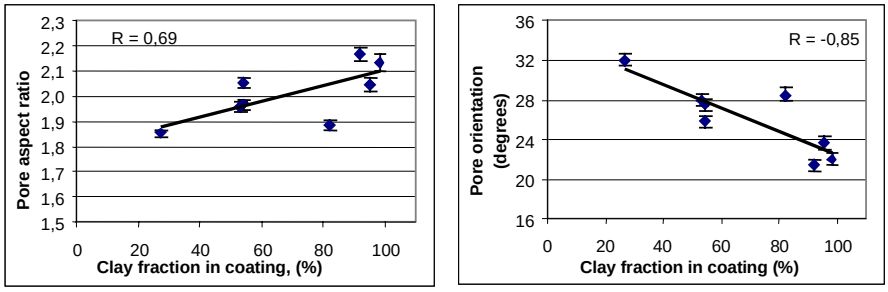

Figure 3 The effect of clay fraction on pore orientation and shape (represented by the aspect ratio). The pore orientation is calculated relative to the surface direction.

7.3.2 The effect of pore geometry on gloss development

For the same pore diameter, coatings containing clay particles tend to yield higher gloss than coatings having mainly $CaCO_3$. Pores with largest diameter increase gloss the most for a given group of pigment particles (Fig. 4, left). Pesenti et al. (1996) also reported higher gloss values for clay coatings compared to PCC coatings for a given surface roughness. This is also in accordance with practical experience.

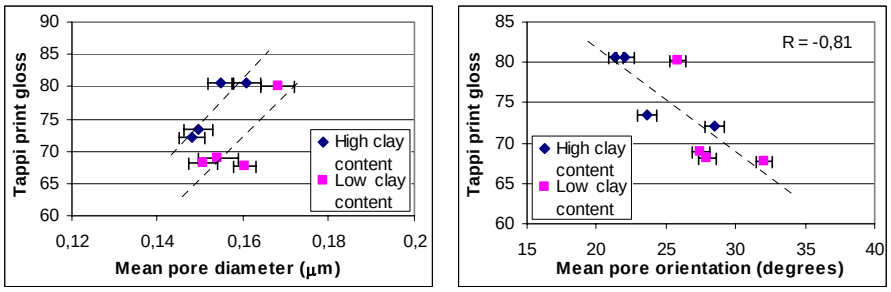

Figure 4 The effect on print gloss by apparent pore size. The presented pore diameters correspond to the average pore minor axis of the ellipses fitted to the pores. The pore orientation is based on the orientation of the major axis of the fitted ellipses relative to the paper surface.

Despite the assumed effect of pore size on absorption, it is likely that other pore geometry parameters affect the printing ink behaviour as well. The pore orientation also seems to affect the gloss of the given paper grade (Fig. 4, right and Fig. 5). Fig. 5 demonstrates the importance of controlling pore geometry, to affect critical end-use properties like print gloss. In Fig. 5 the pore and particle orientations are related to the delta gloss (print gloss-paper gloss). Since it is evident that the pore size and orientation will affect the absorption of ink components into the coating structure it seems recommendable to combine the two parameters and use the pore orientation/diameter (O/D) ratio to describe the geometry of the pores. This ratio seems to be a suitable parameter for predicting the absorption behaviour of the ink fluids, being well correlated with the print and delta gloss.

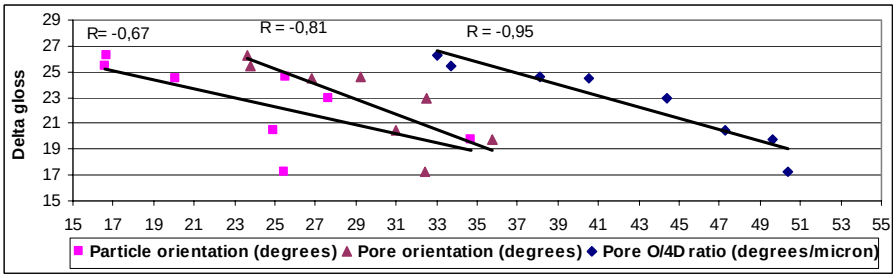

Figure 5 The influence of the pore geometry on print gloss. Although the pores from the uppermost 2.5 micrometers yield similar correlation, the presented pore dimensions are assessed throughout the entire coating structure. The pore diameter is represented by the measured pore minor axis parameter. The particle and pore orientations are based on the orientation of the major axis of the fitted ellipses relative to the paper surface and are given in degrees (for details see Chinga and Helle, 2001a). To fit the values of the scale used in the graph, the pores' orientation/diameter (O/D) ratio are divided by 4.

7.3.3 Coating layer structural details throughout the whole cross-section

Pigment particle orientation has been considered an important parameter affecting the uniformity of the coating structure. It is well known that platy pigment particles like clay are used to increase e.g. the surface smoothness, gloss and the tortuosity of the coating layer as well. As expected, there is a clear relationship throughout the coating layer between particle and pore orientation (Fig. 6). This confirms the influence of pigment particle orientation on the geometry of the formed pores.

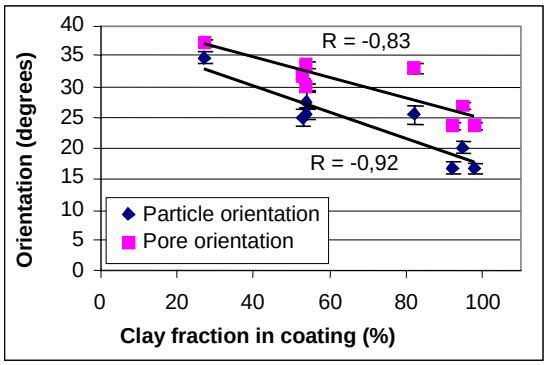

Figure 6 Mean orientation of pores and pigment particles relative to the paper surface as a function of clay fraction for the given paper grades.

The pore size distribution in the Z-direction of the coating layers was assessed. This may be relevant for analysing the pore size variation and explore how process variables affect pore details and thus print quality. Fig. 7 depicts the coating layer pore area fraction distribution for the 8 paper samples. All samples have a compressed structure in the surface when compared to the inner part of the coating layer. Note the pore area fraction distribution of sample F (Fig. 7) which in spite of having a larger fraction of $CaCO_3$ matches the gloss levels of clay coatings.

7.3.4 Mercury porosimetry measurements

As explained above, mercury porosimetry has been widely used for characterising the coating layer porosity. Fig. 8 reveals a reasonable correlation between the mercury porosimetry and the cross-sectional image analysis techniques, although the values tend to be underestimated by the porosimetry method.

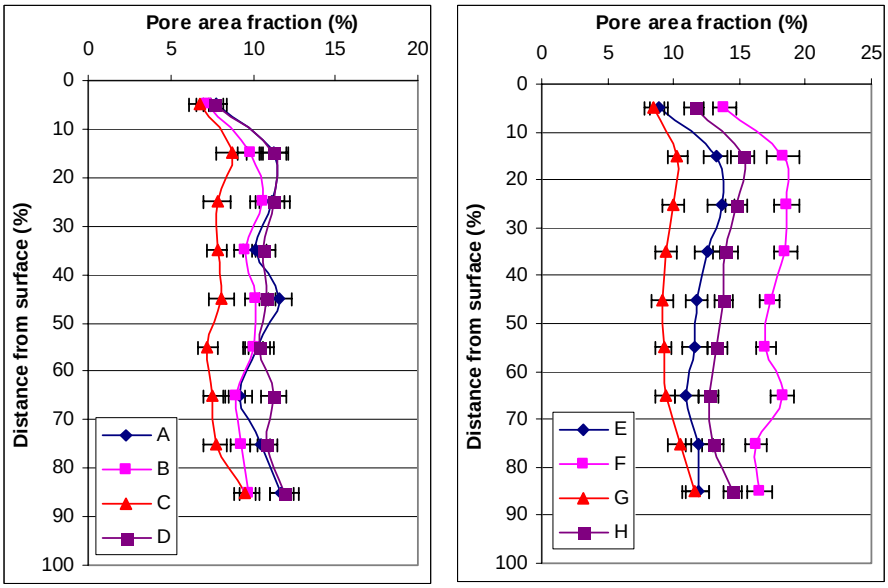

Figure 7 Cross-sectional pore area fraction distribution in the Z-direction for paper samples having coatings with large clay fractions (left) and low clay fractions (right). The coating layers have been divided into 10 layers where the 0-10 level represents the surface layer and the 90-100 level the layer close to the base paper.

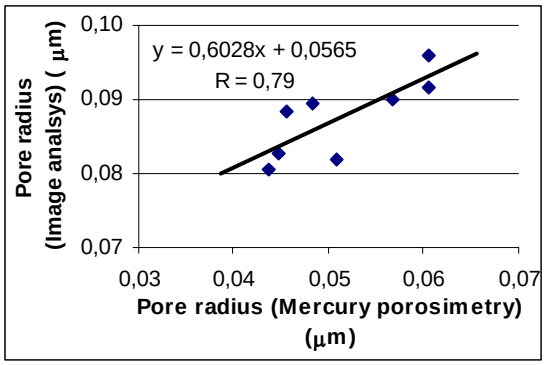

Figure 8 Comparison between mercury porosimetry and cross-sectional image analysis. The values indicate the mean pore radius of the coating layers for the given paper grades obtained by the two methods.

7.4 Discussion

A reaction between OsO_4 and the coating binders applied for the studied paper grades allowed the real pores (air-filled voids) of the coating layer to be studied. The studied papers were all LWC, meaning that the coatings were basically similar and that it can be assumed that OsO_4 reacted with the binders in a similar fashion for all the paper grades in the study. Parameters found to correlate well; like the

clay fraction and porosity details support this assumption. A reduction in the number of pores in coatings containing a large fraction of clay was found, when compared to $CaCO_3$ based coatings. Although these findings are contrary to results reported by Stanislawska and Lepoutre (1995) where the authors concluded that the pores in clay coatings are more numerous, they are supported by the fact that increasing the coating's clay fraction leads to a more compact structure with lower porosity. Moreover, as expected, larger clay fractions lead to pores with higher aspect ratio and consequently higher orientation relative to the paper surface, evidencing the packing ability of clay pigment particles (Fig. 3 and 6).

The absorption rate of the ink vehicle has been attributed mainly to the pore size without considering the actual geometry of the pores. Some studies have even assumed straight capillaries with constant radii. Such studies focus the attention exclusively on the size distribution and disregard other relevant factors like the shape and continuity of the pores (Kent and Lyne, 1989). Hence, besides the average pore size (Fig. 4), the singular geometry of the pores in the different coating structures also seems to play an important role with respect to the ink vehicle absorption. The network of interconnected pores with a large variety in shape, size and orientation must be considered when studying mechanisms like the separation and absorption of ink components into the coating structure. Fig. 4 reveals a clear negative relationship between pore orientation and gloss level. This may indicate a large effect by the vertically aligned pores on the absorption of the ink vehicle. Fig. 5 confirms the effect of pore geometry on offset print gloss. The orientation/diameter (O/D) ratio seems to be well suited to evaluate the paper's ability to reach a high gloss level. For a given pore diameter, the more horizontal oriented, the higher the gloss. This seems to confirm the mechanism leading to a reduction of print gloss for pores more effective in pulling the solvent from the printing ink, thus reducing the levelling of the ink on paper (Donigian et al., 1997).

The pore area distribution throughout the coating layer clarifies the packing ability of the two main groups of pigment particles used in the present study. The remarkable reduction in porosity at the top layer of the coating structure should be noted. All the analysed samples reveal the same trend. Suspicions that it might be caused by an artefact have not been confirmed. It thus indicates an enhanced packing of the surface coating structure upon the calendering due to an increased horizontal alignment of surface pigment particles (Hiorns et al., 1998; Elton et al., 1999). Support for this hypothesis is provided by the measured pore orientation at the top 2.5 μm (Fig. 3, right) and throughout the coating layer (Fig. 6). The pores at the coating surface appear to be more horizontally aligned compared to the pores in the coating bulk, suggesting a denser packing of the coating structure at the top layer. Quantification of the pore distribution in uncalendered coating layers may shed some light into the uncertainty of a presumable artefact at the top layer measurements.

Although the mercury porosimetry method is not capable of yielding such details, it was used to partly verify the obtained results. As expected, mercury porosimetry yields smaller pore radii readings compared to image analysis probably due to the bottle shaped voids (Fig. 8). However, it may also be realised that we are approaching the effective resolution of the scanning electron microscope and small pores may thus tend to be excluded from the segmentation procedure, probably

increasing the average pore area. On the other hand, mercury porosimetry needs extremely high pressures to assess the pores smaller than 0.01 μm reducing the accuracy of the results with decreasing pore size (Furó and Daicic, 1999).

At this point it should be reminded that little was known of the coating formulation, the type of coating procedure and calendering used on the studied commercial paper samples. In spite of such shortcomings much information has been gained, emphasising also the objectiveness of the morphometrical study. Besides, the assessment of real coating structure details increase our knowledge of the pore geometry and its implication on such an important end-use property like print gloss.

7.5 Conclusion

Cross-sectional SEM analysis has been used in the characterisation of coating layers for a group of commercially coated papers. Despite the wide spread of coating formulation and structure, it has been demonstrated that the described techniques including sample preparation and morphometric analysis are well suited to characterise coating layer structures. The complex pore structure with respect to pore size, shape and orientation has been assessed and quantified. The obtained pore details represent valuable information, not accessible by other available techniques. It has been demonstrated that the pore geometry, described by the best fitting ellipse approach, may be essential for the absorption of the ink vehicle and thus critical for the print gloss development. The pore orientation/diameter ratio seems also to be a proper parameter for predicting print gloss. For a given pore diameter, the more horizontally oriented the pores are, the higher the delta gloss.

Acknowledgements

The authors would like to thank Øyvind Gregersen (PFI) for his support and guidance during the present work. Financial support was given by Norske Skog and the Norwegian Research Council.

References

Allem, R. (1998) Characterization of Paper Coatings by Scanning Electron Microscopy and Image Analysis, *J. Pulp Pap. Sci*. 24(10): 329-336

Arai, Y. and Nojima, K. (1998) Coating structure for obtaining high print gloss, *Tappi J*. 81(5): 213-221

Chinga, G. and Helle, T. (2001a) Structure characterisation of pigment coating layer on paper by scanning electron microscopy and image analysis, *Submitted for publication in Nordic Pulp Pap. Res. J.*

Chinga, G. and Helle, T. (2001b) Staining with OsO_4 as a means to explore paper coating structure", *Submitted for publication to Pap. puu*,

Climpson, N.A. and Taylor, J.H. (1976) Pore distributions and optical scattering coefficients of clay structures, *Tappi J*. 59 (7): 89-92

Donigian, D.W., Ishley, J.N. and Wise, K.J. (1997) Coating pore structure and offset printed gloss, *Tappi J*. (5): 163-172

Dullien, F.A.L. and Mehta, P.N. (1971) Particle size and pore (void) size distribution determination by photographic methods, *Powder Technol*, (5): 179-193

Elton, N.J., Gate, L.F. and Hooper, J.J. (1999) Texture and orientation of kaolin in coatings, *Clay Minerals* 34: 89-98.

Fukui, T., Terao, T. and Yamamoto, M. (1996) Effect of porous structure on coated layer ink setting, *Proceedings from the 50th Appita Annual General Conference*, 335-339

Furó, I. and Daicic, J. (1999) NMR cryoporometry: A novel method for the investigation of the pore structure of paper and paper coatings, *Nordic Pulp and Paper Res. J.* 14(3): 221-225.

Hiorns A.G., Elton, N.J., Coggon, L. and Parsons, D.J. (1998) Analysis of differences in coating structure induced through variable calendering conditions, *Proceedings from the coating/papermakers conference* 583- 602

Kent, H.J. and Lyne, M.B. (1989) Influence of paper morphology on short term wetting and sorption phenomena, *Fundamentals of papermaking*, 2: 895-920

Lepoutre, P. (1996) Structure and performance of pigmented coatings: what do we know?, *International paper and coating chemistry symposium*, 205-208

Lepoutre P. and Rezanowich A. (1977) Optical properties and structure of clay-latex coatings, *Tappi J.* 60(11): 86-91

Lohmander, S. (2000) Influence of shape and a shape factor of pigment particles on the packing ability in coating layers, *Nordic Pulp and Paper Res. J*. 15(4): 300-305

Peterson, A. and Williams, L.C. (1992) Determining Paper-Coating Thickness with Electron Microscopy and Image Analysis, *Tappi J.*, (10) 122-126

Pesenti, F., Hassler, J.C. and Lepoutre, P (1996) Influence of pigment morphology on microstructure and gloss of model coatings, *International paper and coating chemistry symposium*, 141-144

Rissa, K., Lepisto, T., Vaha-Nissi, M., Lahti, J. and Savolainen, A. (2000) Orientation of talc particles in dispersion coating, *Nord. Pulp Pap. Res. J.* 15(5): 357-361.

Schoelkopf, J., Gane, P.A.C., Ridgway, C.J. and Mathews, G.P. (2000) Influence of inertia on liquid absorption into paper coating structures, *Nord. Pulp Pap. Res. J.* 15(5): 422-430

Senden, T.J., Knackstedt, M.A. and Lyne, M.B. (2000) Droplet penetration into porous networks: Role of pore morphology, *Nord. Pulp Pap. Res. J.* 15(5): 554-563

Stanislawska, A. and Lepoutre, P. (1995) Consolidation of pigment coatings: Development of porous structure, *Proceedings from the 1995 coating conference*, 67-77

Williams, G.J. and Drummond, J.G. (1994) Preparation of Large Sections for the Microscopical Study of Paper Structure, *Proceedings from the 1994 Papermakers Conference*, 517-523

Wygan, R.W., Pruett, R.J. and Chen, C.Y. (1995) A review of techniques for characterizing the paper coating surfaces, structures and printability. *Proceedings from the 1995 Coating Fundamentals Symposium*, 1-15

Xiang, Y. and Bousfield, D. W. (2000) Influence of coating structure on ink tack dynamics", *J. Pulp Pap. Sci*., 26(6) 221-227

CHAPTER

8

RELATIONSHIPS BETWEEN THE COATING SURFACE STRUCTURAL VARIATION AND PRINT QUALITY (PAPER IV)

G. Chinga
Department of Chemical Engineering
Norwegian University of Science and Technology (NTNU)
N-7491 Trondheim
Norway
e-mail: gary.chinga@pfi.no

T. Helle
Department of Chemical Engineering
Norwegian University of Science and Technology (NTNU)
N-7491 Trondheim
Norway
e-mail: torbjorn.helle@pfi.no

Submitted for publication in Journal of Pulp and Paper Science

Abstract

The coating surface of commercial LWC paper has been studied by microscopy and image analyses. Based on secondary and backscattered electron images, some detailed characterisation of the calendered paper samples' surface was undertaken. Surface areas differing in porosity and roughness were identified and characterised. Significant differences between "closed" and "open" areas with respect to pore area fraction and mean pore diameter were quantified. It is demonstrated that the larger the size of each closed area unit the larger the correlation between the surface variation and mottling. The observed structural differences are likely to cause a non-uniform ink vehicle absorption into the coating structure and may affect the printing ink density on the paper surface. It was also demonstrated that print gloss is influenced by the pore diameter. However, pore geometry, described by the pore size and orientation, seems also important for the gloss development.

Keywords : SEM, image analysis, coating structure, porosity, gloss, mottling.

8.1 Introduction

8.1.1 Characterisation of the paper coating surface

Knowledge of the coating layer structure details is important for the understanding of mechanical, optical and printing characteristics of LWC paper. The variation in the coating layer's porosity, binder content and surface roughness may cause non-uniformities in critical paper characteristics. Several authors have used the scanning electron microscope to study paper structure details, see e.g. [1,2,3]. Most of these studies used cross-section digital images of the coating layer. Much complementary information may however be obtained from surface images. Both secondary (SE) and backscattered electron (BSE) images may give insight into the paper surface structure [2,4,5,6,7]

8.1.2 The effect on print paper quality by paper surface details

The coating layer pore structure is considered as being one of the most important parameters affecting the printing ink behaviour on the paper surface. It is well known that the pore diameter and volume fraction may affect the absorption and setting of the ink vehicle [6,8,9,10,11]. Structures containing small pores seem to lead to faster ink setting.

Print density variation on the paper surface, print mottle, is a well-known print defect. Binder migration is considered a main cause of mottling. Whalen-Shaw and Eby [12] reported that areas having low ink density were characterised by high latex level, corresponding to heavy coat weight areas. A probable relationship between coating layer thickness variation and mottling has been reported by several authors [13,14,15]. Gane [13] argued that the presumptive effect of binder migration on mottle did not occur independently of structural coat-weight variation. Zang and Aspler [16] suggested that binder content affects ink transfer at high printing speed (4.5 m/s). Less ink is transferred to less porous and less absorbent coatings containing more binder, causing reduced printing ink density [16].

The appearance of glossy, low porosity ("closed") areas on the calendered paper surface have been reported by some authors [2,12,17]. Wikström et al. [18] reported the appearance of flattened regions ("closed" areas) on the paper surface after calendering. Such areas were not observed in uncalendered paper, indicating that the surface structural variations were not caused by the drying conditions. Even other authors have found varying paper surface densification due to the calendering [12,19]

Whalen-Shaw and Eby [12] suggested that the closed areas, characterised by higher binder content, might correlate with areas of low ink density. More recently, Xiang et al. [7] proposed a mechanism where drying-induced coat weight variation might lead to the formation of closed and open areas. Contrary to results reported by Whalen-Shaw and Eby [12], the closed areas on the paper surface were found to occur in the low coat weight regions and being characterised by a rather smooth structure. Although Xiang et al. [7] did not find any binder content difference in closed areas compared to more open ones, a clear correlation was found between the closed area fraction of the paper surface and the mottling appearance. They

concluded that mottling might have a structural cause related to the non-uniform distribution of surface pores

Regardless the origin of the closed areas, it is obvious that such paper surface variations may harm the uniformity of prints. However, even though several authors have reported such structural surface variation, little is known of the pore characteristics on these areas. Reported assessments on the closed areas [7] and surface pore structure [6] have been performed manually, thus being prone to errors. Hence, automation of routines for assessing the surface structural characteristic details is necessary. In the present study a method based on microscopy and image analysis has been developed for automatic identification and quantification of the closed area fraction of coating surfaces. Routines for characterising the closed and open area fractions with respect to pore characteristic details were also developed. The methods were applied on commercial LWC papers in order to analyse the paper surface and to study the presumptive implication of the surface structural variation and surface porosity on print gloss and the mottling appearance.

8.2 Materials and methods

A series of commercial LWC paper samples from different suppliers were used. The different paper samples had been coated with different pigment formulations, including clay and $CaCO_3$ pigment particles. Further details about the different paper samples can be found in Table I. Being commercial samples, no complete information of the papers was available.

8.2.1 Calculation of the clay content in the paper samples

The coating layers contained both $CaCO_3$ and kaolin. To assess the relative amounts of the two components, the samples were burnt, first at 490 ^oC. After weighing, the ash was further heated to 800 ^oC and weighed again. Based on the two readings, and knowledge of the ash for the two components at the two temperatures, the relative and then the absolute amounts were calculated by a procedure recommended by Zellcheming.

8.2.2 Print quality measurements

Paper and print gloss were assessed by the TAPPI 75^o specular gloss method (T 480 om-92). Print gloss was measured 24 h after printing the sample on a Prüfbau test printer. 0.3 g ink (Reflecta Magenta 42F8000) was used on every test strip. The printing speed and temperature were 0.5 m/s and 23 ^oC respectively. The paper samples used for mottling evaluation were printed on a M.A.N. Rotoman C printing press, speed approx. 5 m/s. Print mottle was measured at KCL using a method based on band pass filtering and image analysis. Such methods have been found suitable for evaluating print mottle [20].The image size for measurement was 51 x 51 mm^2 and the obtained mottling values represent print density unevenness in the range from 2 to 8 mm. The mottling value for each paper grade is the average of five replicates.

Table I Properties of the studied commercial LWC paper grades. The clay fraction values are based on residues on ignition (ash) determination of the given paper grades.

Paper samples		Clay fraction (%)	Tappi print gloss	Print mottling
A	High clay fraction samples	92	80,6	1,25
B		95	73,5	1,35
C		82	72,1	0,90
D		98	80,7	0,98
E	Low clay fraction samples	54	68,9	1,26
F		54	80,2	1,17
G		53	68,1	0,78
H		27	67,8	1,00

8.2.3 Sample preparation and image acquisition

10x10 mm^2 not printed samples were taken from each paper grade and gold sputtered for 30 s before visualisation in the SEM, SEI and BEI-mode. Table II presents the operation parameters used during image acquisition.

Table II SEM conditions during image acquisition in secondary electron imaging (SEI) and backscattered electron imaging (BEI) mode.

	Low magnification	High magnification
SEM-mode	SEI	BEI
Magnification	250x	5000x
Accelerating voltage	10 kV	5 kV
Working distance	10 mm	8 mm
Image size	1280x960 $pixels^2$	1280x960 $pixels^2$
Image resolution	0.4 μm/pixel	0.02 μm/pixel
Number of images pr. Sample	20	20 “closed” areas 20 “open” areas

8.2.4 Quantification of surface variation based on secondary electron imaging (SEI)

By microscope inspection, “closed“ and “open” areas can easily be observed. They are also observed in SEM micrographs, where the closed areas seem to be smoother, having lower surface porosity than the open areas. The compact closed areas have less specific surface available for electron emission. Fewer electrons being captured by the secondary electron detector may cause the darker grey area level, characteristic for these areas (Fig. 1).

The greyscale images were histogram equalised, segmented using automatic thresholding and binarised (Fig. 1). It is obvious that if not performed with caution, such image processing and analysis may lead to significant changes in the numerical data acquisition. Care must be taken in order to find the optimal

segmentation procedure, avoiding removal of important data. Image analysis routines were developed to automate this part of the process. The segmented images were then subjected to erosion in order to remove the small noisy points. An erosion filter with limit 5 and 20 iterations was found suitable in the present study, for details see Chinga and Helle [21].

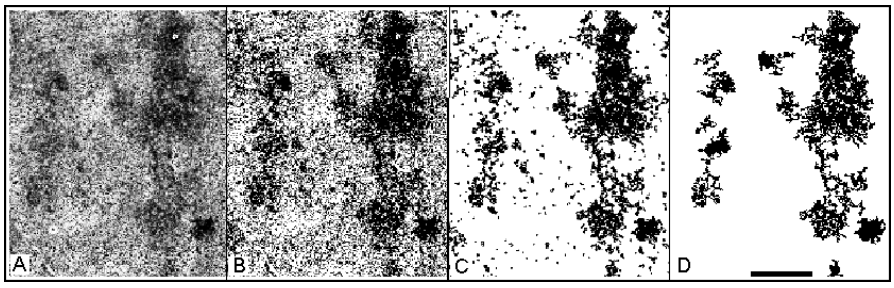

Figure 1 Segmentation procedure of closed areas on images of LWC paper surfaces. A) Original equalised image reflecting differences in topography, B) thresholded image, C) the same area after running erosion filter with limit 5 and 20 iterations and D) noisy particles smaller than 100 pixels have been removed. Bar: 50 μm.

8.2.5 Assessment of pore details on closed and open areas

High magnification BSE images (see Fig. 2) may contribute to the surface characterisation and allow quantification of surface pores. The surface pore segmentation exemplified in Fig. 2C and D is based on the same routine as developed to segment closed areas on the paper surface. To enhance the segmentation procedure the first threshold value was subtracted from the histogram and the resulting image thresholded again and binarised. For low contrast images, as for extremely closed areas, an extra subtraction of the threshold value may be required, otherwise the pore area fraction may be over estimated. After thresholding and binarisation an erosion filter was run over the images. 10 iterations and a limit of 6 neighbour pixels seems to be enough for removing most of the noisy particles, for details see Chinga and Helle [21].

Pore area fractions and pore sizes are easily quantified from the segmented images. Pore area fractions were calculated by determining the total area comprised by the pores relative to the total image area (~ 490 μm^2). The pore diameter corresponds to the minor axis of the ellipses fitted to each pore, for details see Chinga and Helle [3]. In the present study the mean values are given with the corresponding standard errors.

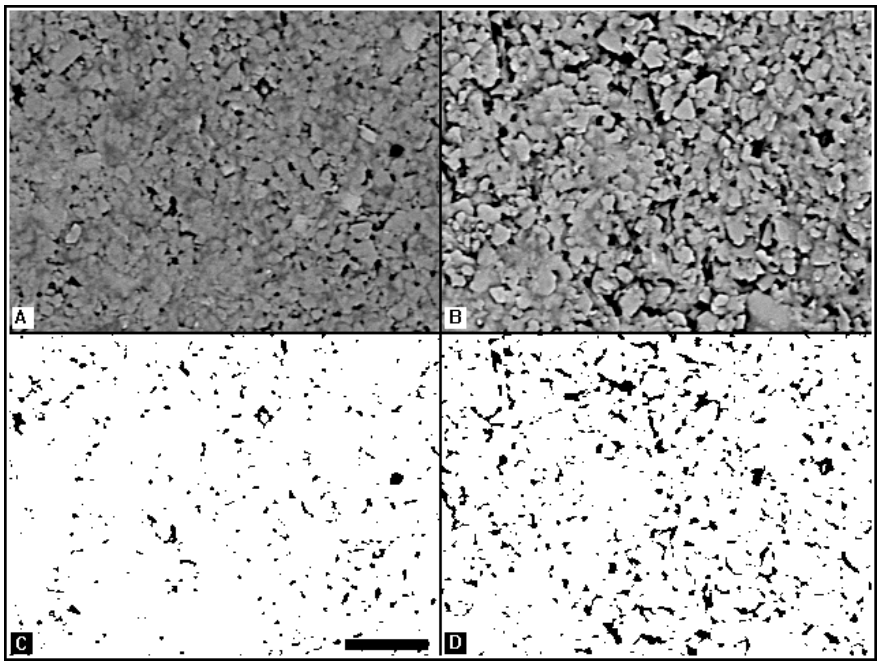

Figure 2 A) and B): Backscattered electron images of closed and open areas resp. C) and D) Surface pore segmentation based on the images shown in A) and B). Bar: 5 μm.

8.3 Results

8.3.1 Origin of the closed areas

Analysis of the paper surface of an uncalendered paper sample, having a large fraction of $CaCO_3$, did not reveal any occurrence of closed areas in the coating surface. This may indicate that closed areas are a consequence of the calendering. It is unclear which areas become closed. However, it seems that the closed areas appear most frequently on "hills"; the top of base paper surface fibres thus corresponding to the thinnest regions of the coating layer. The width of the segmented areas lies in the range of the fibres' width, supporting this assumption (Fig. 1).

8.3.2 The effect of surface structural variation on print density unevenness

Xiang et al. [7] claimed a direct relationship between the paper surface's closed area fraction and mottling. Their quantitative evidence was however subjective and based on manual segmentation of very small images if compared to characteristic mottling areas. As a first attempt in the present study, the closed area fractions from each of the 20 individual micrographs (512 μm x 384 μm) for each paper grade

were measured, and the average calculated. Assuming that the size of the closed area may be of importance, only closed areas > 8000 μm^2 were included. Plotted vs. the KCL mottling readings of the paper reveals no correlation (Fig. 3). From this result, one will conclude that the total closed area will not be critical.

Each of the individual micrographs is very small, related to the typical mottling area. The variation in closed area fraction for the different micrographs of a given paper may be a better way of assessing the variability. The standard deviation between the micrographs from each paper grade was calculated, again limiting the assessed close areas to those > 8000 μm^2. In Fig. 4 (left) the calculated standard deviations are plotted vs. the mottling tendency. Here, there is a good correlation; the larger the standard deviation in closed area fraction, the larger the mottling tendency, as one might expect.

Similar calculations were made when including smaller and smaller individual closed areas in the closed area assessment. Again plotting the standard deviation of the total closed area fraction for the individual micrographs, the results are plotted in Fig. 4, right. One will note that the smaller the individual closed areas included in the calculation, the poorer the correlation with mottling tendency. It thus appears as only the larger closed areas affect the mottling appreciably. The used magnification of 250x did not allow an increase of the minimum size requirement without removing a major part of the segmented areas from the images. Lower magnification should be used in order to cover wider regions of the paper surface.

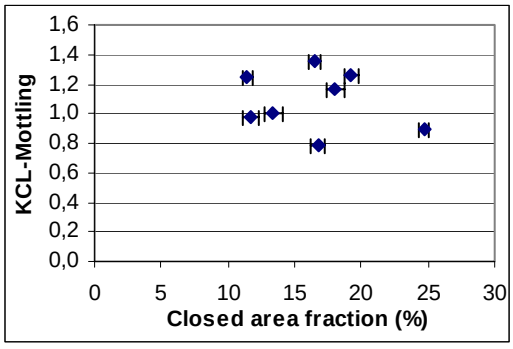

Figure 3 Measured closed area fraction and the mottling values for the 8 analysed samples.

8.3.3 Pore details in closed and open areas on the coated paper surface

From visual inspection it seems that the closed areas are smoother, containing less and smaller pores. Fig. 5 (left) compares pore area fractions for open and closed areas. The differences are quite large. Fig. 5 (right) demonstrates that open areas contain larger pores. The pore diameter distributions over closed and open areas were calculated (Fig. 6 and 7). The closed areas have fewer pores available for absorbing the printing ink vehicle. This suggests a slower consolidation of the transferred printing ink. This supports an assumption of low ink density on closed

areas [12]. Different absorption for closed and open areas will likely harm print homogeneity.

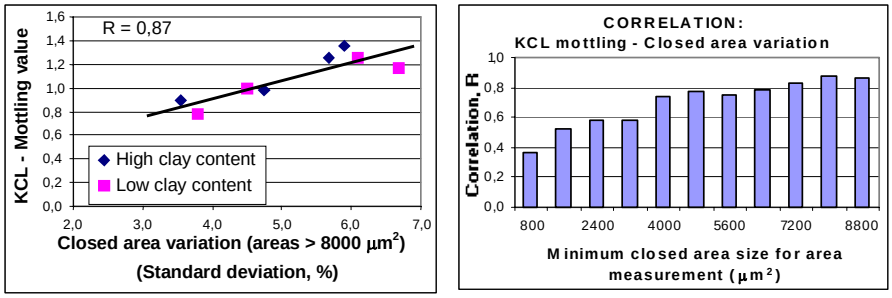

Figure 4 Left: Correlation between the closed area fraction variation and mottling when using a limit size of 8000 µm^2. Right: Correlation between the variation of the closed area fraction, represented by its standard deviation, and the corresponding mottling values. Closed areas below a certain size (x-axis) are removed and not taken into consideration during the measurement.

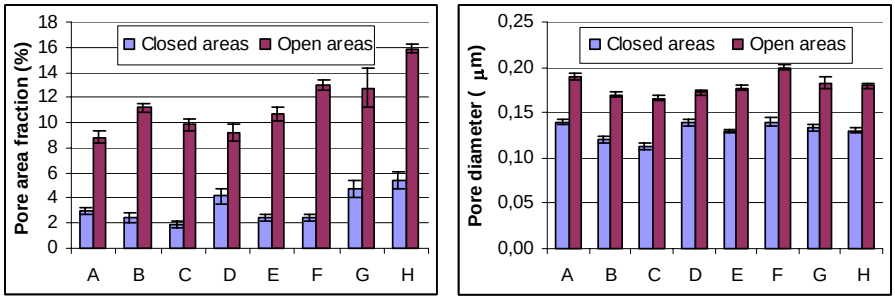

Figure 5 Pore area fraction (left) and mean pore diameter (right) on the closed and open surface areas for some of the tested papers. The pore diameter is represented by the pore minor axis of the fitting ellipses [3].

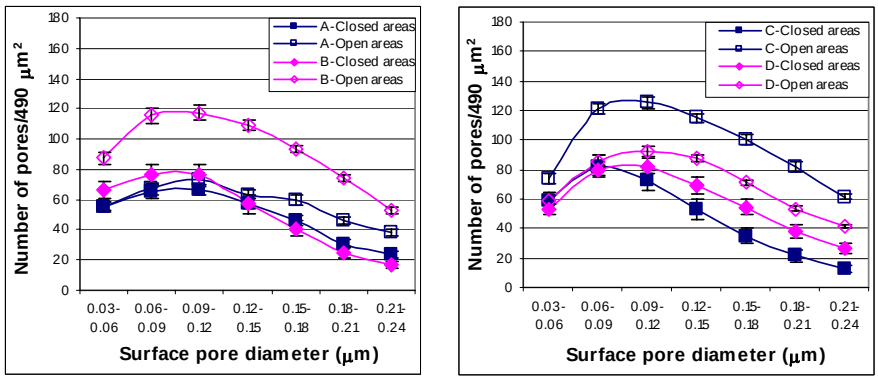

Figure 6 Pore diameter distribution on paper grades with *high clay fraction* in the coating. The number of surface pores in closed and open areas for paper A, B, C and D are given. The pore diameter is represented by the pore minor axis of the ellipses fitted to each pore.

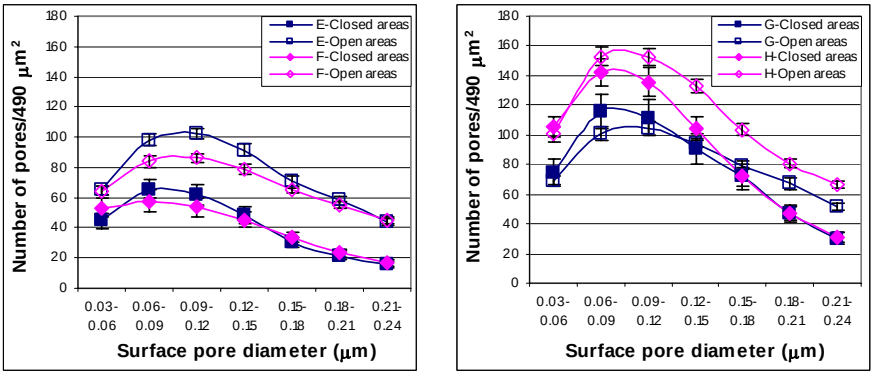

Figure 7 Pore diameter distribution on paper grades with *low clay fraction* in the coating. The number of surface pores from the closed and open areas of paper E, F, G and H are given. The high values for paper H are probably caused by the high $CaCO_3$ fraction in the coating (Table I). The pore diameter is represented by the pore minor axis of the ellipses fitted to each pore.

8.3.4 The influence of surface pore diameter on print gloss

Fig. 8 relates print gloss to mean pore diameter. The larger the pores, the higher the gloss. The same trend was observed in cross-sectional image analysis [22]. Fig. 8 even shows good correlation between cross-sectional and surface pore diameter, though the samples for surface analysis were not OsO_4-treated. This confirms the suitability of the BSE signal to assess surface openings.

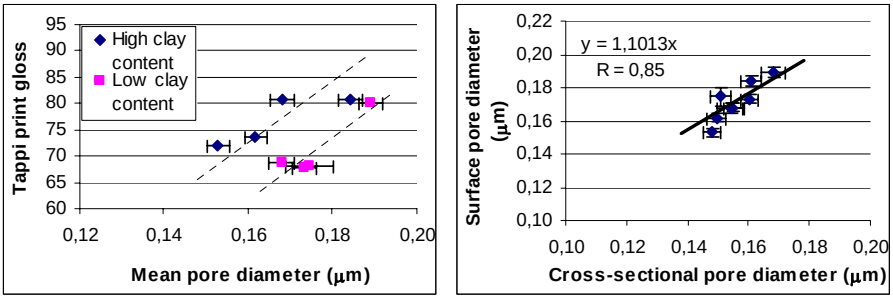

Figure 8 Left: Relationship between mean surface pore diameter and print gloss for the 8 tested papers. Right: relationship between the cross-sectional pore diameter [22] and the surface pore diameter.

8.4 Discussion

SEM surface analysis did not reveal closed areas for the investigated uncalendered sample. Some regions, presumptively having a high local basis weight, are likely to be subjected to high specific loads during calendering, becoming compressed and smoothened [23]. A correlation between thin coating regions on the hills and closed paper surface areas thus appears likely. Such differences between thin and thick coating regions are believed to cause a non-uniform ink transfer and consequently uneven print density due to the porosity variation [12, 24].

The total closed area fraction level was found not to affect the mottling appearance. However, it appears that the size and distribution of the closed area affects mottling. The larger the size of each closed area unit the better the correlation between surface variation and mottling. It is not clear which region yields the higher ink density, closed or open areas. Considering the dimensions and number of pores presumptively responsible for the fast ink setting (Fig. 6 and 7), the results may suggest that the open areas consolidate the ink film faster than the closed areas provided the same amount of transferred ink. Whalen-Shaw and Eby [12] stated that areas of low porosity might correlate with areas of low ink density, however reported that these areas are characterised by thick coating regions and high latex content. Such relationships were not explored in the present study. However, if the closed areas appear after calendering, one would expect to find such areas on regions with high local basis weight and thin coating films.

The findings on the effect of pore diameter on print gloss agree with earlier studies [6,10]. However Arai and Nojima [6] claimed that print gloss is affected by surface pores rather than by the inner pores. This has not been confirmed here. On the other hand, the results may suggest a major influence by the inner pore structure and geometry on the gloss development [22]. The Arai and Nojima [6] study applied two different techniques for assessing the inner and the surface pore structure, mercury porosimetry and SEM surface analysis respectively. This may have induced some uncertainties in the mentioned comparison.

The present study only aimed at exploring the structural parameters affecting the ink/coating interaction. The possible effect of chemical aspects of the coating layers was thus not studied.

8.5 Conclusion

New techniques were developed to study surface details of pigment coated paper, in order to explore their effects on printing defects like mottling. New and semi-automatic routines for image analysis on SEM images, in the SEI and BEI-modes were developed. The automation improves the reliability and reproducibility of the morphometric studies. The study results allowed a division of the surface into smaller and larger areas characterised as either “open” or “closed”, the two groups differing in their surface pores fraction. The open areas are characterised by having large amount of pores, large pore area fraction and high mean pore diameter. The cross-sectional pore diameters correlate well with the surface pore diameter measured by image analysis, though the later is larger. Larger average size of the

pores tends to raise print gloss, however the inner pore geometry is also important for the gloss development. The fraction of open and closed surface areas does not directly affect mottling. The critical factor is rather the distribution of the areas. The more uneven the distribution of open and closed areas, the larger the mottling tendency. And the larger the size of each closed surface area unit of the coating, the larger the correlation between the surface variation and mottling.

Acknowledgements

The authors would like to thank Øyvind Gregersen (PFI) for valuable discussions during the present work. Financial support was given by Norske Skog and the Norwegian Research Council.

References

1. Peterson, A. and Williams, L.C., "Determining Paper-Coating Thickness with Electron Microscopy and Image Analysis", *Tappi J.*, (10): 122-126(1992).
2. Allem, R., "Characterization of Paper Coatings by Scanning Electron Microscopy and Image Analysis", *J. Pulp Pap. Sci.*, 24(10): 329-336(1998).
3. Chinga, G. and Helle, T., "Structure characterisation of pigment coating layer on paper by scanning electron microscopy and image analysis", Submitted for publication in Nordic Pulp Pap. Res. J. (2001).
4. Helle, T. and Johnsen, P.O., "Using stereoscopic and SEM backscatter imaging for studying ink distribution details on paper and fibre surfaces", *J. Pulp Pap. Sci.* 20(7): 189-192 (1994)
5. Gregersen, Ø.W., Johnsen, P.O. and Helle, T., "Small scale topographical variations of paper surfaces, and their effects on printing ink transfer distribution", *Proceedings from the International printing and graphic arts conference,* 271-281 (1994).
6. Arai, Y. and Nojima, K., "Coating structure for obtaining high print gloss", *Proceedings from the 1997 Coating Conference,* 133-142 (1997)
7. Xiang, Y., Bousfield, D. W., Coleman, P. and Osgood, Al., " The cause of backtrap mottle: chemical of physical", *Proceedings from the 2000 Tappi Coating Conference and Trade Fair,* 45-57 (2000).
8. Watanabe, J., Kuhara, Y. and Takahashi, S., "Effects of clay properties on paper coating structure. Printability relationships", *Tappi J.* (1): 43-46 (1980).
9. Fukui, T., Terao, T. and Yamamoto, M., "Effect of porous structure on coated layer ink setting", *Proceedings from the 50th Appita Annual General Conference,* 335-339 (1996)
10. Donigian, D.W., Ishley, J.N. and Wise, K.J., "Coating pore structure and offset printed gloss", *Tappi J.* (5): 163-172 (1997)
11. Xiang, Y. and Bousfield, D. W. "Influence of coating structure on ink tack dynamics", *J. Pulp Pap. Sci.*, 26(6): 221-227 (2000).
12. Whalen-Shaw, M and Eby, T., "An investigation of factors related to backtrap mottle in coated papers using electron probe microanalysis", *Proceedings from the 1991 Coating Conference,* 401-409(1991)

13. Gane, P.A.C.,"Mottle and the influence of coating and binder migration", *Pap. tech.* 34-41 (1989)
14. Ensgtrøm, G., Rigdahl, M., Kline, J. and Ahlroos, J., "Binder distribution and mass distribution of the coating layer - cause and consequence", *Tappi J.* (5): 171-179 (1991)
15. Matasubayashi, H and Saito, Y., "The influence of coating structure on paper quality", *Proceedings from the 1992 Coating Conference*, 161-171 (1992)
16. Zang, Y.-H. and Aspler, J.S., "The effect of surface binder content on print density and ink receptivity of coated paper", *J. Pulp Pap. Sci.*, 24(5): 141-145 (1998)
17. Hiorns, A. and Julin, M., "Optimum paper performance through new calendering technology", *Proceedings from the 2000 Tappi Coating Conference and Trade Fair*, 227-244 (2000).
18. Wikstrøm, M.," Influence of temperature and pressure pulses on the calendering result", *Thesis for the degree of Doctor of technology, STFI*, ISNN 1104-7003 (1999).
19. Lepoutre, P. and De Grâce, J.H., "Ink transfer characteristics and coating structure", *Pap. Tech. Ind.*, 301- 304 (1978)
20. Johansson, P.Å., "Print mottle evaluation by band-pass image analysis", *IARAGAI´s* 22nd International Research Conference, Advances in printing science and technology, p. 403.
21. Chinga, G. and Helle, T., "Variations of LWC paper surfaces and their implications for the printing ink behaviour", *Proceedings, COST Workshop Action E-11, "Characterisation methods for Fibres and Paper"*, (2): 1-9 (2000).
22. Chinga, G., Helle, T. and Forseth, T., "Quantification of structure details of LWC paper coating layers", Submitted for publication in Nordic Pulp Pap. Res. J. (2001).
23. Gregersen, Ø.W., Hansen, A., Tufa, L.D. and Helle, T., "The influence of fibre shives on calender cuts in newsprint", *J. Pulp Pap. Sci.*, 26(5): 176-179 (2000)
24. Engstrom, G., Morin V. and Bi, S.L., "Analysis of porosity distribution in coating layers", *proceedings from the 1997 Advanced coating fundamentals symposium, Philadelphia*, 189-198 (1997).

CHAPTER

9

THREE-DIMENSIONAL RECONSTRUCTION OF A COATING LAYER STRUCTURE (PAPER V)

G. Chinga
Department of Chemical Engineering
Norwegian University of Science and Technology (NTNU)
N-7491 Trondheim
Norway
e-mail: gary.chinga@pfi.no

T. Helle
Department of Chemical Engineering
Norwegian University of Science and Technology (NTNU)
N-7491 Trondheim
Norway
e-mail: torbjorn.helle@pfi.no

Submitted for publication in Journal of pulp and paper science

Abstract

The scanning electron microscope in low-vacuum mode was used to acquire consecutive backscattered electron images after successive grinding and polishing. The high resolution achieved by this technique permits the visualisation of pigment particles and inter-particle volumes. Computer programs available in the Internet were used to process, render and visualise the reconstructed volume. Characteristics of real coating layers like the inter-particle volume network and the pigment particles were volume rendered and visualised in 3-D space. The technique seems promising, however further work is required to improve the efficiency of the image acquisition and to control the thickness of the removed cross-sections, which is important for a true quantification of structure details.

Keywords: 3-D reconstruction, image analysis, SEM, pores, pigment particles

9.1 Introduction

It has been demonstrated that cross-sectional and surface scanning electron microscopy images are well suited for acquiring numerical information of the paper coating structure. The coating layer characteristic details can effectively be assessed and quantified [1,2].

Direct assessment methods like microscopy and image analysis yield insight into the coating layer structure, however has the limitation of being based on two-dimensional (2-D) image analysis [1]. A further step will be a three-dimensional (3-D) characterisation of real pigment coatings. Toivakka and Nyfors [3] developed techniques for characterising the coating structure using 3-D image analysis. However due to the lack of real 3-D datasets of the coating structure, the authors have limited the technique to a characterisation of mathematical models. Unfortunately, such models will severely over-simplify the real coating structures, thus losing the heterogeneity of real samples [4].

Images for 3-D reconstructions may be acquired by different techniques, e.g. magnetic resonance, microscopy and X-ray microtomography [5,6,7,8]. Due to the small size of typical elements in coating layers, the image acquisition device must have high resolution to visualise structure components like pigment particles and pores. Currently available techniques for acquiring 3-D datasets do not have the required resolution to assess the detailed coating structure. However, some techniques have been applied for the analysis of void spaces in base sheets [8,9,10].

High quality images of paper structure may also be obtained by the scanning electron microscope (SEM). Distortions introduced by microtoming [11] are avoided by grinding and polishing of epoxy embedded samples. The SEM has proved to be suitable for acquiring information about the coating layer structure based on 2-D images. A series of SEM images showing cross-sections throughout a paper sample, at given constant small distances would provide a basis for three-dimensional reconstruction. However preparation of paper samples for such image acquisition in not easy. Here, attempts are made to acquire consecutive images of a coating layer and arranging them in a 3-D reconstruction. Such reconstruction may reveal details not available by analysing 2-D images. Particle and inter-particle structure details may be assessed independent of the analysis direction, thus complementing other structural characterisations of the coating layer.

9.2 Material and Methods

9.2.1 Sample description

The paper used in this study was commercially coated with a pigment mix of 70% ground calcium carbonate (GCC), 30% kaolin (clay) (90% <2μm). A detailed description of the paper sample and the applied preparation is given in Chinga and Helle [1].

The sample was not treated with OsO_4. Therefore, the binders cannot be discerned from the embedding epoxy resin in the SEM, backscattered mode electron images. The visualised inter-particle "pores" will thus be filled partly by air (true pores) and partly by coating binders. It seems reasonable to assume a clear relationship between the inter-particle volume fraction (binders and air filled pores) and the air filled volume fraction, although they are not identical. Realising it being not completely correct, the inter-particle volumes will nevertheless be termed "pores" in the following.

9.2.2 Image acquisition

Backscattered electron (BSE) images for 3-D reconstruction of the coating layer were acquired in low vacuum mode (240 MPa), using 15 kV accelerating voltage, 8 mm working distance and 4000x magnification. The spatial resolution of the digital images was 0.025 μm/pixel with 256 grey-levels.

After acquiring the first BSE image, the block with the embedded samples was polished using a 1-micron abrasive cloth. Samples were placed in a STRUERS Rotoforce-4 and polished in a STRUERS Rotopol-22 for 30 sec using a 5 N pressure and 150 rpm. A second, similar BSE image of the coating layer was then acquired. A total of 42 digital images were obtained successively with a separation of some 0.10 μm. Working distance, accelerating voltage and beam current were kept constant during the acquisitions. The brightness and contrast were adjusted to a similar level to avoid grey-level differences between the BSE images. The applied procedure allowed the acquisition of some 4-6 images pr. hour.

9.2.3 Image processing and 3-D visualisation

The obtained digital images were aligned using the Scion Image program. This was accomplished by first rotating all images to a horizontal position using a regression line based on the paper surface, for details see Chinga and Helle [1]. As paper is a planar structure, it was assumed that the paper surface should lie in the same global position in all the images. The vertical-aligned images were finally moved horizontally until the differences between consecutive images were minimal. The pigment particles in the coating layer were also used as markers to verify the alignment process. The stack was visualised in the Object Image program available at http://simon.bio.uva.nl/object-image.html. The program was run under Executor in a Windows NT based computer. Volume rendering with lightning effects was performed by the VolumeJ plug-in [12]. The gaps between the images were filled by the TransformJ plug-in [13]. Interpolated images were thus created between two consecutive images. The plug-ins were used in the ImageJ program (public domain) developed at the U.S. National Institute of Health (NIH) available on Internet at http://rsb.info.nih.gov/ij/.

9.3 Results

9.3.1 3-D visualisation of the coating layer

The consecutive BSE images were aligned as described above and mounted into a 3-D data box (Fig. 1). This is a suitable way of inspecting the 3-D structure, thus gaining information about the pores and the pigment particles. One drawback is the limited knowledge of the distance between each slice. Taking into account the size of the pigment particles and assuming isometric shapes of the $CaCO_3$ particles, distances of approx. 0.10 µm were estimated. However, it seems difficult to maintain a constant thickness of the abraded sections, probably due to softening of the polishing cloth. The transition between the last slices in the stack is smoother compared to the middle ones (Fig 1C).

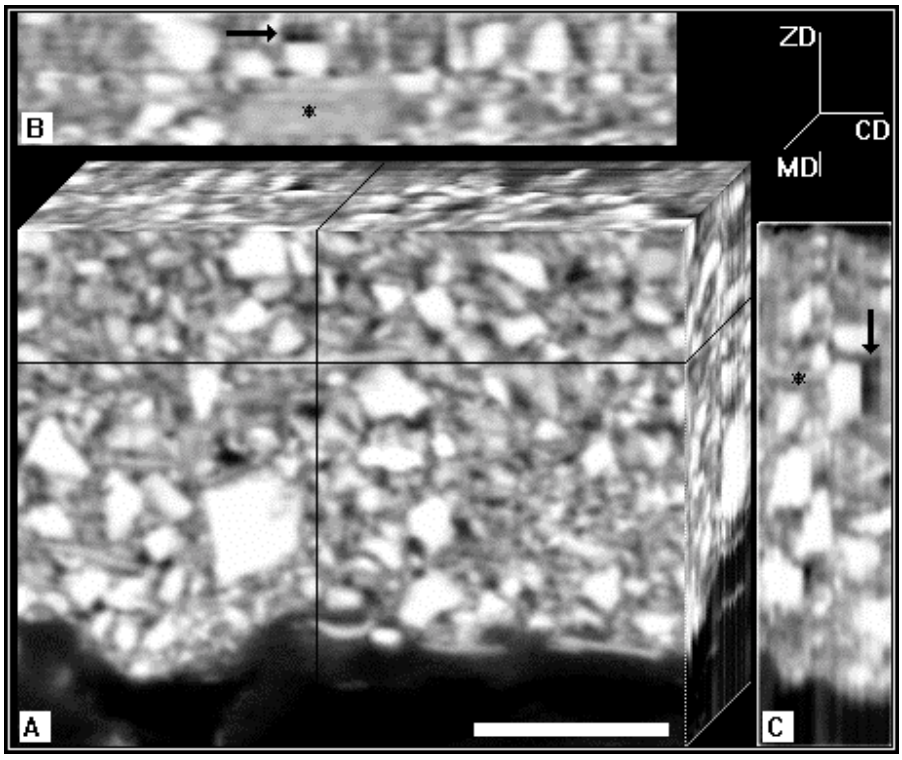

Figure 1 Three-dimensional visualisation of the coating layer. A) Stack of consecutive cross-section images of the coating layer of LWC paper. B) and C) are reconstructed slices seen in z (ZD) and machine (MD) direction respectively. The horizontal and vertical lines in A) correspond to the planes where B) and C) were taken. The arrow indicates a part of a $CaCO_3$ particle removed by polishing (see Fig. 2). The stars in B) and C) indicate the same clay particle seen from different directions. Bar: 5µm.

Some particles also appear to have been removed, probably owing to the polishing (Fig. 1). The embedding epoxy may be softened by the repeated application of ethanol and lubricant during polishing, thus weakening the coating matrix. Fig. 2 depicts two consecutive images of the coating layer with evidence of removal of pigment particles. Parts of 1 clay and 27 $CaCO_3$ pigment particles were removed in the reconstructed coating volume of approx. 750 μm^3. Although the created cavities may be confounded with pores, it is unlikely to find such "false pores" in conventional cross-sectional SEM inspection where grinding and polishing is performed once.

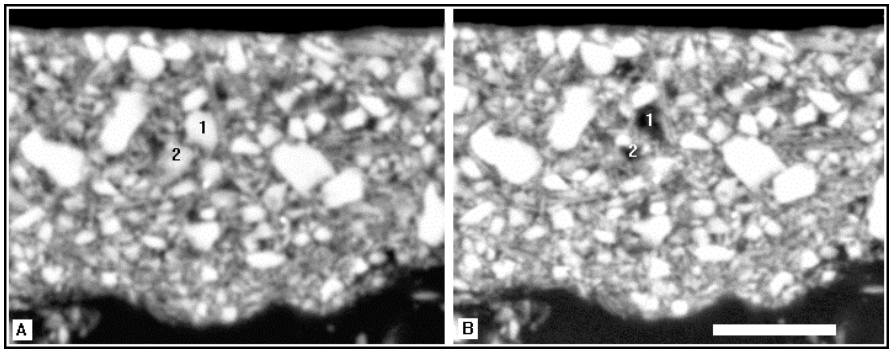

Figure 2 Two consecutive backscattered electron images of the coating layer. 1 and 2 are two $CaCO_3$ particles (A) removed after polishing and creating "false pores" (B). Bar: 5μm

$CaCO_3$ pigment particles were also volume-rendered to visualise the distribution and orientation of the particles in the coating layer (Fig. 3). The rendered volume seems to be composed of a relatively compact lower and a more voluminous upper layer. This may indicate an uneven pigment particle distribution. The more compact lower layer may also reflect the presumptive filter cake formed during coating.

Instead of visualising the pigment particles, one may do the opposite, i.e. visualising the inter-particle voids, the pores. Such detailed visualisation of the pores was obtained by rendering the segmented pore structure (Fig. 4). The rendering yields a volume depicting the coating surface with the surface openings and the inner "pore walls", i.e. the interfaces between pigment particles and pores. Due to the complexity of the pore network only part of the available volume was explored. Even so, the rendered volume exemplifies the complexity of a pore structure, illustrating the simplification of mathematical models. A more detailed visualisation of the pore indicated by the arrow (Fig. 4, left) is given in Fig. 4 (right). Fig. 5 depicts the pore composed of a main body surrounded by several throats. Such throats are assumed to shield larger pores from injection by mercury when using mercury porosimetry [14].

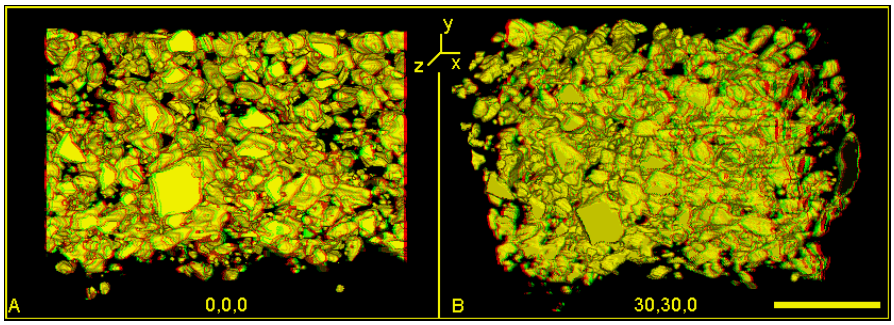

Figure 3 A) Volume rendering of segmented $CaCO_3$ pigment particles (stereo images). B) The same volume rotated around the x and the y axes. The numbers indicate the rotation angle around the x,y and z-axes resp. Bar: 5µm

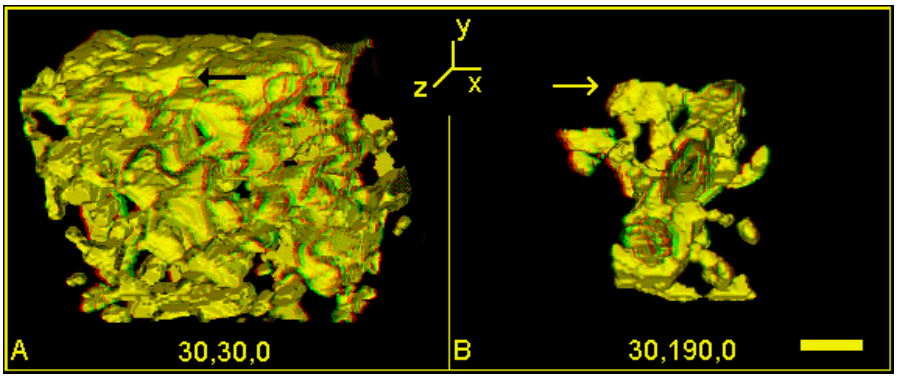

Figure 4 Volume rendering of a portion of the reconstructed coating layer. A) The cross-sectional and surface pore openings are visualised. B) Volume rendering of the pore indicated in A. Note the opening in the middle allowing the visualisation of the throat inner walls. The arrows in A and B indicate the same pore opening seen from different angles. The numbers indicate the rotation angle around the x,y and z-axes resp. A better visualisation of the indicated pore is given in Fig. 5. Bar: 1µm

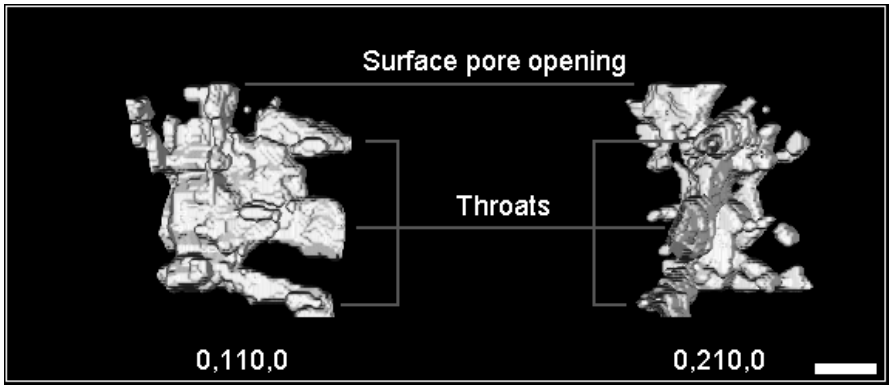

Figure 5 Volume rendering of the pore indicated in Fig. 4. The numbers indicate the rotation angle around the x,y and z-axes resp. Bar: 1µm

Several models of the pore structure are based on arbitrary spheres creating pores with arbitrary connectivity. The pores and throats being aligned either vertically or horizontally [4]. As demonstrated here, this is hardly encountered in reality. Moreover, partition of the pore volume into a main pore and throats have been performed by eroding the binary pore space producing local maxima considered as the pore centres [3]. Even with computer generated models the segmentation of the pore space is not a trivial task and will certainly be challenged by real pore structures.

9.4 Final remarks

3-D reconstruction is a unique way of obtaining information of the coating layer structure in other directions than the vertical cross-section. Complementary information of the spatial distribution of the particles and pores can be collected. In the present qualitative inspection, pigment particles, pores and the coating surface have been reconstructed. The complexity of real structures and the singular pore geometry has also been demonstrated.

Two main problems were encountered with respect to the applied method for acquiring cross-section images. Firstly, it was difficult to determine the accurate thickness of the removed layers during the polishing. Secondly, it seemed that the removed layers' thickness were gradually somewhat reduced for every polishing step, possibly due to the increasing softening of the cloth. The major concern in this respect is to maintain a constant thickness of the removed layers. New reported methods like the focused ion beam (FIB) may be more suitable for sample preparation and image acquisition [15].

Despite the shortcomings with respect to image acquisition, the obtained dataset was considered suitable for making a first attempt of a 3-D reconstruction of the coating structure of LWC paper. The technique was applied for visualising part of a real coating layer 3-D structure, yielding more insight about the pigment particle distribution, pore geometry and the connectivity of surface and inner pores. With improved techniques for serial sectioning and image acquisition, 3-D reconstruction may also become applicable to the micro-structure of paper coatings. Having a 3-D stack, parameters like the volume of objects may be calculated taking into consideration the area comprised by the object in the 2-D sections and the estimated thickness of the abraded sections [16].

Future work, concerning the acquisition of a 3-D dataset, should focus on making the procedure more time-efficient and in regulating the thickness of the removed layers improving the accuracy of the method. Besides, it may be suitable to acquire a series of images in the Z-direction, parallel to the paper's plane, starting at the paper surface and polishing gradually throughout the coating, ever deeper into the paper structure. This would permit a wider region of the coating layer to be assessed.

References

1. Chinga, G. and Helle, T. “Structure characterisation of pigment coating layer on paper by scanning electron microscopy and image analysis”, *Submitted for publication in Nordic Pulp Pap. Res. J.* (2001)
2. Chinga, G. and Helle, T., “Relationships between the coating surface structural variation and print quality”, *Submitted for publication in J. Pulp Pap. Sci.* (2001)
3. Toivakka, M. and Nyfors, K., “Pore space characterisation of coating layers”, *Tappi J.*, 84(3): 1-16 (2001)
4. Matthews, G.P., “Computer modelling of fluid permeation in porous coatings and paper - an overview”, *Nordic Pulp Pap. Res. J.* 15(5): 476-485 (2000)
5. Botto, R. E., Cody, G. D., Dieckman, S. L., French, D. C., Gopalsami, N. and Rizo, P., ”Three-dimensional magnetic resonance microscopy of materials”, *Solid State Nuclear Magnetic Resonance*, 6(4): 389-402 (1996)
6. Chinga,G., Skagen, E., Kittang, A., Beisvaag, T., Iversen, T. and Briarty L., “Three-dimensional reconstruction of *Arabidopsis thaliana* root statocytes exposed to different gravity conditions”, *J. Micros. Ana. (2): 17-19* (2000)
7. Shishido, O., Yoshida, N. and Umino, O., “Image processing experiments for computer-based three-dimensional reconstructions of neurones from electron micrographs from serial ultrathin sections”, *J. Micros.*, 197 (3): 224-238 (2000)
8. Samuelsen, E.J., Gregersen, Ø.W., Houen, P.J. Helle, T., Raven, C. and Snigirev, A., “Three-dimensional imaging of paper by use of synchrotron x-ray microtomography”, *J. Pulp Pap. Sci.* 27(2): 50-53 (2001)
9. Antoine, C., Nygård. P., Holsmtad, R., Gregersen, Ø.W., Weitkamp, T., Rau, C. Solheim, O. and Houen, P.J., “Binarisation of 3D images of paper obtained by phase contrast X-ray microtomography”, *Proceedings from the Cost Action E11 – Characterisation methods for fibres and paper,*1:14 (2001)
10. Holmstad, R., Antoine, C., Silvy, J., Costa, A.-P. and Antoine, J., “Modelling the paper sheet structure according to the equivalent pore concept”, *Proceedings from the Cost Action E11 – Characterisation methods for fibres and paper,* 15:25 (2001)
11. Walbaum, H.H. and Zak, H., “Internal Structure of Paper and Coatings in SEM Cross Sections”, *Tappi J.*, 59(3): 102-105 (1976).
12. Abràmoff, M.D. and Viergever, M.A., “Computation and Visualization of Three Dimensional Motion in the Orbit”, *Accepted for publication in IEEE Trans Med Imag.* (2002)
13. Meijering, E. H. W. Niessen, W. J. and Viergever, M. A., “Quantitative Evaluation of Convolution-Based Methods for Medical Image Interpolation”, *Medical Image Analysis* 5(2): 111-126 (2001)
14. Gane, P.A., Kettle, J.P., Matthews, G.P. and Ridgway, C.J., ”Void space structure of compressible polymer spheres and consolidated calcium carbonate paper-coating formulations”, *Ind. Eng. Chem. Res.* 35: 1753-1764 (1996)

15. Kim, S.T. and Dravid, V.P., “Focused ion beam sample preparation of continuous fibre-reinforced ceramic composite specimens for transmission electron microscopy”, *J. microscopy,* 198(5): 124-133 (2000)
16. Coombs, G.H., Tetley, L., Moss, V.A. and Vickerman, K., “Three-dimensional structure of the leishmania amastigote as revealed by computer-aided reconstruction from serial sections”, *Parasitology* 92:13-23 (1986).

CHAPTER

10

CONCLUDING REMARKS

10.1 Preparation method (Chapter 5)

The results obtained during this study confirm an effective reaction of OsO_4 with material components like mechanical pulp fibres and latex binders for pigment coated paper. With respect to the two staining methods that are compared, OsO_4 dissolved in water (procedure A) causes the best staining of the combined coating/base paper structure. Unfortunately, although the paper samples are not in direct contact with water, the humidity in the sealed containers causes a swelling of the hydroscopic pulp fibres, inducing a roughening of the paper surface.

With respect to the effects of the staining methods on the micro-roughness of the coating surface, and the coating pore details, methods A and B appear to be more or less equivalent, A possibly giving somewhat better image quality. When only the coating layer is under study, either method may be recommended. When even the base paper has to be considered, procedure B should be preferred.

Considering the interesting potentials offered by OsO_4 staining, the method is likely to become a quite common step in the preparation and analysis of fibres and paper even besides coated grades. The chemical is well-suited for visualisation of lignin-containing structures in the base paper and latex films in the coating structure, thus improving the quantification of parameters like porosity and roughness.

Posterior to the staining, the further preparation includes grinding and polishing. With available modern equipment, blocks are prepared quickly and effectively. This is of major importance since fewer steps are required to prepare the samples avoiding distortions on the cross-section surface due to mechanical stress during grinding and polishing.

10.2 Image analysis routines applied to the study of the coating structure (Chapters 3,4,6)

Despite the complexity of surface and cross-sectional images, the automatic thresholding yielded suitable segmentation. The segmented images were thus suitable for further morphometric analysis. The procedures are reproducible, avoiding the large variation experienced with manual assessment. The developed routines are summarised in Table 10.1.

The outlined automation improves the morphometric analysis of coating layers, allowing a direct assessment of critical pore, pigment particle and paper surface details. Besides, the limited operator involvement in the measurement procedures raises the objectivity and reproducibility of the results. Finally, the complementary information obtained by the described methods may be useful for an increased knowledge of the coating layer structure, how it is affected by different process variables and how it will affect the paper end-use properties.

Table 10.1 Developed routines for assessing the coating layer structure.

Structure segmentation	**Morphometric analysis**
Coating layer	Thickness Roughness
Surface closed areas	Closed area fraction
Cross-sectional pores	Pore area fraction Pore area Pore shape Pore orientation Pore size distribution in the Z-direction
Surface pores	Pore area fraction Pore area Pore shape Pore orientation Pore size distribution
Paper coating coverage	Area fraction
Pigment particle's edges	Pigment particle orientation

10.3 Quantification of cross-sectional structure details (Chapter 7)

Cross-sectional SEM analysis has been used in the characterisation of coating layers for a group of commercially coated papers. Despite the wide spread of coating formulation and structure, it has been demonstrated that the described techniques including sample preparation and morphometric analysis are well suited to characterise coating layer structures. The complex pore structure with respect to pore size, shape and orientation has been assessed and quantified. The obtained pore details represent valuable information, not accessible by other available techniques. It has been demonstrated that the pore geometry, described by the best fitting ellipse approach, may be essential for the absorption of the ink vehicle and thus critical for the print gloss development. The pore orientation/diameter ratio also seems to be a proper parameter for predicting print gloss. For a given pore diameter, the more horizontally oriented the pores are, the higher the delta gloss.

10.4 Relationships between surface structural variation and print quality (Chapter 8)

New techniques were developed to study surface details of pigment coated paper, in order to explore their effects on printing defects like mottling. New and semi-automatic routines were developed for image analysis on SEM images, in the SEI and BEI-modes. The automation improves the reliability and reproducibility of the morphometric studies. The study results allowed a division of the surface into different areas characterised as either “open” or “closed”, the two groups differing in their surface pores fraction. The open areas are characterised by having larger amount of pores, larger pore area fraction and higher mean pore diameter. The cross-sectional pore diameters correlate well with the surface pore diameter measured by image analysis, though the later is larger. Larger average size of the pores tends to raise print gloss, however the inner pore geometry is also important for the gloss development. The fraction of open and closed surface areas does not directly affect mottling. The critical factor is rather the distribution of such areas. The more uneven the distribution of open and closed areas, the larger the mottling tendency. And the larger the size of each closed surface area unit of the coating, the larger the correlation between the surface variation and mottling

10.5 3-D reconstruction of real coating layers (Chapter 9)

3-D reconstruction is a unique way of obtaining information of the coating layer in other directions than the cross-section. Complementary information of the spatial distribution of the particles and pores can be collected. In the present qualitative inspection, pigment particles, pores and the coating surface have been reconstructed. The complexity of real structures and the singular pore geometry has also been demonstrated.

Two main problems were encountered with respect to the acquired cross-section images. Firstly, it was difficult to determine the accurate thickness of the removed layers during the polishing. Secondly, it seems that the removed layers’ thickness was reduced for every polishing step, possibly due to the increasing softening of the cloth. The major concern in this respect is to maintain the thickness of the removed layers constant. With improved techniques for serial sectioning and image acquisition, 3-D reconstruction may also become applicable to the micro-structure of paper coatings.

10.6 Suggestions for further work

The presented thesis is based on semi-automatic image processing and analysis routines developed to assess the coating layer structure. Special attention is given to the characterisation of the coating layer micro-structure with respect to pore and characteristic pigment particle details. The automation secures the objectivity and reproducibility of the results. However, being semi-automatic, the routines still need operator involvement in some areas.

10.6.1 Interface between the coating layer and the base paper

When segmenting the coating structure, in high magnification images, some part of the base paper tends to remain as a part of the coating layer. This has to be verified for each image, editing the images when necessary. It is thus recommended to put a border line between the base paper and the coating layer manually before thresholding. New image processing routines may solve this problem, thus improving the automation of the segmentation process.

10.6.2 Pore segmentation

The segmentation procedure seems to yield a suitable segmentation of the pore structure. However, restoration algorithms like the reported wiener filter (Tovey and Hounslow, 1993) might be used to enhance the pores and particles' edges to improve segmentation of small pores. This may also facilitate the particle orientation assessment. There are thus room for the development of such restoration algorithms probably improving the final image quality.

10.6.3 3-D reconstruction

Future work, concerning the acquisition of a 3-D dataset, should focus on making the procedure more time-efficient and in regulating the thickness of the removed layers improving the accuracy of the method. Besides, it may be suitable to acquire a series of images in the Z-direction, parallel to the paper's plane, starting at the paper surface and polishing gradually throughout the coating, ever deeper into the paper structure. This would permit a wider region of the coating layer to be assessed. It is also recommended to verify the suitability of new preparation techniques like the FIB (KIM and Dravid, 2000) for consecutive image acquisition.

10.6.4 Analysis of the paper surface and the bulk pore geometry

The main objective for developing image analysis routines is the direct assessment of critical pore and pigment particle details. This enriches our understanding of the effect of e.g. pore geometry and surface structural variation on print quality. It seems that calendering induces a non-uniform compaction of the coating layer surface, presumptively leading to a non-uniform absorption of ink components. This may affect the homogeneity of prints. Having suitable routines for characterising the paper surface it seems logical to verify the effect of calendering on the paper surface and how different pigment particles and raw stock material affect the pore geometry as well as the development of closed areas. The chemical

aspects of the closed and open areas should also be taken into consideration in future studies. Finally, assessment of the pore geometry underneath the closed and open areas may also be important. In this respect, 3-D reconstruction based on serial images seems essential. Such techniques may even be applied to the study of the surface of printed samples and assess the coating structure below the areas with high and low ink density.

REFERENCES

Abrams, L., Favorite, C.W., Capano, P.J. and Johnson, R.W.,"Using mercury porosimetry to characterise the coating pore structure and its relation to coating optical performance", *Proceedings from the Coating Conference*, 185-192 (1996)

Alberts, B., Bray, D., Lewis, J., Raff, M., Roberts, K. and Watson, J.D., "Molecular biology of the cell", *2nd ed.* ISBN0-8240-3595-6 (1989)

Alkemper, J. and Voorhees, P.W., "Quantitative serial sectioning analysis", *J.* microscopy, *201(3): 388-394* (2001)

Allem, R., "Characterization of Paper Coatings by Scanning Electron Microscopy and Image Analysis", *J. Pulp Pap. Sci.*, 24(10) 329-336 (1998)

Allem, R. and Uesaka, T., "Characterization of Paper Microstructure: A New Tool for Assessing the Effects of Base Sheet Structure on Paper Properties", *Proceedings from the 1999 Microscopy as a Tool in Pulp and Paper Research and Development Symposium*, 43-52 (1999)

Baxes, G.A., "Digital image processing : principles and applications", New York : Wiley, ISBN: 0-471-00949-0, 452p (1994)

Climpson, N.A. and Taylor, J.H., "Pore distributions and optical scattering coefficients of clay structures", *Tappi J.* (7), 89-92 (1976).

Dickson, A., "Quantitative Analysis of Paper Cross-Sections", *Appita J.*, 735-738 (1999).

Dickson, R., Forsström, U. and Grön, J., "Coating coverage of metered size press pre-coated paper", *Proceedings from the 2000 Tappi Coating Conference and Trade Fair*, 167-184 (2000).

Dullien, F.A.L. and Mehta, P.N., "Particle size and pore (void) size distribution determination by photographic methods", *Powder Technol*, (5): 179-193 (1971)

Elton, N.J., Hooper, J. and Gane P.A.C., "Optical microscopy of paper: Methodology and applications", *Proceedings from the 24th EUCEPA Conference, 438-458* (1990)

Elton, N.J., Gate, L.F. and Hooper, J.J., "Texture and orientation of kaolin in coatings", *Clay Minerals* 34: 89-98. (1999)

Fahrenbach, W.H., "Continuous Serial Sectioning for Electron Microscopy", *J. Electron Micros. Tech.*, 1:387-398 (1984).

Forseth, T., Wiik, K. and Helle, T., "Surface Roughening Mechanisms for Printing Paper Containing Mechanical Pulp", *Nordic Pulp Pap. Res. J.*, 1: 67-71 (1997)

Gane, P.A.C., Hooper. J.J. and Baumeister, M." The influence of furnish content on formation and basesheet profile stability during coating", *Tappi J.* (9): 193-201 (1991)

Gane, P. A. C., Hooper, J. J. and Grunwald, A., "Coating pigment orientation: A comparative analysis of the application mechanisms and properties of blade and roll coatings", *Proceedings from 1995 Coating Conference,* 383-390 (1995)

Gane, P.A., Kettle, J.P., Matthews, G.P. and Ridgway, C.J., "Void space structure of compressible polymer spheres and consolidated calcium carbonate paper-coating formulations", *Ind. Eng. Chem. Res.* 35: 1753-1764 (1996)

Gane, P. and Watters, P., "Pigment particle orientation", *Pap. puu* 71(5): 517-533 (1989)

Gibbon, D.L., Simon, G.S. and Cornelius, C., "New Electron and Light Optical Techniques for Examining Papermaking", *Tappi J.*, 72(10): 87- (1989)

Gregersen, Ø.W., Johnsen, P.O. and Helle, T., "Small scale topographical variations of paper surfaces, and their effects on printing ink transfer distribution", *Proceedings from the International printing and graphic arts conference*, 271-281 (1994)

Gregersen, O.W., Helle, T. and Johnsen, P.O., "Qualitative Methods for the Study of Lignin Distribution in Wood and Surface Layers of Unbleached Pulp Fibres and Paper", *J. Pulp Pap. Sci.*, 21(8): 285-287 (1995)

Gregersen, Ø.W., Hansen, A., Tufa, L.D. and Helle, T., "The influence of fibre shives on calender cuts in newsprint", *J. Pulp Pap. Sci.*, 26(5) 176-179 (2000)

Helle, T. and Johnsen, P.O., "Using stereoscopic and SEM backscatter imaging for studying ink distribution details on paper and fibre surfaces", *J. Pulp Pap. Sci.* 20(7): 189-192 (1994)

Kartovaare, I., "Coatweight distribution and coating coverage in blade coating", *Pap. puu*. (9): 1033-1042

Kent, H.J., Hooper, J.J., Climpson, N.A., Gane, P.A.C. and Coggon, L., "Applications of novel techniques for quantitative characterisation of coating structure", *Proceedings from the 1986 coating conference*, 103- 112 (1986)

Kim, S.T. and Dravid, V.P., "Focused ion beam sample preparation of continuous fibre-reinforced ceramic composite specimens for transmission electron microscopy", *J. microscopy*, 198(5): 124-133 (2000)

Krishnagopalan, A. and Simard, G.L., "An improved technique for studying binder migration in coated paper", *Tappi J.* 12: 96- 99 (1976)

Lepoutre P. and Rezanowich A., “Optical properties and structure of clay-latex coatings”, *Tappi J.* 60(11): 86-91 (1977)

Matsubayashi, H., Miyamoto, K., Takagishi, Y. and Kataoka, Y., “A study of blistering by coating structure analysis”, *Tappi J.* (5): 161-170 (1990)

Matasubayashi, H and Saito, Y., “The influence of coating structure on paper quality”, Proceedings from the 1992 Coating Conference, 161-171 (1992)

McCoy, J.W., ”Metallographic Preparation of Coated Papers for Backscattered Electron Imaging of Coating Structures in Cross-section”, *Proceedings from the 1998 Coating/Papermaking Conference*, 121-132 (1998)

Ozaki, Y. and Kimura, M., “Visualisation of printing ink vehicle on paper surfaces by a SEM technique”, *Appita J.* 3: 216-219 (2000)

Peterson, A. and Williams, L.C., “Determining Paper-Coating Thickness with Electron Microscopy and Image Analysis”, *Tappi J.*, (10) 122-126 (1992)

Quackenbush, D., ”Case Studies on the Use of the Optical Microscope in the Analysis of Coated Papers”, *Tappi J.*, 71: 70-75 (1988)

Reme, P.A. and Kure, K.-A. “Quantitative assessment of changes in paper structure topography details during printing, using SEM”, *Proceedings from the 2000 International paper physics seminar*, 79-83. (2000)

Ridler, T.W. and Calvard, S., “Picture Thresholding Using an Iterative Selection Method”, *IEEE Transactions on Systems, Man, and Cybernetics*, smc-8 (8): 630-632 (1978)

Rissa, K., Lepisto, T., Vaha-Nissi, M., Lahti, J. and Savolainen, A., “Orientation of talc particles in dispersion coatings”, *Nordic Pulp Pap. Res. J.*, 15: 5, 357- 361 (2000)

Rissa, K., Lepistö, T., Vähä-Nissi, M. and Savolainen, A., “Characterization of Pigment and Dispersion Coatings using Atomic Force Microscopy and Scanning Electron Microscopy”, *proceedings from the 1999 Microscopy as a Tool in Pulp and Paper Research and Development Symposium*, 195-206 (1999)

Russ, J.C., “The image processing handbook”, 3rd Ed. ISBN 3-540-64747-3 (1999)

Tovey, N.K. and Hounslow, M.W., “Quantitative micro-porosity and orientation analysis in soils and sediments”, *J. Geol. Soc.* 152: 119-129 (1995)

Walbaum, H.H. and Zak, H., “Internal Structure of Paper and Coatings in SEM Cross Sections”, *Tappi J.*, 59(3): 102-105 (1976)

Whalen-Shaw, M. and Eby, T., “An investigation of factors related to backtrap mottle in coated papers using electron probe microanalysis”, *Proceedings from the 1991 Tappi Coating Conference and Trade Fair*, p. 401 (1991)

Williams, G.J. and Drummond, J.G., ”Preparation of Large Sections for the Microscopical Study of Paper Structure”, *Proceedings from the 1994 Papermakers Conference,* 517-523 (1994)

Wygan, R.W., Pruett, R.J. and Chen, C.Y. “A review of techniques for characterizing the paper coating surfaces, structures and printability”, *Proceedings from the 1995 Coating Fundamentals Symposium,* 1-15 (1995)

APPENDIX A

A.1 Coating layer thickness

The coating layer thickness of the 8 paper samples presented in Chapter 7, Fig. 1 is given in Fig. A.1. The readings are based on 24 BSE cross-section images acquired according to Chapter 3, section 3.3. The coating thickness of each paper grade was measured as described in Chapter 3, section 3.6.

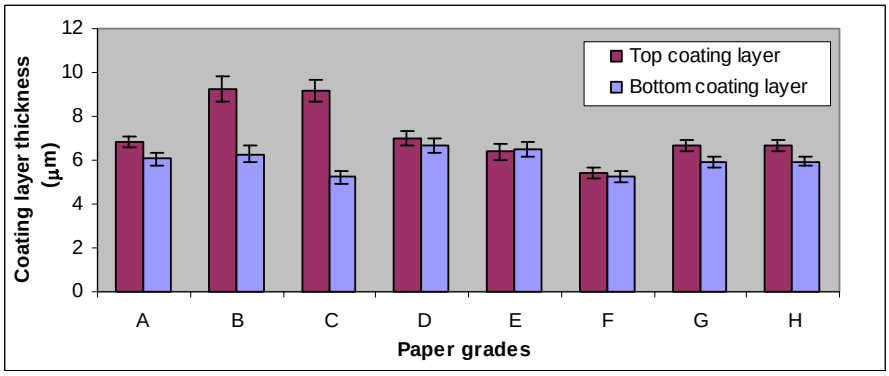

Figure A.1 Thickness measurements on the studied paper samples. The thickness measurements were taken with 3 µm step size.

A.2 The pore size distribution of calendered and uncalendered samples

Analysis of the paper surface of an uncalendered paper sample, having a large fraction of $CaCO_3$ pigments, has not revealed any occurrence of closed areas at the coating surface. This may indicate that the closed areas is a result of the calendering (Fig. A.2). It is unclear which areas become closed. However, it seems that the closed areas appear frequently on the hills of the fibres and may thus correspond to the thinnest regions of the coating layer. These regions, presumptively having a high local basis weight, are likely to be subjected to high specific loads during calendering, becoming compressed and smoothened (see e.g. Gregersen et al., 2000).The width of the segmented areas is in the range of the fibres' width, supporting this assumption (Chapter 8, Fig. 1).

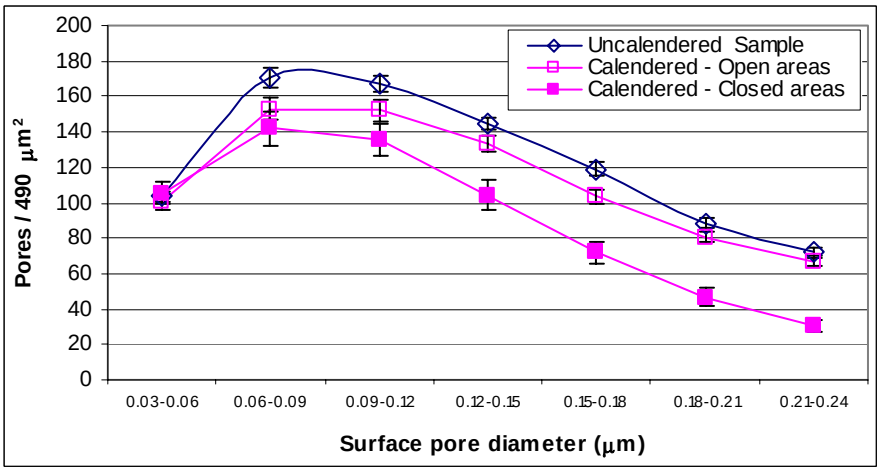

Figure A.2 The presumptive effect of calendering on the paper surface densification.

A.3 Paper coating coverage

The paper coating coverage (Fig. A.3) of the 8 samples described in Chapter 7 and 8 was measured as explained in Chapter 4, section 4.3.3 and Table 4.1. 10 kV accelerating voltage seems to be suitable for coverage characterisation and may represent information from some 0.5 µm of the uppermost part of the coating layer (see e.g. Helle and Johnsen, 1994; Allem, 1998). The dark areas visualised in the SEM, BEI- mode images (Fig. 4.6) correspond thus to areas with no coating or having a coating thickness less than 1 µm. The readings are based on 20 BSE images taken from the surface of each sample.

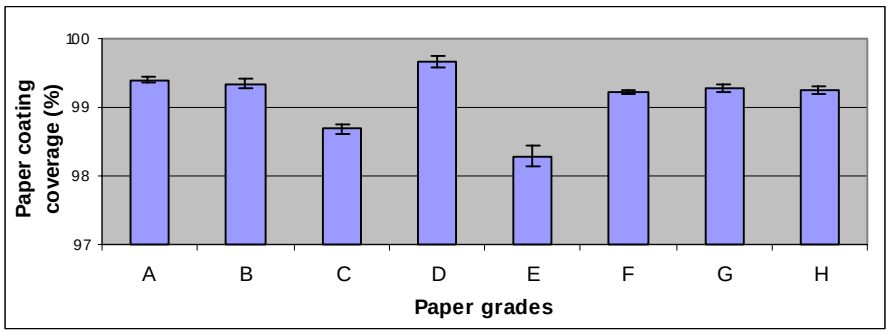

Figure A.3 The paper coating coverage of the 8 samples described in Chapter 7 and 8.